Al-Farabi Kazakh National University

UDC 530.12:524.3 On manuscript rights

ZHAMI BAKYTZHAN

Investigation of hot rotating white dwarfs in general relativity

6D060400 – Physics

Dissertation submitted in fulfillment of the requirements for the degree of Doctor of Philosophy (PhD)

Scientific advisors:
PhD, associate professor
Kuantay Boshkayev;
Doctor of Science, professor
Remo Ruffini

Republic of Kazakhstan
Almaty, 2020

CONTENT

ABBREVIATIONS..... 4

INTRODUCTION……5

1 EQUATIONS OF STATE OF WHITE DWARF MATTER.....10
1.1 The Chandrasekhar equation of state at zero temperature…….....10
1.2 The Chandrasekhar equation of state at finite temperatures.....12
1.3 The Salpeter equation of state……....13
1.4 The Feynman-Metropolis-Teller equation of state…….....15
1.5 The Feynman-Metropolis-Teller equation of state at finite temperatures…....18
1.6 Summary……....19
2 EXTERIOR METRICS OF COMPACT OBJECTS AND THEIR COMPARISON……....20
2.1 Correspondence of the Kerr and Hartle-Thorne metrics……... 21
2.1.1 The exterior Hartle-Thorne metric…….……21
2.1.2 The Kerr metric…… 24
2.2 Correspondence of the Fock and the Kerr metrics…… 27
2.2.1 Fock's approach…….……....27
2.2.2 The interior solution…….. 28
2.2.3 Fock's metric for a deformed body……... 29
2.2.4 Fock's metric for a spherically symmetric body……... 29
2.2.5 Relation between the Kerr and Fock metrics…… 30
2.3 On the equivalence of Hartle-Thorne and Sedrakyan-Chubaryan solutions…. 32
2.3.1 The Sedrakyan-Chubaryan solution…….. 33
2.3.2 Relation between the Hartle-Thorne and Sedrakyan-Chubaryan metrics……. 37
2.4 Summary……....39
3 EQUILIBRIUM CONFIGURATIONS OF STATIC WHITE DWARFS…….. 42
3.1 Effects of general relativity to the structure of white dwarfs..... 43
3.1.1 Newtonian and general relativistic equations of stellar structur……....43
3.1.2 Dimensionless form…….…….45
3.1.3 Boundary conditions……..46
3.1.4 Results of numerical calculations……..47
3.2 Static white dwarfs taking into account the effects of finite temperatures and general relativity……..... 51
3.2.1 Main parameters of white dwarfs and their relations……... 51
3.2.2 Binary systems: white dwarf and millisecond pulsar……..…. 53
3.3 Static white dwarfs taking into account nuclear composition in general relativity……,……....57
3.3.1 The catalog of white dwarfs from the Sloan Digital Sky Survey…….……57
3.3.2 Results of numerical calculations……..61
3.4 Summary…….……...65
4 EQUILIBRIUM CONFIGURATIONS OF ROTATING WHITE

DWARFS..... 67
4.1 Rotating white dwarfs in Newtonian gravity..... 67
4.1.1 Definition of coordinates.....70
4.1.2 Spherical harmonics..... 71
4.1.3 Mass and central density..... 74
4.1.4 The shape of a star and numerical integration.....76
4.1.5 Moment of inertia.....77
4.1.6 Gravitational binding energy and rotational kinetic energy.....79
4.1.7 Quadrupole moment.....80
4.1.8 Ellipticity and gravitational Love number.....80
4.1.9 Equations of structure.....83
4.1.10 An example: white dwarfs..... 86
4.1.11 The mass-shedding limit and scaling law..... 95
4.1.12 Comparison with other results in the literature..... 97
4.2 Rotating white dwarfs in general relativity.....98
4.2.1 Equations of structure..... 98
4.2.2 Rotating white dwarfs at zero temperature 100
4.2.3 Rotating white dwarfs at finite temperatures.....102
4.3 Summary.....103
5 I-LOVE-Q RELATIONS FOR WHITE DWARF STARS.....106
5.1 Equations of structure.....106
5.2 Stability criteria for rotating white dwarfs.....107
5.2.1 Inverse β-decay instability.....107
5.2.2 Mass-shedding limit.....107
5.2.3 The turning-point criterion and secular axisymmetric instability..... 108
5.3 Results and discussion.....108
5.4 I-Love-Q and I-Q-e relations forwhite dwarfs.....114
5.5 Summary.....121
CONCLUSIONS.....123
REFERENCES..... 125

ABBREVIATIONS

EoS	Equation of state
GR	General relativity
NG	Newtonian gravity
WDs	White dwarfs
NSs	Neutron stars
BHs	Black holes
HF	Hartle formalism
CGS units	Centimeter-gram-second system of units
TOV equation	Tolman-Oppenheimer-Volkoff equation
SDSS DR 4	Sloan Digital Sky Survey Data Release 4
SDSS DR 10	Sloan Digital Sky Survey Data Release 10
SDSS DR 12	Sloan Digital Sky Survey Data Release 12
I-Love-Q relations	Inertia-Love Number-Quadrupole moment relations
I-Q-e relations	Inertia-Quadrupole moment-eccentricity relations
FMT EoS	Feynman-Metropolis-Teller equation of state

INTRODUCTION

The general characteristics of the dissertation. The PhD dissertation is devoted to the theoretical research of properties of stable white dwarfs (WDs) with a main focus on the effects of general relativity (GR), finite temperatures, nuclear composition and rotation.

The relevance of the dissertation. A white dwarf or degenerate dwarf is one of the classes of compact objects which are the end-products of stellar evolution. In general, there are three main classes of compact objects: WDs, neutron stars (NSs) and black holes (BHs). These objects are called compact objects because of their large masses and small sizes and, correspondingly, high densities. A WD is the final stage in the evolution of main sequence stars with masses from $0.07\,M_\odot$ to $8\,M_\odot$ [1] (even up to $12\,M_\odot$ according to some studies [2]). This range covers the overwhelming majority of normal stars formed in our galaxy (the Milky Way), including our Sun, and that is why WDs will present the most common end-products of stellar evolution. The lower limit of a main sequence star mass is associated with the impossibility of the occurrence of a thermonuclear helium synthesis reaction. If the mass of the main sequence star is more than the upper limit it will become a NS, not a WD. It is thought that more than 97% of the normal stars in our galaxy will finally end as a WD [1].

After, a main sequence star of low or medium mass runs out of the nuclear fusion of hydrogen into helium, it expands, becoming a red giant. The red giant is supported by thermonuclear reactions of the converting helium into carbon and oxygen. If the mass of the red giant is insufficient to raise the core temperature to the level necessary for thermonuclear reactions involving the obtained carbon, it accumulates in the star's core, together with oxygen. A star discards its outer shell, forming a planetary nebula, and the former core of the star becomes a white dwarf composed of carbon and oxygen. However, depending on the initial mass of the star, thermonuclear reactions can also stop on helium (for stars with a very small mass) or on neon (for massive stars), which will lead to the formation of WDs consisting respectively of helium or oxygen, neon and magnesium [3, 4].

There is no nuclear fusion in the interior of the WD like in a normal star. Consequently, it is not the thermal pressure force keeping the white dwarf in hydrostatic equilibrium. The pressure support in the WD is provided by a degenerate electron gas, whereas most of the mass density is due to a nondegenerate gas of ions [5, 6]. The maximum mass of a non-rotating white dwarf cannot exceed the Chandrasekhar mass limit of $1.44M_\odot$ [7] beyond which even the degenerate electron gas cannot prevent the WD from gravitational collapse or type Ia supernova explosion [8], which takes place as a result of accretion or merger. However, the maximum mass of a rotating white dwarf can exceed the Chandrasekhar mass limit [9-17].

WDs are important to understand the expansion of the universe in cosmology in terms of type Ia supernova explosions, since they can provide independent information about the age of our galaxy and their distribution contains information

about star formation history and subsequent evolution. Also, type Ia supernovae are used as standard candles in astronomy to estimate distances to remote galaxies and study the nature of dark energy [18, 19]. Since the progenitors of white dwarfs lose carbon, nitrogen and oxygen on the stage of the main sequence star, they make a significant contribution to the chemical evolution of our galaxy, and possibly are an important source of life sustaining chemical compounds. Thus, all these facts fully justify **the relevance** of this PhD thesis. Therefore, it is important to study the formation, physical properties, stability and evolution of WDs and to construct a realistic model for them.

Relation of the dissertation with other research projects. The work has been carried out within the plans of the following research projects of Ministry of Education and Science of the Republic of Kazakhstan: 1) «Investigation of white dwarfs taking into account temperature and rotation in general relativity» (2015-2017, 3101/GF4, State registration No. 0115RK01047); 2) «Investigations on rotating and deformed objects in general relativity and relativistic astrophysics» (2013-2015, 1597/GF3, State registration No. 0113PK00369).

The purpose of the dissertation is to investigate the properties of equilibrium configurations of white dwarfs with a main focus on the effects of general relativity, finite temperatures, nuclear composition and rotation.

To achieve the purpose of the dissertation the following **research tasks** have been posed:

- To study both interior and exterior metrics of Einstein's field equations in order to describe gravitational field of white dwarfs;
- To study the effects of general relativity, finite temperatures and nuclear composition on the structure of non-rotating white dwarfs;
- To study the influence of rotation on the structure of white dwarfs both in Newtonian gravity and general relativity;
- To study dependence of I-Love-Q and I-Love-e relations in the case of rotating white dwarfs with different equations of state.

The object of the research. Equilibrium configurations of cold and hot, static and rotating, classic and relativistic white dwarfs.

The subject of the research. The main parameters of stable, cold and hot, static and rotating white dwarfs such as mass, radius, central density, central pressure, moment of inertia etc.

Research methods. The methods of tensor analysis and general relativity, the numerical methods for integrating differential equations, the method of perturbation theory and the Hartle formalism are used.

Scientific and practical value of the dissertation. The obtained results can be directly used to explain the observational data in the analysis and in the investigations of problems in astronomy, relativistic astrophysics, physics of white dwarfs and cosmology.

The main provisions submitted for the defense:

1. The mathematical and physical equivalence of the approximate stationary axially symmetric the Hartle-Thorne and Sedrakyan-Chubaryan solutions of Einstein

field equations (up to second order in angular velocity) that describe the gravitational field of astrophysical compact objects including white dwarfs in the limiting case of slow rotation and small deformation.

2. The effects of general relativity become significant in the mass-radius relation for white dwarf masses closer to the Chandrasekhar limit, thermal effects are most clearly pronounced for white dwarf masses lower than the Chandrasekhar limit, while rotation and nuclear composition are important for the entire mass range of white dwarfs.

3. The core temperatures of white dwarf-satellites in the binary systems of millisecond pulsars PSR J1738+0333, PSR J1012+5307 and PSR J1911-5958A estimated to be in the range $(1.55\text{-}6.5)\times10^7$ K, $(1.4\text{-}2.4)\times10^7$ K and $(0.4\text{-}9.5)\times10^7$ K, respectively.

4. The I-Love-Q (the moment of inertia, the rotational Love number and the quadrupole moment) and I-Q-e (the moment of inertia, the quadrupole moment and the eccentricity) relations are universal and independent of the equations of state (Chandrasekhar and Salpeter equations of state) of white dwarfs.

Novelty of the work. The following results have been obtained for the first time within this dissertation:

– A set of algebraic expressions relating the total mass, angular momentum and mass quadrupole moment of the Hartle-Thorne solution with the integration constants of the Sedrakyan-Chubaryan solution. Alternatively, the relevant multipole moments of both solutions have been calculated and it has been shown that they are identical. The mathematical and physical equivalence of the two metrics has also been proven.

– The mass-radius relations of white dwarfs taking into account the effects of general relativity, finite temperatures, nuclear composition and rotation were calculated.

– The core temperatures of white dwarf-satellites in the binary systems of millisecond pulsars PSR J1738+0333, PSR J1012+5307 and PSR J1911-5958A, have been estimated using the graphical method..

– The I-Love-Q and I-Love-e relations for white dwarfs have been shown to be universal and independent of the Chandrasekhar and Salpeter equations of state.

The personal contribution of the author. The author was directly involved in setting the research task together with scientific advisers, carrying out all the analytical and numerical calculations, doing comparisons and analysis of the results, summarising conclusions, presenting the obtained results at the international conferences, preparing the results of the work for publications.

Reliability and validity of the results. The well-known physical models, mathematical methods approved and generally accepted in scientific community have been used in the thesis. The results obtained in the thesis are in good agreement with the ones in the literature and observational data. Furthermore, the reliability and validity of the thesis results are confirmed by publications in the journals with high impact factors indexed by Scopus and Web of Science and in the journals

recommended by the Committee for the Control of Education and Science of the Ministry of Education and Science of the Republic of Kazakhstan and in the materials of local and foreign international scientific conferences.

Approbation of the dissertation. The results of the work were presented and discussed at the following foreign and local international conferences:

– XII-th International Conference on Gravitation, Astrophysics and Cosmology, Dedicated to the centenary of Einstein's General Relativity theory (Peoples' Friendship University of Russia, Moscow, Russia, June 28-July 5, 2015);

– The Fourteenth Marcel Grossmann Meeting on Recent Developments in Theoretical and Experimental General Relativity, Astrophysics, and Relativistic Field Theories (Sapienza University of Rome, Rome, Italy, July 12-18, 2015);

– The V-th International scientific conference «Physics and Physical Education: Achievements and Development Prospects» (Kyrgyz National University, Bishkek, Kyrgyzstan, September 21, 2015);

– 9-th Alexander Friedmann International Seminar on Gravitation and Cosmology and 3-rd Satellite Symposium on the Casimir Effect (Saint Petersburg, Russia, June 21-27, 2015);

– 9-th International scientific conference «Modern achievements of physics and fundamental physical education» (Al-Farabi Kazakh National University, Almaty, Kazakhstan, October 12-14, 2016);

– Supernovae, Hypernovae and Binary Driven Hypernovae, An Adriatic Workshop (International Center for Relativistic Astrophysics Network, Pescara, Italy, June 20-30, 2016);

– Phenomenology of Strong Gravity Workshop (Nazarbayev University, Astana, Kazakhstan, September 14-16, 2016);

– 5-th International conference on Cosmology, Relativistic and Nuclear Astrophysics (Al-Farabi Kazakh National University, Almaty, Kazakhstan, October 31-November 4, 2017);

– International Scientific Conference dedicated to the 80-th anniversary of Academician of the NAS RK Abdildin M.M. Abdildin readings: Actual Problems of Modern Physics (Al-Farabi Kazakh National University, Almaty, Kazakhstan, April 12-15, 2018);

– International scientific conference of students and young scientists «FARABI ALEMI» (Al-Farabi Kazakh National University, Almaty, Kazakhstan, April 13-16, 2015; April 14-16, 2016; April 10-13, 2017; April 10-13, 2018; April 8-11, 2019);

– The 6-th International Workshop «Nuclear Physics, Nuclear Astrophysics and Cosmic Rays» (Al-Farabi Kazakh National University, Almaty, Kazakhstan, April 16-18, 2019).

Publications. According to materials presented in the dissertation 30 works have been published in total. 6 articles were published in the international journals and conference proceedings indexed in Scopus (Elsevier, Netherlands) and Web of Science (Clarivate Analytics, USA). 7 articles were published in journals recommended by Control Committee of Education and Science of the Ministry of Education and Science of the Republic of Kazakhstan. 1 article was published in the

scientific journal of the Republic of Kazakhstan. 16 abstracts and articles were published in the materials of local and foreign international scientific conferences.

The volume and structure of the dissertation. The dissertation consists of a title page, content, abbreviation list, introduction, five sections, conclusion and reference list with 161 sources. It contains 7 tables and 65 figures. The total volume of the dissertation is 135 pages.

1 EQUATIONS OF STATE OF WHITE DWARF MATTER

In this section, the Chandrasekhar [7], the Salpeter [20, 21], and the Feynman-Metropolis-Teller (FMT) [22] equations of state and their extensions which can be used to describe WD matter are considered. The classical work of Feynman, Metropolis and Teller [22] for compressed atoms is extended to the relativistic regimes in the work of Rotondo et al. [23], as well as, to the case of finite temperatures by S.M. de Carvalho et al [24, 25]. As a result, they have constructed the corresponding EoSs of the system.

1.1 The Chandrasekhar equation of state at zero temperature

The EoS of a degenerate WD substance, in the simplest case, determines the dependence of the total pressure on the total energy density. The substance of WDs consists of electrons and positively charged ions (naked nuclei). In this case, electrons are considered as a completely degenerate free electron gas and they are described by Fermi-Dirac statistics. In the Chandrasekhar approximation [7, 24, 26], the Coulomb interaction between nuclei and electrons and of course, between electrons is ignored and the distribution of electrons, as well as ions, is assumed to be locally constant. Consequently, the condition of local charge neutrality is given by

$$n_{\mathrm{e}} = \frac{Z}{A} n_n , \tag{1.1}$$

where n_{e} is the electron number density, Z is the number of protons, A is the average atomic weight, n_n is the number density of nucleons. At the complete degeneracy, all the lower energy levels are filled up to some maximum level, called the Fermi level. The number density of total degenerate electron gas at the Fermi level is defined as

$$n_{\mathrm{e}} = \int_0^{p_{\mathrm{e}}^F} \frac{2}{(2\pi\hbar)^3} d^3 p = \frac{8\pi}{(2\pi\hbar)^3} \int_0^{p_{\mathrm{e}}^F} p^2 dp = \frac{\left(p_{\mathrm{e}}^F\right)^3}{3\pi^2\hbar^3}, \tag{1.2}$$

where p_{e}^F is the Fermi momentum of electron, $\hbar$ is the reduced Planck constant.

Within the Chandrasekhar's approximation, the total pressure is due to the pressure of electrons P_{e} since the pressure of positive ions P_n (naked nuclei) is insignificant whereas the energy density is due to the energy density of nuclei ε_n as the energy density of the degenerate electrons ε_{e} is negligibly small. Thus, the Chandrasekhar EoS at zero temperature is given by

$$\varepsilon_{Ch} = \varepsilon_n + \varepsilon_{\mathrm{e}} \approx \varepsilon_n = \frac{A}{Z} m_n c^2 n_{\mathrm{e}} , \tag{1.3}$$

$$P_{Ch} = P_n + P_{\mathrm{e}} \approx P_{\mathrm{e}}, \tag{1.4}$$

where m_n is the mass of the nucleon, ε_n is the energy density of nucleons, ε_{e} is the energy density of degenerate electrons, P_n is the pressure of nucleons (positive ions or naked nuclei), P_{e} is the pressure of electrons. The ratio of the atomic number A to the number of protons Z is usually denoted in the literature as $\mu = A/Z$ and in our diagrams, for simplicity all calculations for the Chandrasekhar EoS were carried out taking the value of $\mu = 2$.

The total energy density of degenerate electron gas is written in the following form, although it is neglected in the Chandrasekhar EoS

$$\varepsilon_{\mathrm{e}} = \frac{2}{(2\pi\hbar)^3}\int_0^{p_e^F} \sqrt{p^2c^2 + m_{\mathrm{e}}^2c^4}\, 4\pi p^2 dp = \frac{m_{\mathrm{e}}^4 c^5}{8\pi^2\hbar^3}\left[y_{\mathrm{e}}\sqrt{1+y_{\mathrm{e}}^2}\left(1+2y_{\mathrm{e}}^2\right) - \operatorname{arsinh}\left(y_{\mathrm{e}}\right)\right], \tag{1.5}$$

and the total electron pressure is defined as

$$P_{\mathrm{e}} = \frac{1}{3}\frac{2}{(2\pi\hbar)^3}\int_0^{p_e^F} \frac{p^2c^2}{\sqrt{p^2c^2 + m_{\mathrm{e}}^2c^4}}\, 4\pi p^2 dp = \frac{m_{\mathrm{e}}^4 c^5}{8\pi^2\hbar^3}\left[y_{\mathrm{e}}\sqrt{1+y_{\mathrm{e}}^2}\left(2y_{\mathrm{e}}^2/3 - 1\right) + \operatorname{arsinh}\left(y_{\mathrm{e}}\right)\right], \tag{1.6}$$

where $y_{\mathrm{e}} = p_{\mathrm{e}}^F/(m_{\mathrm{e}}c)$ is the dimensionless Fermi momentum of electrons, m_{e} the electron mass. It should be noted that $\operatorname{arsinh}(y_{\mathrm{e}})$ in the equations (1.5) and (1.6) can be replaced by $\ln\left(y_{\mathrm{e}} + \sqrt{1+y_{\mathrm{e}}^2}\right)$.

The expressions of the Chandrasekhar EoS system at zero temperature (1.3) and (1.4) are given by

$$\varepsilon_{Ch} = \rho c^2 = \frac{32}{3}\left(\frac{m_{\mathrm{e}}}{m_n}\right)^3 K_n \left(\frac{A}{Z}\right) y_{\mathrm{e}}^3, \tag{1.7}$$

$$P_{Ch} = \frac{4}{3}\left(\frac{m_{\mathrm{e}}}{m_n}\right)^4 K_n \left[y_{\mathrm{e}}\left(2y_{\mathrm{e}}^2 - 3\right)\sqrt{1+y_{\mathrm{e}}^2} + \ln\left(y_{\mathrm{e}} + \sqrt{1+y_{\mathrm{e}}^2}\right)\right], \tag{1.8}$$

where K_n is defined by $K_n = \left(m_n^4 c^5\right)/\left(32\pi^2\hbar^3\right)$. As it was mentioned above the energy density $\varepsilon_{Ch} = \varepsilon_{Ch}(R)$ is determined only by the nuclei, while the pressure $P_{Ch} = P_{Ch}(R)$ is determined by means of the degenerate electron gas.

Let us consider an EoS of the form $P = P(\rho)$. In the following, we will focus on two extreme cases: $y_{\mathrm{e}} << 1$ and $y_e >> 1$, i.e. $p_{\mathrm{e}}^F << m_{\mathrm{e}}c$ and $p_{\mathrm{e}}^F >> m_{\mathrm{e}}c$, respectively. In the former case, the kinetic energy is much smaller than the rest mass of the

electrons, i.e. that is the nonrelativistic case. Considering the equation for the pressure for $p_{\mathrm{e}}^{F} << m_{\mathrm{e}}c$, one finds that

$$P = K_{non-rel}\rho^{\frac{5}{3}}, \tag{1.9}$$

where $K_{non-rel} = \left(3^{2/3}\pi^{4/3}\hbar^{2}\right)/\left(5m_{\mathrm{e}}m_{u}^{5/3}\mu_{\mathrm{e}}^{5/3}\right)$ is the constant.

For the relativistic case $p_{\mathrm{e}}^{F} >> m_{\mathrm{e}}c$, we obtain

$$P = K_{rel}\rho^{\frac{4}{3}} \tag{1.10}$$

where $K_{rel} = \left(3^{1/3}\pi^{2/3}\hbar c\right)/\left(4m_{u}^{4/3}\mu_{\mathrm{e}}^{4/3}\right)$ is the constant. In general, the relation of the form

$$P = K\rho^{\Gamma} \tag{1.11}$$

is called a polytropic EoS. In the polytropic of form of EoS both K and Γ are constants. It is also important to note that the EoS (1.3, 1.4) and (1.7, 1.8) can be written in the approximate polytropic form as in (1.9) and (1.10) [5].

1.2 The Chandrasekhar equation of state at finite temperatures

In general, the expression for the electron number density follows from the Fermi-Dirac statistics and, when temperature is taken into account, it is determined by

$$n_{\mathrm{e}} = \frac{2}{\left(2\pi\hbar\right)^{3}}\int_{0}^{\infty}\frac{4\pi\, p^{2}dp}{\exp\left[\dfrac{E(p)-\mu_{\mathrm{e}}(p)}{k_{B}T}\right]+1}, \tag{1.12}$$

where $k_{B} = 1.38\times10^{-16}\, erg\cdot K^{-1}$ is the Boltzmann constant, μ_{e} is the electron chemical potential without the rest-mass, and $E(p) = \sqrt{c^{2}p^{2}+m_{\mathrm{e}}^{2}c^{4}} - m_{\mathrm{e}}c^{2}$ is the kinetic energy, with p and m_{e} being the electron momentum and rest-mass, respectively.

Formula (1.12) takes into account the effects of finite temperatures, and can be written in the following alternative form [27]

$$n_{\mathrm{e}} = \frac{2\pi\sqrt{2}}{\left(2\pi\hbar\right)^{3}}m^{3}c^{3}\beta^{\frac{3}{2}}\left[F_{1/2}(\eta,\beta)+\beta F_{3/2}(\eta,\beta)\right], \tag{1.13}$$

where

$$F_{k}(\eta,\beta) = \int_{0}^{\infty}\frac{t^{k}\sqrt{1+(\beta/2)t}}{1+e^{t-\eta}}dt \tag{1.14}$$

is the relativistic Fermi-Dirac integral, $\eta = \mu_e/(k_B T)$, $t = E/(k_B T)$ and $\beta = k_B T/m_e c^2$ are degeneracy parameters.

Consequently, the energy density of degenerate electron gas at finite temperatures is given by

$$\varepsilon_e = \frac{2^{3/2}}{3\pi^2\hbar^3} m_e^4 c^5 \beta^{5/2}\left[F_{3/2}(\eta,\beta) + \beta F_{5/2}(\eta,\beta)\right], \tag{1.15}$$

the electron pressure at finite temperatures

$$P_e = \frac{\sqrt{2}}{\pi^2\hbar^3} m_e^4 c^5 \beta^{5/2}\left[F_{3/2}(\eta,\beta) + \frac{\beta}{2} F_{5/2}(\eta,\beta)\right]. \tag{1.16}$$

1.3 The Salpeter equation of state

The extension of the Chandrasekhar approximation has been developed in the so-called "lattice" model which introduces the concept of a Wigner-Seitz cell, as well as, takes into account the contribution of the electrostatic interactions to the pressure of the degenerate electron gas. The Wigner-Seitz cell contains a point-like nucleus of charge $+eZ$ with A nucleons located at the center and surrounded by a uniformly distributed cloud of Z fully-degenerate electrons [24, 26]. However, the electron distribution cannot be uniform. A further improvement to the lattice model was made by Salpeter [20, 21] who considered the corrections due to the following effects: the Coulomb interaction energy, the non-uniform distribution of electrons inside a Wigner-Seitz cell (Thomas-Fermi correction), exchange energy, correlation energy. But, only main interactions as the Coulomb interaction, Thomas-Fermi correction are considered here. According to the general approach of Migdal et al. [24, 28], it has been shown that these effects are negligible in the relativistic regime [23]. There are not electrostatic interactions between the different Wigner-Seitz cells by the global neutrality of each cell. The condition of the global charge neutrality is

$$Z = V_{WS} n_e = \frac{n_e}{n_{WS}}, \tag{1.17}$$

where $V_{WS} = 4\pi R_{WS}^3/3$ is the Wigner-Seitz cell volume of radius R_{WS} and n_{WS} is the Wigner-Seitz cell density.

The total energy of the Wigner-Seitz cell will be written

$$E_{Sal} = E_{Ch} + E_C + E_{TF}^{Sal}, \tag{1.18}$$

where $E_{Ch} = \varepsilon_{Ch} V_{WS}$, ε_{Ch} is the energy density of the Chandrasekhar approximation and the total Coulomb energy E_C is the sum of the electron-nucleus E_{e-n} and the electron-electron E_{e-e} Coulomb energies

$$E_C = E_{e-n} + E_{e-e} = -\frac{9}{10}\frac{Z^2 e^2}{R_{WS}}, \tag{1.19}$$

where

$$E_{e-n} = -\int_0^{R_{WS}} \left(\frac{Ze}{r}\right) e\, n_e 4\pi r^2 dr = -\frac{3}{2}\frac{Z^2 e^2}{R_{WS}}, \quad E_{e-e} = \frac{3}{5}\frac{Z^2 e^2}{R_{WS}}, \tag{1.20}$$

and the Thomas-Fermi correction E_{TF}^{Sal}

$$E_{TF}^{Sal} = -\frac{162}{175}\left(\frac{4}{9\pi}\right)^{2/3} \alpha^2 Z^{7/3} \mu_e . \tag{1.21}$$

The self-consistent pressure of the Wigner-Seitz cell is then given by

$$P_{Sal} = P_{Ch} + \frac{1}{3}\frac{E_C}{V_{WS}} + \frac{1}{3}\left(\frac{p_e^F}{\mu_e}\right)^2 \frac{E_{TF}^{Sal}}{V_{WS}}, \tag{1.22}$$

where $\mu_e = (\varepsilon_e + P_e)/n_e = \sqrt{c^2 (p_e^F)^2 + m_e^2 c^4}$ is the electron free-chemical potential.

Here, for the sake of simplicity, we will define the energy density exactly as in the case of Chandrasekhar [7]. However, the electron-electron and electron-nuclei Coulomb interactions and the Thomas-Fermi corrections, which consider deviations of the electron charge distribution from uniformity, have been accounted when constructing the expression for the pressure of the degenerate WD matter [20, 21],

$$\varepsilon_{Sal} = \varepsilon_{Ch}, \tag{1.23}$$

$$P_{Sal} = P_{Ch} + P_C + P_{TF}, \tag{1.24}$$

where $P_C + P_{TF}$ are the contributions to the pressure due to the Coulomb interactions and the Thomas-Fermi corrections. This sum is given by

$$P_C + P_{TF} = -m_e c^2 \left(\frac{m_e c}{\hbar}\right)^3 \left[\frac{\alpha Z^{2/3}}{10\pi^2}\left(\frac{4}{9\pi}\right)^{1/3} y_e{}^4 + \frac{162}{175}\frac{(\alpha Z^{2/3})^2}{9\pi^2}\left(\frac{4}{9\pi}\right)^{2/3} \frac{y_e^5}{\sqrt{1+y_e^2}}\right], \tag{1.25}$$

where $\alpha = 1/137.036$ is the fine structure constant, m_e is the electron mass, c is the speed of light, $\hbar$ is the reduced Planck constant, Z is the number of protons, y_e is the dimensionless Fermi momentum of electrons [29].

1.4 The Feynman-Metropolis-Teller equation of state

Feynman, Metropolis, and Teller have demonstrated in their work [22-24] how to derive the EoS of matter at high pressures by considering a Thomas-Fermi model confined in a Wigner-Seitz cell of radius R_{WS}.

The condition of equilibrium of the degenerate nonrelativistic electrons in an atom is expressed by

$$E_{\mathrm{e}}^{F} = \frac{\left(p_{\mathrm{e}}^{F}\right)^{2}}{2m_{\mathrm{e}}} - eV, \tag{1.26}$$

where E_{e}^{F} is constant Fermi energy of electrons, p_{e}^{F} is the electron Fermi momentum, m_{e} is the electron mass, e is the elementary charge which is the magnitude of the electric charge carried by a single electron, V is the Coulomb potential.

The electrostatic potential (for $r>0$) can be found solving the differential Poisson equation

$$\nabla^{2}V = 4\pi e n_{\mathrm{e}}, \tag{1.27}$$

where $\vec{\nabla}$ is the nabla operator and we know from the Eq. (1.2) that the electron number density n_{e} is related to the Fermi momentum p_{e}^{F} by

$$n_{\mathrm{e}} = \frac{\left(p_{\mathrm{e}}^{F}\right)^{3}}{3\pi^{2}\hbar^{3}}. \tag{1.28}$$

It is very convenient to use dimensionless units in the numerical consideration of differential equations. Defining a function $\phi(\eta)$ by the expression

$$eV + E_{e}^{F} = e^{2}Z\frac{\phi(\eta)}{r}, \tag{1.29}$$

and introducing the new dimensionless radial coordinate η as

$$r = b\eta\ , \tag{1.30}$$

where $b = \left(9\pi^{2}/128Z\right)^{1/3} r_{Bohr}$ and $r_{Bohr} = \hbar^{2}/\left(m_{\mathrm{e}}e^{2}\right)$ is the Bohr radius.

The expression for the electron number density (1.28) takes the following form

$$n_{\mathrm{e}} = \frac{1}{3\pi^{2}\hbar^{3}}\left[2m_{\mathrm{e}}\left(E_{\mathrm{e}}^{F} + eV\right)\right]^{3/2} = \frac{Z}{4\pi b^{3}}\left[\frac{\phi(\eta)}{\eta}\right]^{3/2}, \tag{1.31}$$

when one takes into account the expressions (1.26), (1.29) and (1.30). After some simple transformations Eq. (1.27) can be written in the form

$$\frac{d^2\phi(\eta)}{d\eta^2} = \frac{\phi(\eta)^{3/2}}{\eta^{1/2}}, \tag{1.32}$$

which is the classic Thomas-Fermi equation [30, 31]. A first boundary condition for the equation (1.32) follows from the pointlike structure of the nucleus

$$\phi(0) = 1. \tag{1.33}$$

A second boundary condition comes from the global neutrality of the Wigner-Seitz cell

$$\left.\frac{d\phi(\eta_0)}{d\eta}\right|_{\eta=\eta_0} = \frac{\phi(\eta_0)}{\eta_0}, \tag{1.34}$$

where $\eta_0 = R_{WS}/b$ defines the radius R_{WS} of the Wigner-Seitz cell. As you can see, Eq. (1.32) is nonlinear second order differential equation and it has to be solved numerically with the given boundary conditions.

If one considers the relativistic case, the relativistic equilibrium condition of compressed atoms for the degenerate case is expressed by

$$E_{\mathrm{e}}^F = \sqrt{\left(p_{\mathrm{e}}^F c\right)^2 + m_{\mathrm{e}}^2 c^4} - m_{\mathrm{e}} c^2 - eV(r), \tag{1.35}$$

which generalizes the Eq. (1.26). Traditionally the radius of an extended nucleus is given by the phenomenological relation $R_C = r_0 A^{1/3}$, where A is the number of nucleons and $r_0 = 1.2 \times 10^{-13}$ cm. It was assumed a constant distribution of protons confined in a radius R_C defined by

$$R_C = \Delta \frac{\hbar}{m_\pi c} Z^{1/3}, \tag{1.36}$$

where Δ is a parameter such that $\Delta \approx 1$ $(\Delta < 1)$ corresponds to nuclear (supranuclear) densities when applied to ordinary nuclei and m_π is the pion mass.

The proton density can be written as

$$n_p(r) = \frac{N_p}{\frac{4}{3}\pi R_C^3}\theta(r - R_C) = \frac{3}{4\pi}\frac{m_\pi^3 c^3}{\hbar^3}\frac{1}{\Delta^3}\theta(r - R_C), \tag{1.37}$$

where $\theta(r - R_C)$ is the Heaviside function.

The electron density is given by

$$n_{\mathrm{e}}(r)=\frac{\left(p_{\mathrm{e}}^{F}\right)^{3}}{3\pi^{2}\hbar^{3}}=\frac{1}{3\pi^{2}\hbar^{3}c^{3}}[e^{2}V^{2}(r)+2m_{\mathrm{e}}c^{2}eV(r)]^{3/2}, \tag{1.38}$$

where V is the Coulomb potential. The Coulomb potential satisfies the Poisson equation

$$\nabla^{2}V=4\pi e\left(n_{p}-n_{\mathrm{e}}\right), \tag{1.39}$$

By substituting the proton number density (1.37) and the electron number density (1.38) into the Poisson equation (1.39), moreover, by introducing the new dimensionless quantities $x=r/\lambda_{\pi}$, $x_{\mathrm{C}}=R_{C}/\lambda_{\pi}$, where $\lambda_{\pi}=\hbar/(m_{\pi}c)$ and the function, $\chi=\alpha Z\phi$, one can obtain the relativistic dimensionless Thomas-Fermi equation

$$\frac{1}{3x}\frac{d^{2}\chi(x)}{dx^{2}}=-\frac{\alpha}{\Delta^{3}}\theta(x-x_{C})+\frac{4\alpha}{9\pi}\left[\frac{\chi^{2}(x)}{x^{2}}+\frac{2m_{\mathrm{e}}}{m_{\pi}}\frac{\chi(x)}{x}\right]^{\frac{3}{2}}, \tag{1.40}$$

where $\alpha=e^{2}/(\hbar c)$is the fine-structure constant in CGS units. The relativistic dimensionless Thomas-Fermi equation can be integrated by the boundary conditions

$$\chi(0)=0\,,\quad \left.\frac{d\chi(x)}{dx}\right|_{x=0}>0\,,\quad \left.\frac{d\chi(x)}{dx}\right|_{x=x_{WS}}=\frac{\chi(x_{WS})}{x_{WS}}, \tag{1.41}$$

where $x_{WS}=R_{WS}/\lambda_{\pi}$ is the dimensionless Wigner-Seitz cell radius.

The total energy of the Wigner-Seitz cell can be written as the sum of the nucleus, kinetic and Coulomb energy of the cell

$$E_{WS}=E_{n}+E_{k}+E_{C}, \tag{1.42}$$

and the energies are given by

$$E_{n}=M_{n}(A,Z)c^{2}, \tag{1.43}$$

$$E_{k}=\int_{0}^{R_{WS}}4\pi r^{2}\left(\varepsilon_{\mathrm{e}}-m_{\mathrm{e}}n_{\mathrm{e}}\right)dr, \tag{1.44}$$

$$E_{C}=\frac{1}{2}\int_{R_{C}}^{R_{WS}}4\pi r^{2}e\left[\left(n_{p}(r)-n_{\mathrm{e}}(r)\right)\right]V(r)dr\,. \tag{1.45}$$

where $M_{n}$is the nucleus mass, ε_{e} is the electron energy density which is given by the Eq. (1.5)

The total pressure of the Wigner-Seitz cell is

$$P_{FMT}^{rel} = \frac{1}{3}\frac{2}{(2\pi\hbar)^3}\int_0^{p_e^{F,WS}} \frac{c^2 p^2}{\sqrt{c^2 p^2 + m_e^2 c^4}} 4\pi p^2 dp = \\ = \frac{m_e^4 c^5}{8\pi^2\hbar^3}\left[y_{e,WS}\sqrt{1+y_{e,WS}^2}\left(2y_{e,WS}^2/3-1\right)+\operatorname{arsinh}\left(y_{e,WS}\right)\right], \tag{1.46}$$

where $y_{e,WS}$ is the dimensionless Fermi momentum of electrons at the border of the Wigner-Seitz cell.

The total pressure at the border of the Wigner-Seitz cell is determined by the pressure of the relativistic degenerate electron gas as in the case of the Chandrasekhar EoS. Undoubtedly, the total energy density ε_{WS} or the mass density ρ_{WS} can be obtained from the Eq. 1.42. Overall, the functional dependence of the total pressure on the total energy density (or the total mass density) defines the FMT EoS.

1.4 The Feynman-Metropolis-Teller equation of state at finite temperatures

The work of Feynman-Metropolis-Teller for compressed atoms has been recently generalized to relativistic regimes in [23]. Further, this treatment was extended to the case of finite temperatures and constructed the corresponding EoS of the system in [24, 25]. It is considered the equations of equilibrium of a relativistic gas of electrons at a temperature $T \neq 0$ surrounding a finite-sized and positively charged nucleus of mass and atomic numbers A and Z, respectively. The electron cloud is confined within a radius R_{WS} of a globally neutral Wigner-Seitz cell and the system is isothermal. For the further details see the Ref. [24, 25].

In the work de Carvalho et al. [25] they have considered temperatures that satisfy $T << m_e c^2/k_B \approx 6\times10^9$ K, so they did not take into account the presence of antiparticles. In this case, the Thomas-Fermi equilibrium condition for the relativistic electron gas is defined as

$$\tilde{\mu}_e(r) - eV(r) = k_B T\eta(r) - eV(r) = \text{const}, \tag{1.47}$$

where $V(r)$ is the Coulomb potential.

The total energy of each Wigner-Seitz cell for the case of finite temperatures is

$$E_{WS} = E_n + E_k + E_C, \tag{1.48}$$

where E_n is the nucleus energy, E_k is the kinetic and E_C is the Coulomb energy. They are defined as

$$E_n = M_n(A,Z)c^2 + U_{ther}, \tag{1.49}$$

$$E_k = \int_0^{R_{WS}} 4\pi r^2(\varepsilon_e - m_e n_e)dr, \tag{1.50}$$

$$E_C = \frac{1}{2}\int_{R_C}^{R_{WS}} 4\pi r^2 e\left[\left(n_p(r) - n_e(r)\right)\right]V(r)dr \tag{1.51}$$

where $U_{ther} = 3/2\,k_B T$ is the thermal energy of nuclei, $V(r)$ is the Coulomb potential, the number density of electrons n_e is given by the Eq. (1.13), the number density of protons is given by the Eq. (1.37) and the electron energy density ε_e is given by

$$\varepsilon_e = m_e c^2 n_e + \frac{2^{1/2}}{\pi^2\hbar^3} m_e^4 c^5 \beta^{5/2}\left[F_{3/2}(\eta,\beta) + \beta F_{5/2}(\eta,\beta)\right], \tag{1.52}$$

The total density and pressure at finite temperatures are then given by

$$\rho = E_{WS}/(c^2 V_{WS}), \qquad P = P_n + P_e\ , \tag{1.53}$$

where

$$P_n = (2U_{ther})/3V_{WS} = (k_B T)/V_{WS}\ , \tag{1.54}$$

$$P_e = \frac{2^{3/2}}{3\pi^2\hbar^3} m_e^4 c^5 \beta^{5/2}\left[F_{3/2}(\eta,\beta) + \beta F_{5/2}(\eta,\beta)\right], \tag{1.55}$$

with η_{WS} being the value of η at the boundary of the Wigner-Seitz cell.

1.5 Summary

In the section 1, we analyzed the equations of state which are used to describe the interior matter of WDs, in particular, the Chandrasekhar EoS at zero temperature and its approximate polytropic forms at non-relativistic and relativistic cases, the Salpeter EoS and the Feynmann-Metropoilis-Teller EoS at zero temperature and finite temperatures. The EoS completes the equations of stellar structure and allows to define the main parameters of WDs. These EoS are used in sections 3, 4 and 5.

2 EXTERIOR METRICS OF COMPACT OBJECTS AND THEIR COMPARISON

In section 2 the exterior metrics of compact objects and their comparisons are considered, precisely, the comparison the Hartle-Thorne metric, which is an approximate solution of the Einstein equations, with an approximate Kerr metric, between the Fock and Kerr metrics. Furthermore, the exterior Sedrakyan-Chubaryan solution is derived explicitly and established its relationship with the Hartle-Thorne solution.

In subsection 2.1 the procedure of comparison the exterior solutions of the Einstein gravitational field equations such as the approximate Hartle-Thorne solution and the exact Kerr solution is considered. To this end, the Kerr metric in the Boyer-Lindquist coordinates was expanded in the Taylor series accurate within the quadratic terms in the rotation parameter, and thereby was presented in the approximate form. Furthermore, the coordinate transformations with a given accuracy, which link the approximate Kerr and Hartle-Thorne solutions were found using the methods of the perturbation theory. Despite the fact that the quadrupole moment implicitly enters into the Kerr metric, it was shown that one can express it via the angular momentum and the total mass of the source of the gravitational field. Thus, it was demonstrated that the physical quantities contained in the Hartle-Thorne solution such as the total mass, angular momentum and quadrupole moment directly connected to the total mass and the rotation parameter of the Kerr solution. The coordinate transformations obtained here can be used to write the Hartle-Thorne metric in the Boyer-Lindquist coordinates, and in turn it is equivalent to the approximate Kerr solution with the quadrupole parameter. From the practical standpoint, the approximate Kerr solution with the quadrupole parameter has wider application for the description of the geometry around real objects, because in the absence of the quadrupole momentum the solution reduces to the initial approximate Kerr solution within the accuracy up to the second order terms in the rotation parameter [32].

In subsection 2.2 the procedure of comparison between the Fock approximate solution and the Kerr exact solution is considered. Since the Kerr and Fock metrics are widely known in the scientific communities, we will use the final form of the metrics without going into their detailed derivation. The methods of perturbation theory are applied within the approximation $\sim 1/c^2$. Approximate coordinate transformations, allowing the comparison between the Fock and Kerr metrics, have been obtained analytically. The proposed method is applicable to other external approximate solutions of Einstein's equations [33, 34].

In subsection 2.3 stationary axially symmetric solutions of the Einstein vacuum field equations are studied. They can be used to describe the gravitational field of astrophysical compact objects in the limiting case of slow rotation and slight deformation. The exterior Sedrakyan-Chubaryan approximate solution is derived explicitly, and expressed it in an analytical form, which makes it practical in the context of astrophysical applications. In the limiting case of vanishing angular momentum, the solution reduces to the well-known Schwarzschild solution in

vacuum. It is demonstrated that the new solution is equivalent to the exterior Hartle-Thorne solution [35-37].

2.1 Correspondence of the Kerr and Hartle-Thorne metrics

The Kerr metric is an exact vacuum solution of the Einstein gravitational field equations in GR, describing the geometry around rotating uncharged bodies, thereby generalizes the Schwarzschild metric taking into account the rotation parameter [38]. The Kerr solution is the only known exact solution that can serve to describe a stationary axisymmetric asymptotically flat field outside a massive rotating object with two basic parameters, such as mass and the Kerr parameter (rotation parameter). According to scientific consensus, the Kerr solution is, apparently, the only possible exterior solution for rotating BHs [39]. It should be noted that there is also the Kerr-Newman metric for rotating but charged BHs, which, in the absence of a charge, becomes the Kerr metric [40, 41]. It follows from the Kerr metric that some part of black hole energy can theoretically be extracted in the form of rotational energy [42]. This conclusion is essential for the models of quasars and active nuclei of galaxies, in which BHs are considered as the central source of all types of radiation [42]. However, until now it has not been possible to find the interior Kerr solution even in an approximate form [39]. This fact shows that the Kerr metric can be used only for a limited class of astrophysical objects, and it is not suitable for describing the exterior field of rotating real objects [39].

The Hartle-Thorne solution, often used in the literature to describe geometry around slowly rotating and slightly deformed objects in strong gravitational fields, is characterized by three multipole moments, such as total mass, angular momentum, and quadrupole moment [43, 44]. These parameters, in turn, allow us to describe real astrophysical objects from planet-like celestial bodies up to NSs [45, 46]. One of the most important characteristics of this family of solutions is that the corresponding equations of state were constructed using realistic models of the internal structure of relativistic stars. Semi-analytical and numerical generalizations of the Hartle-Thorne metric with more complex equations of state were proposed by various authors [47]. The most complete review of these solutions is given in [48]. In all these cases, however, it is assumed that the multipole (quadrupole and octupole) moments are relatively small and the rotation is slow [32].

2.1.1 The exterior Hartle-Thorne metric

Taking into account second-order corrections in angular velocity, the structure of compact objects can be approximately described by means of total mass, angular momentum, and quadrupole moment. An important consequence of this approximation is that the equations of equilibrium reduce to a system of ordinary differential equations. Hartle and Thorne [43, 44] have investigated the gravitational field of rotating stars in the approximation of slow rotation. This formalism can be applied to most of compact objects, including pulsars with millisecond rotation periods.

An additional property of this formalism is that it can be used to match an interior metric with an approximate exterior metric. In this regard, it is worth noting that the problem of junction of interior and exterior solutions implies many mathematical and physical difficulties [48], including the calculation of metric functions and coordinates on the junction surface, as well as the physical behavior of such internal parameters as pressure and density distribution of substance.

The Hartle-Thorne metric in coordinates (t, R, Θ, φ), describing the exterior field of a slowly rotating and slightly deformed object has the following form:

$$\begin{aligned} ds^2 = &\left(1-\frac{2M}{R}\right)\left[1+2k_1 P_2(\cos\Theta)+2\left(1-\frac{2M}{R}\right)^{-1}\frac{J^2}{R^4}\left(2\cos^2\Theta-1\right)\right]dt^2 - \\ &-\left(1-\frac{2M}{R}\right)^{-1}\left[1-2k_2 P_2(\cos\Theta)-2\left(1-\frac{2M}{R}\right)^{-1}\frac{J^2}{R^4}\right]dR^2 - \\ &-R^2\left[1-2k_3 P_2(\cos\Theta)\right]\left(d\Theta^2+\sin^2\Theta d\varphi^2\right)+\frac{4J}{R}\sin^2\Theta dt d\varphi \end{aligned} \tag{2.1}$$

where

$$k_1 = \frac{J^2}{MR^3}\left(1+\frac{M}{R}\right)+\frac{5}{8}\frac{Q-J^2/M}{M^3}Q_2^2\left(\frac{R}{M}-1\right),$$

$$k_2 = k_1 - \frac{6J^2}{R^4},$$

$$k_3 = k_1 + \frac{J^2}{R^4}+\frac{5}{4}\frac{Q-J^2/M}{M^2R}\left(1-\frac{2M}{R}\right)^{-1/2}Q_2^1\left(\frac{R}{M}-1\right),$$

are functions of the coordinate R. In turn, the functions

$$Q_2^1(x) = \left(x^2-1\right)^{1/2}\left[\frac{3x}{2}\ln\frac{x+1}{x-1}-\frac{3x^2-2}{x^2-1}\right],$$

$$Q_2^2(x) = \left(x^2-1\right)\left[\frac{3}{2}\ln\frac{x+1}{x-1}-\frac{3x^2-5x}{\left(x^2-1\right)^2}\right],$$

are the associated Legendre polynomials of the second kind, whereas $P_2(\cos\Theta)=(1/2)(3\cos^2\Theta-1)$ is the ordinary Legendre polynomial of the first kind and $x = R/M - 1$, the constants M, J, and Q, and are the total mass, angular momentum and quadrupole moment of the rotating object, respectively. This kind of metric corrects some typos in the original work of Hartle and Thorne [43, 44].

Unlike other solutions of the Einstein equations, the Hartle-Thorne solution has an internal counterpart, which makes it more practical with respect to the exact solutions. All internal functions are interrelated with the external ones. Thus, the total mass, angular momentum and quadrupole moment of a rotating star are determined through the constants obtained by numerical integration of both interior and exterior solutions, by applying the matching conditions on the surface of the star [32].

In general, this metric represents an approximate vacuum solution with accuracy up to the second order in angular momentum J and up to the first order in the quadrupole moment Q. In the case of ordinary stars, such as the Sun, in view of the gravitational constant G and the speed of light c, the metric (2.1) can be simplified because of the smallness of the parameters:

$$\frac{GM_{Sun}}{c^2R_{Sun}} \approx 2\times10^{-6}, \qquad \frac{GJ_{Sun}}{c^3R_{Sun}^2} \approx 10^{-12}, \qquad \frac{GQ_{Sun}}{c^2R_{Sun}^3} \approx 10^{-10}. \tag{2.2}$$

For this particular case, we can calculate the corresponding approximate metric from (2.1) in the limit of $c\to\infty$. These calculations are simple and lead the metric to the following form

$$\begin{aligned} ds^2 \approx &\left[1-\frac{2GM}{c^2R}+\frac{2GQ}{c^2R^3}P_2(\cos\Theta)+\frac{2G^2MQ}{c^4R^4}P_2(\cos\Theta)\right]c^2dt^2+\frac{4GJ}{c^2R}\sin^2\Theta dtd\varphi- \\ &-\left[1+\frac{2GM}{c^2R}-\frac{2GQ}{c^2R^3}P_2(\cos\Theta)\right]dR^2-\left[1-\frac{2GQ}{c^2R^3}P_2(\cos\Theta)\right]R^2\left(d\Theta^2+\sin^2\Theta d\varphi^2\right) \end{aligned} \tag{2.3}$$

It describes the gravitational field for a wide range of celestial bodies, and only in the case of very dense $\left(GM\sim c^2R\right)$ or rapidly rotating $GJ\sim c^3R^2$ objects, it shows large discrepancies.

In the case where the source does not rotate and its angular velocity is zero $\Omega=0,$ then, respectively $J=0,\quad Q=0$, and the Hartle-Thorne solution reduces to an exact exterior Schwarzschild solution in standard coordinates. In the absence of a quadrupole moment, the Hartle-Thorne solution reduces to the Lense-Thirring solution, while preserving the linear terms with respect to the angular momentum. It can also be shown that in the absence of angular momentum, the Hartle-Thorne metric can be compared with the approximate Erez-Rosen solution using the appropriate coordinate transformations. For this, the Erez-Rosen metric is expanded in a series with an accuracy up to linear terms in the quadrupole parameter [49]. However, these calculations are beyond the scope of this work and are not considered here. On the other hand, it would be logical to assume that the Hartle-Thorne metric can be compared with the approximate Kerr metric in the absence of a quadrupole moment, preserving the angular momentum. In this subsection we will find out why this assumption has not been shown by anyone yet. In this connection, we follow the work of Hartle and Thorne and show that the approximate Kerr metric, with an accuracy up to quadratic terms with respect to the rotation parameter, is compared with the Hartle-Thorne metric, only in the unique case when there is a genuine quadrupole moment of the field source, defined through its angular momentum.

It should be noted that, unlike the exact axially symmetric, stationary and asymptotically flat solutions of the Einstein equations, the exterior Hartle-Thorne metric has its own internal counterpart, i.e., interior metric. It is this difference in the

Hartle-Thorne metric that makes it popular in the scientific field and gives it a wider applied character [32].

2.1.2 The Kerr metric

To describe the gravitational field of a rotating body outside the source, it is physically reasonable to assume that the exterior vacuum metric must be asymptotically flat. In this case, the first obvious candidate is the Kerr solution in the appropriate limit. The Kerr metric [38] in the Boyer-Lindquist coordinates (t, r, θ, φ) [50] can be written in the form:

$$ds^2 = \left(1-\frac{2mr}{r^2+a^2\cos^2\theta}\right)dt^2 - \frac{r^2+a^2\cos^2\theta}{r^2-2mr+a^2}\,dr^2 - \left(r^2+a^2\cos^2\theta\right)d\theta^2 - \\ -\left(r^2+a^2+\frac{2mra^2\sin^2\theta}{r^2+a^2\cos^2\theta}\right)\sin^2\theta\, d\varphi^2 + \frac{4mra\sin^2\theta}{r^2+a^2\cos^2\theta}\,dt\,d\varphi, \qquad (2.4)$$

where m is the total mass and a is the rotation parameter of the field source.

We recall that in the absence of a rotation parameter $a=0$, the Kerr metric reduces to the exact exterior Schwarzschild metric in standard coordinates. Then it will be clear that the total masses in the Kerr and Hartle-Thorne metrics are identical, i.e. $m=M$. If we expand the Kerr metric with an accuracy up to linear terms with respect to the rotation parameter, then we will undoubtedly obtain the Lense-Thirring metric, which implies that the rotation parameter of the body is directly related to the angular momentum $a=J/m=J/M$ of the body [49].

To compare the Kerr metric and the Hartle-Thorne metric, the Kerr metric must be expanded in a Taylor series with respect to the quadratic terms of the rotation parameter, so that both metrics have the same approximations (accuracy). For the convenience of calculations, we introduce the expansion parameter ε, which is directly proportional to the angular momentum (angular velocity) of the body. Thus, by replacing $a\to a\varepsilon$ and expanding ε it with respect to terms of order $\sim\varepsilon^2$, we obtain:

$$ds^2 = \left(1-\frac{2m}{r}+\frac{2ma^2\varepsilon^2\cos^2\theta}{r^3}\right)dt^2 - \left(\frac{r}{r-2m}-\frac{a^2\varepsilon^2\left(r+2m\cos^2\theta-r\cos^2\theta\right)}{r(r-2m)^2}\right)dr^2 - \\ -\left(1+\frac{a^2\varepsilon^2\cos^2\theta}{r^2}\right)r^2d\theta^2 - \left(1+\frac{a^2\varepsilon^2}{r^2}\left(1+\frac{2m\sin^2\theta}{r}\right)\right)r^2\sin^2\theta d\varphi^2 + \frac{4ma\varepsilon\sin^2\theta}{r}d\varphi dt. \qquad (2.5)$$

In order to establish the relationship between two axially symmetric metrics, we represent the coordinates in the Kerr metric as a function of the coordinates of the Hartle-Thorne metric, that is, in the form $r=r(R,\Theta)$, $\theta=\theta(R,\Theta)$. Then, using the perturbation theory, coordinate transformations should be sought in the following way: $r=R+a^2\varepsilon^2 f_1(R,\Theta)$, $\theta=\Theta+a^2\varepsilon^2 f_2(R,\Theta)$, where $f_1(R,\Theta)$ and $f_2(R,\Theta)$ are the unknown functions. The differentials of the coordinates, respectively, will have the following form:

$$dr = \frac{\partial r}{\partial R}dR + \frac{\partial r}{\partial \Theta}d\Theta = \left(1 + a^2\varepsilon^2 \frac{\partial f_1(R,\Theta)}{\partial R}\right)dR + a^2\varepsilon^2 \frac{\partial f_1(R,\Theta)}{\partial \Theta}d\Theta,$$
$$d\theta = \frac{\partial \theta}{\partial R}dR + \frac{\partial \theta}{\partial \Theta}d\Theta = a^2\varepsilon^2 \frac{\partial f_2(R,\Theta)}{\partial R}dR + \left(1 + a^2\varepsilon^2 \frac{\partial f_2(R,\Theta)}{\partial \Theta}\right)d\Theta. \quad (2.6)$$

After this, the Kerr solution will be written in coordinates R and Θ

$$\begin{aligned} ds^2 = &\left(1 - \frac{2M}{R} + \frac{2J^2\varepsilon^2}{MR^3}\left\{\cos^2\Theta + Rf_1(R,\Theta)\right\}\right)dt^2 - \\ &-\left(\frac{R}{R-2M} - \frac{2J^2\varepsilon^2}{M^2(R-2M)^2}\left\{\frac{1}{2}\sin^2\Theta + \frac{M}{R}\cos^2\Theta + Mf_1(R,\Theta) - R(R-2M)\frac{\partial f_1(R,\theta)}{\partial R}\right\}\right)dR^2 - \\ &-\left(1 + \frac{2J^2\varepsilon^2}{M^2R^2}\left\{\frac{1}{2}\cos^2\Theta + Rf_1(R,\Theta) + R^2\frac{\partial f_2(R,\Theta)}{\partial \Theta}\right\}\right)R^2d\Theta^2 - \\ &-\left(1 + \frac{2J^2\varepsilon^2}{M^2R^2}\left\{\frac{1}{2} + \frac{M}{R}\sin^2\Theta + Rf_1(R,\Theta) + \frac{\cos\Theta}{\sin\Theta}R^2 f_2(R,\Theta)\right\}\right)R^2\sin^2\Theta d\varphi^2 - \\ &-\frac{2J^2\varepsilon^2R}{M^2(R-2M)}\left(\frac{\partial f_1(R,\Theta)}{\partial \Theta} + R(R-2M)\frac{\partial f_2(R,\Theta)}{\partial R}\right)dRd\Theta + \frac{4J\varepsilon\sin^2\Theta}{R}d\varphi dt \end{aligned} \quad (2.7)$$

where we took advantage of the replacement $a = J/M$.

Now the Kerr metric is written in the same coordinates as the Hartle-Thorne metric. Taking into account the fact that the metrics are axially symmetric, we are only interested in the g_{tt} and $g_{\varphi\varphi}$ components of the metric tensor, since these components remain invariant quantities because of the above-mentioned axial symmetry. Consequently, equating the components of the metric tensor with their analogs in the Hartle-Thorne metric, with a preliminary replacement $J \to J\varepsilon$, $Q \to Q\varepsilon^2$, we find the required functions $f_1(R,\Theta)$ and $f_2(R,\Theta)$:

$$\begin{aligned} f_1(R,\Theta) = &\frac{5}{8}\frac{Q - J^2/M}{M^3}\left(\frac{MR^2}{J^2}\right)\left(1 - \frac{2M}{R}\right)Q_2^2(x)P_2(\cos\Theta) - \\ &-\frac{1}{2R}\left[\left(1 + \frac{2M}{R}\right)\left(1 - \frac{M}{R}\right) - \cos^2\Theta\left(1 - \frac{2M}{R}\right)\left(1 + \frac{3M}{R}\right)\right] \end{aligned}$$
$$\begin{aligned} f_2(R,\Theta) = &\frac{5}{8}\frac{Q - J^2/M}{M^3}\left(\frac{MR}{J^2}\right)\left\{\frac{2M^2}{R^2}\left(1 - \frac{2M}{R}\right)^{-1/2}Q_2^1(x) - \left(1 - \frac{M}{R}\right)Q_2^2(x)\right\}P_2(\cos\Theta)\tan\Theta - \\ &-\frac{1}{2R^2}\left(1 + \frac{2M}{R}\right)\cos\Theta\sin\Theta, \end{aligned} \quad (2.8)$$

where, as before $x = R/M - 1$.

Now we consider the $g_{R\Theta}$ component of the metric tensor in the expression (2.7). Since there are no metric tensor $g_{R\Theta}$ components in the original Kerr and Hartle-Thorne metrics, we need to substitute the values of the functions $f_1(R,\Theta)$ and $f_2(R,\Theta)$ into it, and also find a condition that $g_{R\Theta}$ vanishes. As a result, it turns out that the only condition that satisfies this requirement is the expression of the quadrupole moment through the angular momentum, i.e. $Q = J^2/M$. The appearance of such a quadrupole moment is purely relativistic.

Soon after Hartle and Thorne [43, 44] obtained this algebraic expression, based on the work of Hernandez [51], the quantity $Q = Q_{Kerr} = J^2/M$ became known in the scientific literature as the "Kerr quadrupole moment", since it is exclusively determined by the ratio of the square of the angular momentum to the mass.

Taking into account the Kerr quadrupole moment, the coordinate transformation has the following form:

$$\begin{aligned} r &= R - \frac{a^2}{2R}\left[\left(1+\frac{2M}{R}\right)\left(1-\frac{M}{R}\right) - \cos^2\Theta\left(1-\frac{2M}{R}\right)\left(1+\frac{3M}{R}\right)\right], \\ \theta &= \Theta - \frac{a^2}{2R^2}\left(1+\frac{2M}{R}\right)\cos\Theta\sin\Theta \end{aligned} \tag{2.9}$$

These coordinate transformations translate the Kerr solution (2.5) into the Hartle-Thorne solution (2.1) with an accuracy up to a second order in angular momentum, with a replacement $m = M$, $a = J/M$, and a specific quadrupole parameter $Q = J^2/M$. Thus, we have shown that the approximate Kerr solution is equivalent to the exterior Hartle-Thorne solution with a definite value of the quadrupole parameter.

For the inverse transition from the Hartle-Thorne metric to the Kerr metric, the coordinate transformations (2.9) must be written in the form of $R(r,\theta)$ and $\Theta(r,\theta)$:

$$\begin{aligned} R &= r + \frac{a^2}{2r}\left[\left(1+\frac{2m}{r}\right)\left(1-\frac{m}{r}\right) - \cos^2\theta\left(1-\frac{2m}{r}\right)\left(1+\frac{3m}{r}\right)\right], \\ \Theta &= \theta + \frac{a^2}{2r^2}\left(1+\frac{2m}{r}\right)\cos\theta\sin\theta \end{aligned} \tag{2.10}$$

with the same approximation $\sim\varepsilon^2$. Here we also need to take into account the algebraic relations between the parameters of both metrics: $m = M$, $a = J/M$, and $Q = J^2/M$ [32].

We note that by introducing a new dimensionless quadrupole parameter $\delta = (1/M^3)(Q - J^2/M)$ into the original Hartle-Thorne metric, and using the coordinate transformations (2.10) in the approximation $\sim\varepsilon^2$, one can obtain an approximate Kerr metric with a quadrupole parameter. This metric is known in the literature as a "quasi-Kerr metric" [52, 53] and is widely used to describe processes around compact objects such as gravitational waves, quasi-periodic oscillations, etc. [54, 55]. It is

obvious that for $a = J/M$, $Q = J^2/M$ and the quasi-Kerr metric reduces to the usual approximate Kerr metric (5). This explains its wide application in various astrophysical calculations [56].

2.2 Correspondence of the Fock and the Kerr metrics

The Fock metric [57-59] is a post-Newtonian approximate solution of the Einstein equations, which is used to describe geometry around an astrophysical object with a weak gravitational field and slow rotation. This metric was obtained in different years by Chandrasekhar (1965) and Abdildin (1985) in a general integral form [57, 58]. Although it was in the work [57] that the Fock metric was first obtained for a slowly rotating spherically symmetric object (liquid and solid) [60]. It was demonstrated that the exact solution of the Einstein equations for a rotating body, the so-called Kerr metric [38], reduces in a nontrivial way to the Fock metric corresponding to coordinate transformations in the weak-field and small velocity approximation [39, 58, 60]. However, until now it has not been possible to find an interior Kerr solution, even in an approximate form [39]. This fact shows that the Kerr metric, characterized by two multipole moments, such as the total mass and rotation parameter, can be used only for a limited class of astrophysical objects such as, for example, BHs [39].

One of the most important conceptual problems of GR is the determination of the gravitational field inside compact objects. In fact, it is known that in the case of static spherically symmetric objects, the gravitational field is completely described by the interior and exterior solutions of Schwarzschild [61]. However, even with allowance for the rotation of the body (the original equations are much more complicated), only the exterior exact metric is known as the Kerr metric, [38]. Physicists have been searching for an interior solution to the Kerr metric for more than 50 years, but so far any reasonable physical solution has not been found yet. In this regard,we will focus only on Fock's exterior solution, since there is an interior analogue for it [39,62].

To compare the Fock metric with the Kerr metric, the one should first compute in the Fock metric the integrals for an axially symmetric deformed body, depending on the internal structure [60, 39, 62, 63]. As a result, the Fock metric is derived for a slowly rotating deformed body with three parameters: total mass, angular momentum, quadrupole moment [39, 62]. Then we consider the limiting case for a spherically symmetric mass distribution, where the quadrupole moment of the body disappears [39, 60]. The Kerr metric is then written in approximation $\sim 1/c^2$ in the Boyer-Lindquist coordinates and coordinate transformations between the two metrics are found. As a result, both exterior solutions written in the same coordinates are compared with each other by very simple algebraic expressions [33].

2.2.1 Fock's approach

To study the physical properties of solutions of the Einstein equations, Fock [63] proposed an alternative method in which the parameters entering the exterior metric are obtained using physical models for the internal structure of the body. This

approach takes into account the intrinsic properties of the gravitational source, and reduces the problem of finding an approximate interior solution to the calculation of some integrals that clearly depend on the physical characteristics of the object [59, 60, 64]. Consequently, the significance of external parameters becomes more realistic and it is possible to determine certain aspects of the internal structure of an object with the help of observations conducted in the outer region of the body. Thus, in this subsection we present the main results of this approach and study the possibility of comparing with the Kerr metric.

2.2.2 The interior solution

The Fock metric of the first approximation was obtained and investigated in a rather simple form [58-60]. Initially, the metric was written in the harmonic coordinate system as follows:

$$ds^2 = \left[c^2 - 2U + \frac{2U^2}{c^2} - \frac{2G}{c^2}\int \frac{\rho\left(\frac{3}{2}v^2 + \Pi - U\right) + 3p}{|\vec{r} - \vec{r}'|}(dx')^3 \right] dt^2 - \\ - \left(1 + \frac{2U}{c^2}\right)\left(dx_1^{\,2} + dx_2^{\,2} + dx_3^{\,2}\right) + \frac{8}{c^2}\left(U_1 dx_1 + U_2 dx_2 + U_3 dx_3\right)dt, \tag{2.11}$$

where c is the speed of light in vacuum, G is the gravitational constant, U is the Newtonian gravitational potential, ρ is the body mass density, v is the particle velocity inside the body, Π is the elastic energy per unit mass, p is the pressure, and $\vec{U}$ is the gravitational vector potential. Note that the values ρ, v, Π and U, characterizing the internal structure of the source, depend only on the "internal" coordinates x_i', which are determined only inside the body. To simplify the notation, we omit the arguments that determine the coordinates of this dependence. The corresponding energy-momentum tensor is given by

$$T^{00} = \frac{\rho}{c^2}\left[1 + \frac{1}{c^2}\left(\frac{v^2}{2} + \Pi - U\right)\right], \quad T^{0i} = \frac{\rho}{c^2}v^i, \quad T^{ij} = \frac{1}{c^2}\left(\rho v^i v^j + p\delta^{ij}\right), \tag{2.12}$$

where δ^{ij} is the Kronecker symbol and $i, j = 1, 2, 3$. The Newton potential satisfies the equation $\Delta U = -4\pi G\rho$. The solution of this equation, which satisfies the conditions at infinity, can be written in the form of a volume integral:

$$U = G\iiint \frac{\rho}{|\vec{r} - \vec{r}'|}dx_1'dx_2'dx_3'. \tag{2.13}$$

In addition, the gravitational vector potential must directly satisfy the equation $\Delta U_i = -4\pi G\rho v_i$, then the general asymptotical flat solution can be represented in the form

$$U_i = G\iiint \frac{\rho v_i}{|\vec{r}-\vec{r}'|}\,dx_1'dx_2'dx_3'. \qquad (2.14)$$

2.2.3 Fock's metric for a deformed body

Consider the case of deformed objects, such as, for example, a rotating ellipsoid. Obviously, if the shape of the body slightly deviates from the spherical symmetry, the body acquires additional multipole moments, in particular, the quadrupole moment [61]; moments of a higher order are insignificant, especially for a slowly rotating ellipsoid. We generalize the Fock metric so that the quadrupole moment can appear explicitly in the integration (2.11), as well as in the Newtonian potential. It should be noted that the definition of exterior and interior Newtonian potentials for a rotating ellipsoid is one of the classical problems of both theoretical and mathematical physics. Some examples for a homogeneous ellipsoid were considered in [61], but the most detailed information on this question was given in [65] and most recently in [66].

Thus, Fock's exterior solution describing the gravitational field of a slowly rotating and slightly deformed body in harmonic coordinates looks like this:

$$ds^2 = \left[c^2 - \frac{2GM}{r} - \frac{GD}{r^3}P_2(\cos\theta) + \frac{2}{c^2}\left(\frac{GM}{r}\right)^2 + \frac{2}{c^2}\frac{G^2MD}{r^4}P_2(\cos\theta) - \frac{G\mathsf{D}}{c^2r^3}P_2(\cos\theta)\right]dt^2 -$$

$$-\left[1+\frac{2GM}{c^2r}+\frac{GD}{c^2r^3}P_2(\cos\theta)\right]\left[dr^2 + r^2(d\theta^2+\sin^2\theta d\phi^2)\right] + \frac{4GS_0}{c^2r}\sin^2\theta d\phi dt\,, \qquad (2.15)$$

where M is the total mass of a body, D is the Newtonian quadrupole moment, D/c^2 is the relativistic correction to the Newtonian quadrupole moment D, that is, the quadrupole moment arising due to rotation, S_0 is the angular momentum of the body, $P_2(\cos\theta) = \frac{1}{2}\left(3\cos^2\theta - 1\right)$ is the Legendre polynomial, θ is the angle between the radial coordinate r and the z axis. This solution is axially symmetric with respect to the z axis, and the direction of S_0 coincides with z [33, 39, 62].

2.2.4 Fock's metric for a spherically symmetric body

In the limiting case with zero rotation $S_0 = 0$ and with the vanishing quadrupole moments $D = \mathsf{D} = 0$, the metric represents the approximate Schwarzschild solution in harmonic coordinates [63, 64]:

$$ds^2 = \left[c^2 - \frac{2GM}{r} + \frac{2}{c^2}\left(\frac{GM}{r}\right)^2\right]dt^2 - \left[1+\frac{2GM}{c^2r}\right]\left[dr^2 + r^2(d\theta^2+\sin^2\theta d\phi^2)\right], \qquad (2.16)$$

The investigation of the metric (2.15) shows that in the rough (zero) approximation for the case of slow rotation $S_0 \neq 0$, and with the conservation of

spherical symmetry, this metric reduces to the approximate Fock metric considered in [58, 60] with the total mass M, and

$$D = 0, \quad \mathsf{D} = -\frac{2\kappa S_0^2}{M}. \tag{2.17}$$

Here κ is the numerical factor characterizing the internal structure of the body, which is equal to [39, 58, 60]

$$\kappa = \begin{cases} \kappa_L = \dfrac{4}{7}, & \textit{for a liquid body}, \\ \kappa_S = \dfrac{15}{28}, & \textit{for a solid body}. \end{cases} \tag{2.18}$$

Then the Fock metric takes the following form:

$$ds^2 = \left[c^2 - \frac{2GM}{R} + \frac{2}{c^2}\left(\frac{GM}{R}\right)^2 + \frac{2\kappa G}{c^2 M}\frac{S_0^2}{R^3}P_2(\cos\Theta)\right]dt^2 -$$

$$-\left[1+\frac{2GM}{c^2 R}\right]\left[dR^2 + R^2(d\Theta^2 + \sin^2\Theta d\phi^2)\right] + \frac{4GS_0}{c^2 R}\sin^2\Theta d\phi dt. \tag{2.19}$$

This is the refined Fock metric for the spherically symmetric mass distribution, obtained for the first time by Abdildin [58, 60]. Note that r and θ were redefined by R and Θ in (2.19) in order to find relations of the metrics [33].

2.2.5 Relation between the Kerr and Fock metrics

The Kerr metric is given in the geometric unit system by (2.4). Rewriting the Kerr metric with G and c by making following substitutions $m = M$, $a = -S_0/(cM)$ and performing an expansion in a Taylor series with respect to $\sim 1/c^2$, we obtain:

$$ds^2 = \left[c^2 - \frac{2GM}{r} + \frac{2GS_0{}^2}{c^2 M r^3}\cos^2\theta\right]dt^2 - \left(1+\frac{2GM}{c^2 r} - \frac{S_0{}^2}{c^2 M^2 r^2}\sin^2\theta\right)dr^2 -$$

$$-r^2\left(1+\frac{S_0{}^2}{c^2 M^2 r^2}\cos^2\theta\right)d\theta^2 - r^2\left(1+\frac{S_0{}^2}{c^2 M^2 r^2}\right)\sin^2\theta\, d\varphi^2 + \frac{4GS_0}{c^2 r}\sin^2\theta\, d\varphi dt. \tag{2.20}$$

For purposes of comparison with the exterior Fock metric for a rotating spherically symmetric mass distribution, in addition, we introduce new coordinates $r = r(R,\Theta)$, $\theta = \theta(R,\Theta)$; accordingly, coordinate transformations are necessary to seek with the help of perturbation theory methods in the form:

$$r = R + \frac{1}{c^2} F_1(R,\Theta), \qquad \theta = \Theta + \frac{1}{c^2} F_2(R,\Theta) \tag{2.21}$$

Substituting (2.21) into (2.20) and expanding in a Taylor series with respect to $\sim 1/c^2$, we obtain:

$$ds^2 = \left[c^2 - \frac{2GM}{R} + \frac{2GS_0^2\cos^2\Theta}{c^2MR^3} + \frac{2GM}{c^2R^2}F_1(R,\Theta)\right]dt^2 - \left[1 + \frac{2GM}{c^2R} - \frac{S_0^2\sin^2\Theta}{c^2M^2R^2} + \frac{2}{c^2}\frac{dF_1(\mathrm{R},\Theta)}{dR}\right]\times$$

$$\times dR^2 - \frac{2}{c^2}\left[\frac{dF_1(R,\Theta)}{d\Theta} + R^2\frac{dF_2(R,\Theta)}{dR}\right]dRd\Theta - \left[1 + \frac{S_0^2\cos^2\Theta}{c^2M^2R^2} + \frac{2}{c^2}\frac{F_1(R,\Theta)}{R} + \frac{2}{c^2}\frac{dF_2(R,\Theta)}{d\Theta}\right]R^2\times$$

$$\times d\Theta^2 - \left[1 + \frac{S_0^2}{c^2M^2R^2} + \frac{2}{c^2}\frac{F_1(R,\Theta)}{R} + \frac{2}{c^2}\frac{\cos\Theta}{\sin\Theta}F_2(R,\Theta)\right]R^2\sin^2\Theta d\phi^2 + \frac{4GS_0}{c^2R}\sin^2\Theta d\phi dt. \tag{2.22}$$

In order to find $F_1(R,\Theta)$ and $F_2(R,\Theta)$, we equate the tt and $\varphi\varphi$ components of the metric functions in the Fock (2.19) and Kerr metric (2.22), respectively, we obtain:

$$F_1(R,\Theta) = GM - \frac{\left[k + (2-3k)\cos^2\Theta\right]S_0^2}{2M^2R}$$

$$F_2(R,\Theta) = -\frac{\left[k + (3k-2)(2\cos^2\Theta - 1)\right]S_0^2}{4M^2R^2}\frac{\sin\Theta}{\cos\Theta} \tag{2.23}$$

To find the parameter of the internal structure k, we use the found values $F_1(R,\Theta)$ and $F_2(R,\Theta)$ in the $R\Theta$ component of the metric tensor (2.22) and equate this component to zero, since it must disappear because of its absence in the original metrics. It follows that $k = 1$ and finally obtain

$$r = R + \frac{1}{c^2}\left(GM - \frac{S_0^2\sin^2\Theta}{2M^2R}\right), \qquad \theta = \Theta - \frac{S_0^2\sin\Theta\cos\Theta}{2c^2M^2R^2} \tag{2.24}$$

Then the approximate Kerr metric (2.20) in harmonic coordinates can be reduced to the following form:

$$ds^2 = \left[c^2 - \frac{2GM}{R} + \frac{2}{c^2}\left(\frac{GM}{R}\right)^2 + \frac{2G}{c^2M}\frac{S_0^2}{R^3}P_2(\cos\Theta)\right]dt^2 -$$

$$-\left[1 + \frac{2GM}{c^2R}\right]\left[dR^2 + R^2(d\Theta^2 + \sin^2\Theta d\phi^2)\right] + \frac{4GS_0}{c^2R}\sin^2\Theta d\phi dt \tag{2.25}$$

which coincides with (2.19) only for $k=1$. Consequently, the refined Fock metric (2.19) can be interpreted as a metric describing the exterior gravitational field of a rotating body of second order with respect to the angular velocity. The advantage of using this method is to find an approximate solution that allows us to determine an arbitrary constant k. In fact, in the case $k=k_L=4/7$ for a liquid sphere and $k=k_S=15/18$ for a solid sphere, the value of $k=k_K=1$ for the Kerr metric does not correspond to any specific internal model. On the other hand, all attempts to find a physically reasonable interior solution to the Kerr metric failed. Perhaps the relation with the formalism of Fock can shed light on the structure of the internal model of the Kerr metric [33].

2.3 On the equivalence of Hartle-Thorne and Sedrakyan-Chubaryan solutions

Hartle have introduced a new method in the slow rotation approximation, extending the well-known interior and exterior Schwarzschild solutions, in order to investigate the gravitational field of uniformly slowly rotating and slightly deformed relativistic stellar objects [43]. This approach allows one to study the physical properties of hydrostatic equilibrium configurations of rotating astronomical bodies. Hartle and Thorne applied it for the first time to real astronomical bodies [44], using the Tsuruta-Cameron, Harrison-Wheeler and Harrison-Wakano-Wheeler EoS. Later, the approach became known as Hartle-Thorne's approach. There appeared a new series of researches modifying, extending and improving the original work of Hartle and Thorne by including higher-order multipole moments, corrections in the angular momentum and so on [48, 67]. In addition, the HF was tested, compared and contrasted with numerical calculations in full GR [45, 46]. Consequently, it was shown that the HF can be safely applied to investigate celestial bodies with intermediate periods of rotation. It shows noteable discrepancies from the full general relativistic simulations only for higher angular velocities, close to the mass-shedding limit [45, 46, 48].

Bradley and co-authors have developed similar methods in [68-71], where the slow rotation case is applied to build internal and external solutions for Einstein's gravitational field equations. In contradistinction to Hartle, Bradley and co-authors have solved the 6 independent Einstein equations without including the integral of the hydrostatic equilibrium equation in the case of uniformly rotating configurations. Additionally, Darmois-Israel's method was used to sew the external and internal solutions. For particular cases, Bradley and co-authors [68-71] have added the electric charge by solving Einstein-Maxwell's equations.

Additionally, Konno and others [72] generalized the HF for in the non-rotating case to add deformations of relativistic stars owing to the presence of magnetic fields. Furthermore, Konno and co-authors [73] derived the ellipticity of deformed stars owing to the presence of both rotation and magnetic field, developing their previous works. This approach has become popular and found a wide application in physics of all types of magnetic stars [74-78].

Independently from Hartle, Sedrakyan and Chubaryan have devised own specific method for calculation of the exterior gravitational structure of equilibrium uniformly rotating superdense stars within the approximation of small angular velocity. However this approach isn't so popular in the scientific community [79]. The corresponding internal solution and sewing technique were derived in Sedrakyan-Chubaryan's subsequent work [80]. The solution way of Einstein's field equations was very diverse from the Hartle formalism. Subsequent applications of Sedrakyan-Chubaryan's solution to WDs and NSs have been considered in several scientific articles, for exmaple, in [15, 81, 82]. The results of numerical calculation of Arutyunyan and his coworkers [15] were in accordance with the ones calculated by Hartle and Thorne [44], showing no contradiction between two solutions. In addition, Sedrakyan-Chubaryan's external solution was given in an analytical form in [15, 79-82] and it needed an extra integration of one of the metric functions with a thorough consideration of the boundary conditions. This was possibly one of the basic reasons of why Sedrakyan-Chubaryan's solution isn't still well-known in scientific world. Actually, the aforementioned fact doesn't allow one to contrast and compare it directly with Hartle-Thorne's external metric. Indeed, it will be shown here that Sedrakyan-Chubaryan's and Hartle-Thorne's external solutions are related through a transformation of coordinates whose non-trivial term includes only the radial coordinate and the parameters' redefinition entering to the solution [35].

2.3.1 The solution of Sedrakyan-Chubaryan

In this section, Sedrakyan-Chubaryan's approximate solution [79] is derived in detail. We restrict ourselves on the external solution for which all the metric functions will be derived.

According to the procedure introduced in [79], the metric of axially symmetric rotating stars is considered in the following form

$$ds^2 = \left(\omega^2 e^{\mu}\sin^2\theta - e^{\nu}\right)dt^2 + e^{\lambda}dr^2 + e^{\mu}\left(d\theta^2 + \sin^2\theta d\varphi^2\right) + 2\omega e^{\mu}\sin^2\theta d\varphi dt \qquad (2.26)$$

where $\lambda = \lambda(r,\theta)$, $\mu = \mu(r,\theta)$, $\omega = \omega(r,\theta)$ and $\nu = \nu(r,\theta)$ functions depend on the radial r and angular θ coordinates. Notice that λ, μ and ν are proportional to even powers of the angular velocity Ω, although ω is proportional to odd powers of Ω. Here, the approximation of the second order in Ω will be considered. It is required that the preceding line element satisfy the Einstein equations of the following form

$$G_{\beta}^{\alpha} = R_{\beta}^{\alpha} - \frac{1}{2}R\delta_{\beta}^{\alpha} = 0 \qquad (2.27)$$

Both the angular velocity Ω and the function ω is zero ($\Omega = 0, \omega = 0$) for the particular case so-called non-rotating configuration, in that case, the functions λ, ν and μ depend only on the radial coordinate r. Apparently, for this particular case one easily gets Schwarzschild's external solution

$$e^{\nu} = e^{\nu_0} = \left(1 - \frac{2m}{r}\right), \tag{2.28}$$

$$e^{\lambda} = e^{\lambda_0} = \left(1 - \frac{2m}{r}\right)^{-1}, \tag{2.29}$$

$$e^{\mu} = e^{\mu_0} = r^2, \tag{2.30}$$

m is the mass of a non-rotating configuration.

One can expand the functions λ, μ, ν, and ω in the metric (2.26) for a rotating relativistic star in Taylor series with respect to the angular velocity Ω, supposing that Ω to be small. It is suitable to use a dimensionless quantity $\beta = \Omega^2/(8\pi\rho_c)$ as a parameter for the Taylor expansion of the components of the metric tensor, where ρ_c is the density at the center of a star. Therefore, the metric functions are defined as

$$e^{\nu(r,\theta)} = e^{\nu_0}\left[1 + \beta\Phi(r,\theta)\right], \tag{2.31}$$

$$e^{\lambda(r,\theta)} = e^{\lambda_0}\left[1 - \beta f(r,\theta)\right], \tag{2.32}$$

$$e^{\mu(r,\theta)} = e^{\mu_0}\left[1 + \beta U(r,\theta)\right], \tag{2.33}$$

$$\omega(r,\theta) = \sqrt{\beta}\, q(r), \tag{2.34}$$

where U, Φ, f are unknown functions and Schwarzschild's solution is represented by the functions μ_0, ν_0, λ_0. The following relations are used for the purpose of finding the independent differential equations from Einstein's field equations

$$G_1^1 - G_0^0 = 0, \quad G_2^2 + G_3^3 = 0, \quad G_2^1 = 0, \quad G_0^3 = 0. \tag{2.35}$$

We expand all the metric functions in spherical harmonics in order to solve equations (2.35). As a result of this procedure, separation of variables becomes possible. After leaving only the parts that is responsible to the quadrupolar deformation, we get

$$\Phi(r,\theta) = \sum_{l=0}^{\infty} \Phi_l(r) P_l(\cos\theta) \approx \Phi_0(r) P_0(\cos\theta) + \Phi_2(r) P_2(\cos\theta), \tag{2.36}$$

$$f(r,\theta) = \sum_{l=0}^{\infty} f_l(r) P_l(\cos\theta) \approx f_0(r) P_0(\cos\theta) + f_2(r) P_2(\cos\theta), \tag{2.37}$$

$$U(r,\theta) = \sum_{l=0}^{\infty} U_l(r) P_l(\cos\theta) \approx U_0(r) P_0(\cos\theta) + U_2(r) P_2(\cos\theta), \tag{2.38}$$

where $P_0(\cos\theta)$ and $P_2(\cos\theta)$ are the first kind Legendre's polynomials

$$P_0(\cos\theta)=1 \tag{2.39}$$

$$P_2(\cos\theta)=-\frac{1}{2}\left(1-3\cos^2\theta\right) \tag{2.40}$$

The spherical harmonics expansion contains only even values of l due to orientation of the symmetry axis along the axis of rotation. Note that there are only two of l in the case of slow rotation approximation: $l=0$ and $l=2$.

The Einstein tensor components G_3^0 or G_0^3 give a following differential equation proportional to Ω,

$$\frac{\partial^2 q}{\partial r^2}+\frac{4}{r}\frac{\partial q}{\partial r}=0, \tag{2.41}$$

The general solution of the preceding differential equation is

$$q(r)=\frac{C_q}{r^3}, \tag{2.42}$$

where C_q is a constant to be defined from sewing of the internal and extertal solutions.

We insert the equations (2.36), (2.37) and (2.38) to the equation (2.35), then expand the resultant equation with respect to β (up to the first order) for different values of l. As a result, one gets the following equations for the case of $l=0$:

$$U_{0,rr}+\frac{1}{r}\left[2U_{0,r}+f_{0,r}-\Phi_{0,r}\right]=0, \tag{2.43}$$

$$\Phi_{0,rr}+U_{0,rr}+\frac{1}{r(r-m)}\left[(m+r)\Phi_{0,r}+(r-m)\left(f_{0,r}+2U_{0,r}\right)-\frac{6}{r^4}C_q^2\right]=0, \tag{2.44}$$

The number of unknown functions is more than the number of equations in the above-mentioned system of differential equations that is why it is impossible to find their solution. Thus, an additional equation is needed for closing this system of equations. An analysis of the metric (2.26) shows that the relationship $g_{rr}=-1/g_{tt}$ is fulfilled to the g_{tt} and g_{rr} components of metric tensor in the lowest approximation of a spherically symmetric field. As a result, it is assumed that the condition $f_0(r)=\Phi_0(r)$ allows us to easily find a solution of the equations [79]. Additionally, if we set the following conditions $U_0(r\to\infty)=0$, $\Phi_0(r\to\infty)=0$, then $f_0(r\to\infty)=0$ at large distances, we get

$$U_0(r)=\frac{C_{U_0}}{r}, \tag{2.45}$$

$$\Phi_0(r)=f_0(r)=\frac{C_q^2+2C_{U_0}mr^2-2C_{f_0}r^3}{2r^3(r-2m)}, \tag{2.46}$$

where C_{U_0} and C_{f_0} are the constants of the integration for the functions U_0 and f_0.

Further, we can find the $l=2$ terms of the field equations from the equations (2.35) as

$$U_{2,rr}+\frac{1}{r}\left[2U_{2,r}+f_{2,r}-\Phi_{2,r}+\frac{3}{r-2m}(\Phi_2+f_2)\right]=0, \tag{2.47}$$

$$\Phi_{2,rr}+U_{2,rr}+\frac{r-m}{r(r-2m)}\left[2U_{2,r}+f_{2,r}+\frac{1}{r-m}\left((r+m)\Phi_{2,r}+3(f_2-\Phi_2)+\frac{6C_q^2}{r^4}\right)\right]=0, \tag{2.48}$$

$$\Phi_{2,r}+U_{2,r}-\frac{1}{r(r-2m)}\left[(r-3m)\Phi_2-(r-m)f_2\right]=0. \tag{2.49}$$

We express $U_{2,r}$ from the equation (2.49) in order to solve the above set of equations, after that we find $U_{2,rr}$, then insert the resultant expressions to (2.48). In the result, we obtain the following relation

$$f_2(r)=\Phi_2(r)-\frac{3C_q^2}{r^4}. \tag{2.50}$$

Therefore, the solutions of the equations (2.47), (2.48), and (2.49) can be represented in the forms

$$\Phi_2(r)=\frac{C_q^2}{2}\left(\frac{1}{mr^3}+\frac{1}{r^4}\right)-\frac{3C_{\Phi_2}}{4}\left(1-\frac{2m}{r}\right)r^2\ln\left(1-\frac{2m}{r}\right)-\frac{(3r^2-6mr-2m^2)(r-m)mC_{\Phi_2}}{2r(r-m)}, \tag{2.51}$$

$$f_2(r)=\frac{C_q^2}{2}\left(\frac{1}{mr^3}-\frac{5}{r^4}\right)-\frac{3C_{\Phi_2}}{4}\left(1-\frac{2m}{r}\right)r^2\ln\left(1-\frac{2m}{r}\right)-\frac{(3r^2-6mr-2m^2)(r-m)mC_{\Phi_2}}{2r(r-2m)}, \tag{2.52}$$

$$U_2(r)=-\frac{C_q^2}{2}\left(\frac{1}{mr^3}+\frac{2}{r^4}\right)+\frac{3C_{\Phi_2}}{4}\left(1-\frac{2m^2}{r^2}\right)r^2 ln\left(1-\frac{2m}{r}\right)+\frac{(3r^2+3mr-2m^2)mC_{\Phi_2}}{2r}. \tag{2.53}$$

The constant of integration of (2.53) relates with C_{Φ_2} as

$$C_{\Phi_2} = -\frac{C_{U_2}}{3m^2}\,, \tag{2.55}$$

because of the condition for the asymptotic flatness $U_2(r\to\infty)\to 0$.

In the end, the components of the metric tensor for the metric given by (2.26) are expressed as

$$g_{00} = \omega^2 e^{\mu}\sin^2\theta - e^{\nu} \approx \beta\left(\frac{C_q}{r^3}\right)^2 r^2\sin^2\theta - \left(1-\frac{2m}{r}\right)\left[1+\beta\left\langle\Phi_0(r)+\Phi_2(r)P_2(\cos\theta)\right\rangle\right] =$$

$$= \left(1-\frac{2m}{r}\right)\left\{1+\beta\left\langle\frac{C_q^2+2C_{U_0}mr^2-2C_{f_0}r^3}{2r^3(r-2m)}+\left[\frac{C_q^2}{2}\left(\frac{1}{mr^3}+\frac{2}{r^4}\right)-\frac{3C_{\Phi_2}}{4}\left(1-\frac{2m}{r}\right)r^2\times\right.\right.$$

$$\left.\left.\times\ln\left(1-\frac{2m}{r}\right)-\frac{(3r^2-6mr-2m^2)(r-m)mC_{\Phi_2}}{2r(r-2m)}\right]P_2(\cos\theta)-\left(1-\frac{2m}{r}\right)^{-1}\frac{C_q^2}{r^4}\sin^2\theta\right\rangle\right\}, \tag{2.56}$$

$$g_{11} = e^{\lambda} \approx \left(1-\frac{2m}{r}\right)^{-1}\left[1-\beta\left\langle f_0(r)+ f_2(r)P_2(\cos\theta)\right\rangle\right] = \left(1-\frac{2m}{r}\right)^{-1}\times$$

$$\times\left\{1-\beta\left\langle\frac{C_q^2+2C_{U_0}mr^2-2C_{f_0}r^3}{2r^3(r-2m)}-\left[\frac{C_q^2}{2}\left(\frac{1}{mr^3}-\frac{5}{r^4}\right)-\frac{3C_{\Phi_2}}{4}\left(1-\frac{2m}{r}\right)r^2\times\right.\right. \tag{2.57}$$

$$\left.\left.\times ln\left(1-\frac{2m}{r}\right)-\frac{(3r^2-6mr-2m^2)(r-m)mC_{\Phi_2}}{2r(r-2m)}\right]P_2(\cos\theta)\right\rangle\right\},$$

$$g_{22} = e^{\mu} \approx r^2\left[1+\beta\left\langle U_0(r)+U_2(r)P_2(\cos\theta)\right\rangle\right] =$$

$$= r^2\left\{1+\beta\left\langle\frac{C_{U_0}}{r}+\left[-\frac{C_q^2}{2}\left(\frac{1}{mr^3}+\frac{2}{r^4}\right)+\frac{3C_{\Phi_2}}{4}\left(1-\frac{2m^2}{r^2}\right)r^2\times\right.\right. \tag{2.58}$$

$$\left.\left.\times\ln\left(1-\frac{2m}{r}\right)+\frac{(3r^2+3mr-2m^2)mC_{\Phi_2}}{2r}\right]P_2(\cos\theta)\right\rangle\right\},$$

$$g_{33} = g_{22}\sin^2\theta, \tag{2.59}$$

$$g_{30} = g_{03} = \omega e^{\mu}\sin\theta \approx \frac{C_q\sqrt{\beta}}{r}\sin^2\theta. \tag{2.60}$$

The values of all the constants must be defined via sewing the external solution with the corresponding internal solution on the star's surface [35].

2.3.2 Relation of the Hartle-Thorne and Sedrakyan-Chubaryan solutions

Generally, one has to carry out a full analysis of the corresponding tensors of curvature as well as their covariant derivatives in order to set up the equivalence

between these two metrics in an invariant form. If it is possible to discover an obvious isomorphism of smooth manifolds which relates these metrics, in turn, the problem can be simplified in a significant manner. The current problem is even further simplified when the metrics are approximate solutions of Einstein's equations, since the transformation of coordinates has to be valid only approximately. Both Sedrakyan-Chubaryan's and Hartle-Thorne's metric is to be written in the same coordinates in order to compare them, therefore one should first find a coordinate transformation. A detailed examination of the Sedrakyan-Chubaryan metric finds that it is possible to choose the radial coordinate transformation as follows

$$r \to r\left(1-\frac{\beta}{2}U_0(r)\right), \tag{2.61}$$

and keep the remaining coordinates unchanged. The practical effect of this transformation is to exclude the function $U_0(r)$. This means that, without loss of generality, we can set $U_0(r)=0$ (or, equivalently, $C_{U_0}(r)=0$) in the Sedrakyan-Chubaryan metric, and therefore it becomes equivalent to the Hartle-Thorne solution up to a redefinition of the constants entering the metric. In fact, we now have only three integration constants, namely, C_{f_0}, C_q and C_{Φ_2}, which are directly related to the total mass, angular momentum and quadrupole moment of the Hartle-Thorne metric. Indeed, by comparing the g_{tt} and $g_{t\varphi}$ components of the metric tensor, we obtain

$$M = m+\frac{\beta}{2}C_{f_0}, \tag{2.62}$$

$$J = -\frac{\sqrt{\beta}}{2}C_q, \tag{2.63}$$

$$Q = \frac{\beta}{2}\left(\frac{C_q^2}{2m}-\frac{4m^5 C_{\Phi_2}}{5}\right). \tag{2.64}$$

Notice that M in the Hartle-Thorne metric is actually composed of two terms, $M = m+\delta m$, where m is the "static mass" and δm is the contribution due to the rotation of the source. This means that in fact the last equations relate four constants of the Hartle-Thorne metric to four constants of the Sedrakyan-Chubaryan metric, implying that the inverse transformation is well defined. This proves the mathematical and physical equivalence of the two space-times up to the first order in the quadrupole moment Q and the second order in the angular momentum J.

There is an additional way to prove the equivalence of two spacetimes, namely, in terms of their multipole moments. Indeed, it has been proved that two space-times with the same set of multipole moments are isomorphic to each other (see, for example, [83] for a review). In the case of approximate solutions, one can assure that two spacetimes are isomorphic if they have the same set of multipole moments up to the validity order of the approximation. For the approximate space-times under

consideration in this section, this means that the Hartle-Thorne metric and the Sedrakyan-Chubaryan metric are equivalent if their mass, angular momentum and quadrupole moment are the same. In [84] and [85] it has been shown that in the approximate case, the moments can be derived from the explicit expression of the g_{tt} metric component. For the Hartle-Thorne metric we have

$$g_{tt}^{HT} = -1 + \frac{2M}{R} + \frac{2}{3}\frac{J^2}{R^4} + \left[\frac{2\left(Q - 2J^2/M\right)}{R^3} + \frac{2\left(QM - 4J^2/3\right)}{R^4}\right] \times P_2\left(\cos\theta\right), \tag{2.65}$$

while the corresponding expression for the Sedrakyan-Chubaryan metric is

$$\begin{aligned} g_{tt}^{SC} = -1 + \frac{2m + \beta C_{f_0}}{R} - \frac{\beta m C_{U_0}}{R^2} + \frac{1}{6}\frac{\beta C_q^2}{R^4} - \\ - \beta\left(\frac{\frac{1}{2m}C_q^2 + \frac{4}{5}m^5 C_{\Phi_2}}{R^4} + \frac{\frac{1}{6}C_q^2 + \frac{4}{5}m^6 C_{\Phi_2}}{R^4}\right) \times P_2\left(\cos\theta\right). \end{aligned} \tag{2.66}$$

A comparison of Eqs. (2.65) and (2.66) shows that if we define the constants as

$$M = m + \frac{\beta}{2}C_{f_0}, \tag{2.67}$$

$$C_{U_0} = 0 \tag{2.68}$$

$$J = -\frac{\sqrt{\beta}}{2}C_q, \tag{2.69}$$

$$Q = \frac{\beta}{2}\left(\frac{C_q^2}{2m} - \frac{4m^5 C_{\Phi_2}}{5}\right). \tag{2.70}$$

then the moments are exactly the same, which proves the equivalence of the two metrics up to the fourth order in $1/R$ [35].

2.4 Summary

First, we considered the correspondence of approximate solutions of Einstein's equations, such as the Kerr metric and the Hartle-Thorne metric in strong gravitational fields with slow rotation. In the general case, when the Kerr metric has an exact and not an approximate form, it describes the gravitational field of rapidly rotating compact objects. Nevertheless, the fact that the quadrupole moment in the Kerr solution is completely determined by the angular momentum is a sign that it can be applied only to describe the gravitational field of a certain class of compact objects, for example, BHs. In turn, the Hartle-Thorne metric characterizes the gravitational field of slowly rotating and slightly deformed real compact astrophysical objects. In obtaining the correspondence between the two solutions, we took into account that the Hartle-Thorne metric is given up to the second order in the

angular velocity of rotation. For the same reason, the Kerr metric was considered in the same approximation. With the help of perturbation theory methods, we searched for coordinate transformations for a given approximation. After two metrics were written in the same coordinates, coordinate transformations and the relation between the quadrupole moment in the Hartle-Thorne metric and the rotation parameter in the Kerr metric were found. All the coordinate transformations were calculated with the same approximation as the metric functions in the original Hartle-Thorne solution. Therefore, the procedure for comparing the metrics presented here can be extended in a similar way to other approximate and exact solutions. To compare exact solutions, the situation is quite different. Here we need new methods, the development of which requires further research.

Second, we have investigated solutions of Einstein's equations, which are widely used in the literatures to describe the gravitational fields of compact objects. In particular, the interior and exterior approximate solutions of Fock, the Fock solution with a quadrupole moment, the solution for the spherically symmetric mass distribution, and the Kerr solution have been considered. We have shown that the specific parameter k, entering into the refined Fock metric, subsequently, takes on special values in the case of a liquid and a solid sphere. It was also found out that in the case of the approximate Kerr metric, this parameter does not correspond to any of the known internal models of a body analyzed in the framework of the Fock formalism. To avoid technical problems that usually arise in the process of comparing solutions, we derived coordinate transformations in the approximation of $\sim 1/c^2$ using the method of perturbation theory. In the cases, presented here, this is done in a relatively simple way only because all the coordinate transformations are not calculated accurately, but with the same approximation as the metric functions. This approach allows us to reduce the corresponding problems in the comparison of metrics on the corresponding given surface: thus, only algebraic conditions appear. Using this method, we could show that the technique presented in this section, is applicable to comparison of other approximate solutions of Einstein's equations.

Third, we have reviewed the original papers by Hartle (1967) and Hartle and Thorne (1968) and discussed their main properties, extensions and modifications. We revisited the results of Sedrakyan and Chubaryan (1968) for the metric that describes the exterior field of an axially symmetric mass distribution. Using a perturbation procedure, we have derived the Sedrakyan-Chubaryan solution explicitly, which includes several integration constants. Instead of using the interior Sedrakyan-Chubaryan solution in order to find the integration constants, we compare the exterior metric with the exterior Hartle-Thorne space-time solution in the same coordinates. As a result, we obtain a set of simple algebraic expressions relating the main parameters of the Hartle-Thorne metric with the integration constants of the Sedrakyan-Chubaryan solution. Alternatively, we calculated the relevant multipole moments of both solutions and showed that they are the same. In this way, we have also proved the mathematical and physical equivalence of the two space-times. We conclude that the Sedrakyan-Chubaryan solution can be considered as an alternative approach to describing the gravitational field of a slightly deformed stationary axially

symmetric mass distribution in the slow rotation approximation. Moreover, the Sedrakyan-Chubaryan solution with its internal counterpart can be applied to various astrophysical problems together with the Hartle-Thorne solution on equal rights.

On the other hand, in a previous work [39] it was shown that the Hartle-Thorne formalism for the approximate description of rotating mass distributions is equivalent to the Fock-Abdildin approach. The latter, however, allows us to interpret the parameters of the interior solution in terms of physical quantities like the rotational kinetic energy or the mutual gravitational attraction between the particles of the source. Therefore, the results obtained in this work imply that it should be possible to find a direct relationship between the interior Sedrakyan-Chubaryan solution and the corresponding counterpart in the Fock-Abdildin approach. It is interesting that different approaches that were developed independently in different places and under diverse circumstances turn out to be equivalent from a mathematical point of view. It would be interesting to perform a more detailed analysis of all physical characteristics of each approach in order to propose a unique formalism that would incorporate the advantages of all known approaches.

3 EQUILIBRIUM CONFIGURATIONS OF STATIC WHITE DWARFS

In subsection 3.1, the main parameters of static and zero temperature WDs such as mass, radius, central density, central pressure, gravitational potential and compactness have been theoretically determined both in NG and GR. For this purpose, the system of differential equations which consists of the EoS of the degenerate electron gas within Chandrasekhar approximation, the mass balance equation and the hydrostatic equilibrium equation has been reduced to a dimensionless form and has been solved by the methods of numerical integration. The mass-central density, mass-radius, mass-compactness parameter and gravitational potential-radius relations have been constructed both in NG and GR, and their results have been compared with each other. It has been shown that the effects of GR play an important role near the Chandrasekhar limit, more precisely, for large masses and small radii, i.e. in strong gravitational fields. However, it is also shown that the difference between NG and GR decreases for small masses and large radii due to the weakness of the gravitational field. In addition, the analytical expression for the classical and relativistic mass-radius relation has been found and its accuracy has been estimated. The importance of the simple analytical expression has been clarified in theoretical calculations, studies of the dynamics of a binary star system and practical analyses [86-89].

In subsection 3.2, cold and hot WDs are investigated in the framework of GR using the Chandrasekhar EoS. Basic parameters of WDs such as the central density, pressure, mass, radius, the temperature of an isothermal core and logarithm of surface gravity have been calculated. It has been shown that it is necessary to take into account the effects of finite temperatures in WDs with low masses. The consideration of the effects of temperature can explain observational data from Sloan Digital Sky Survey Data Release 4. Additionally, the core temperatures have been estimated for white dwarfs – satellites of the millisecond pulsars PSR J1738+0333, PSR J1012+5307 and PSR J1911-5958A [27, 90-96].

In subsection 3.3, static cold WDs are investigated by means of the Salpeter EoS within GR. The main parameters of WDs such as mass, radius, central density and pressure are calculated solving the TOV equation, employing the Salpeter EoS. In addition, the WD characteristics from the SDSS DR 4, 10 and 12 are analyzed. The histogram and the Gaussian distribution of mass and radius are constructed for the catalogues. The maximum, minimum and average values of the logarithm of the surface gravity, effective temperature, mass and radius are found. The theoretical mass-radius relations are compared with the observational data. Finally, it has been shown that taking into account nuclear composition, neutronization threshold, the Thomas-Fermi corrections and Coulomb interactions is very important to describe some WDs in the catalogues of the SDSS DR 10 and 12 [29, 97].

3.1 Effects of general relativity to the structure of white dwarfs

3.1.1 Newtonian and general relativistic equations of stellar structure

a) Newtonian equations. There are two forces that act any non-rotating (static) star: the first one is the inward force of gravity and the second one is the outwrd force of interior pressure gradient. For the hydrostatic equilibrium configuration of stars, the inward force of gravity is counterbalanced with the outward force of the interior pressure gradient of the star, as these forces are equal in magnitude, but opposite in direction.

For example, it is the thermal pressure for the normal stars, the degenerate electron pressure for WDs, and the degenerate neutron pressure in case of NSs. On the basis of the equality of these forces, the equation of hydrostatic equilibrium of stellar structure can be derived. For Newtonian, static, spherically symmetric stars, the equation of hydrostatic equilibrium and mass balance equation are given by

$$\frac{dP(r)}{dr} = -\rho(r)\frac{Gm(r)}{r^2} \tag{3.1}$$

and

$$\frac{dm(r)}{dr} = 4\pi r^2 \rho(r), \tag{3.2}$$

where $P(r)$, $\rho(r)$, and $m(r)$ are the pressure, the mass density, and the mass, respectively, which depend on the radial coordinate of r and G is the gravitational constant. The equations of stellar structure describe how the mass and the pressure of a star changes by the radial coordinate of r [5, 98, 99].

The interior gravitational potential of Newtonian static spherically symmetric stars is defined by

$$\frac{d\varphi(r)}{dr} = \frac{Gm(r)}{r^2} \tag{3.3}$$

and the exterior potential outside the star is

$$\varphi(r) = -\frac{GM}{r}, \tag{3.4}$$

where $M = m(r = R)$ is the total mass of a star, R is the total radius.

b) General relativistic equations.To find the general relativistic stellar structure equations, one should substitute the components of the general static, spherically symmetric metric

$$ds^2 = -e^{2\nu(r)}c^2dt^2 + e^{2\lambda(r)}dr^2 + r^2d\theta^2 + r^2\sin^2\theta d\phi^2, \tag{3.5}$$

to the Einstein equations written in the geometrized unit system ($G = c = 1$)

$$G_{ik} = R_{ik} - (1/2) g_{ik} R = 8\pi T_{ik}\,, \tag{3.6}$$

where G_{ik}, R_{ik}, g_{ik}, R, and T_{ik} are the Einstein tensor, the Ricci tensor, the metric tensor, the Ricci scalar and the energy-momentum tensor, respectively, and $i,k = 0,1,2,3.$ To high precision, the matter inside any star is a perfect fluid, including WDs. The energy-momentum tensor of a perfect fluid is given by

$$T_{ik} = \left[P(r) + \rho(r)\right] u_i u_k + P(r) g_{ik}\,, \tag{3.7}$$

where u_i and u_k are the four-velocity [99].

By calculating the Einstein tensor and the energy-momentum tensor, one can find G_{00}, G_{11}, G_{22} and G_{33} components of the Einstein equations

$$G_{00} = \frac{1}{r^2} e^{2(\nu-\lambda)} \left[2r \frac{d\lambda}{dr} - 1 + e^{2\lambda} \right] = 8\pi e^{2\nu} \rho\,, \tag{3.8}$$

$$G_{11} = \frac{1}{r^2} \left[2r \frac{d\nu}{dr} + 1 - e^{2\lambda} \right] = 8\pi \mathrm{e}^{2\lambda} P\,, \tag{3.9}$$

$$G_{22} = r^2 e^{-2\lambda} \left[\frac{d^2\nu}{dr^2} + \left(\frac{d\nu}{dr} \right)^2 - \frac{d\nu}{dr}\frac{d\lambda}{dr} + \frac{1}{r}\left(\frac{d\nu}{dr} - \frac{d\lambda}{dr} \right) \right] = 8\pi r^2 P\ , \tag{3.10}$$

$$G_{33} = \sin^2\theta\, r^2 e^{-2\lambda} \left[\frac{d^2\nu}{dr^2} + \left(\frac{d\nu}{dr} \right)^2 - \frac{d\nu}{dr}\frac{d\lambda}{dr} + \frac{1}{r}\left(\frac{d\nu}{dr} - \frac{d\lambda}{dr} \right) \right] = 8\pi r^2 \sin^2\theta\, P\,. \tag{3.11}$$

The G_{22} and G_{33} components of the Einstein equation are the same, so there is no need to consider them separately. From G_{00} and G_{11} components of the Einstein equation one obtains the mass balance equation and the expression for the gradient of the potential in GR, respectively

$$\frac{dm(r)}{dr} = 4\pi r^2 \frac{\varepsilon(r)}{c^2}\,, \tag{3.12}$$

$$\frac{d\nu(r)}{dr} = \frac{Gm(r)}{c^2 r^2} \left(1 + \frac{4\pi r^3 P(r)}{m(r) c^2} \right) \left(1 - \frac{2Gm(r)}{c^2 r} \right)^{-1}\,, \tag{3.13}$$

and from the law of the local energy and momentum conservation $T^{ik}{}_{;k} = 0$

$$\frac{dP(r)}{dr} = -\left[\varepsilon(r) + P(r)\right]\frac{d\nu(r)}{dr} = -\frac{Gm(r)\rho(r)}{r^2}\left[1 + \frac{P(r)}{\rho(r)c^2}\right]\left(1 + \frac{4\pi r^3 P(r)}{m(r)c^2}\right)\left(1 - \frac{2Gm(r)}{c^2 r}\right)^{-1}, \quad (3.14)$$

where $\nu(r)$ is the dimensionless gravitational potential, which is related to the physical potential as $\varphi(r) = c^2\nu(r)$, $\varepsilon(r) = \rho(r)c^2$ is the energy density, c is the speed of light. The equation (3.14) is called the Tolman-Oppenheimer-Volkoff (TOV) equation of hydrostatic equilibrium for a non-rotating spherically symmetric star within the framework of general relativity. A detailed derivation of the equations (3.12)-(3.14) can be found in [100-103]. Expessions (3.12)-(3.14) reduces to the expressions (3.2), (3.3) and (3.1) in their Newtonian limit. By integrating equation (3.13) with $P(r = R) = 0$ and $m(r \geq R) = M$ and using the boundary condition $\nu(\infty) = 0$, one obtains

$$\varphi(r) = \frac{c^2}{2} ln\left(1 - \frac{2GM}{c^2 r}\right), \quad (3.15)$$

which is the expression for the gravitational potential outside a star.

The main parameters of WDs can be found by solving the equations of stellar structure (3.1) and (3.2) (or (3.12) and (3.14)). However, the number of equations is two, the number of unkowns is three $(m(r), \rho(r), P(r))$. The EoS of the WD matter closes the system of equations being as the third equation.

3.1.2 Dimensionless form

The system of differential equations of stellar structure (3.1) and (3.2) ((3.12) and (3.14)) can not be solved analytically, therefore we seek a numerical solution. At first, all the equations should be nondimensionalized in order to simplify numerical calculations. For this purpose, we write down all physical quantities in their dimensionless forms by

$$r = bx, \quad (3.16)$$

$$m(r) = \frac{c^2 b}{G} m^*(x), \quad (3.17)$$

$$\rho(r) = \frac{c^2}{Gb^2} \rho^*(x), \quad (3.18)$$

$$P(r) = \frac{c^4}{Gb^2} P^*(x), \quad (3.19)$$

$$\varphi(r) = c^2 \varphi^*(x), \quad (3.20)$$

where $b = \left(\hbar^3 / Gcm_e^4\right)^{1/2}$, x, $m^*(x)$, $\rho^*(x)$, $P^*(x)$, $\varphi^*(x)$ are the dimensionless radial coordinate, mass, mass density, pressure and potential, respectively [86].

Consequently, the corresponding dimensionless Newtonian equations of stellar structure are obtained by substituting the expressions (3.16)-(3.19) into the equations (3.1) and (3.2)

$$\frac{dm^*(x)}{dx} = 4\pi x^2 \rho^*(x), \tag{3.21}$$

$$\frac{dP^*(x)}{dx} = -\rho^*(x)\frac{m^*(x)}{x^2}. \tag{3.22}$$

By the same procedure, one can derive the dimensionless relativistic equations of stellar structure as

$$\frac{dm^*(x)}{dx} = 4\pi x^2 \rho^*(x), \tag{3.23}$$

$$\frac{dP^*(x)}{dx} = -\rho^*(x)\frac{m^*(x)}{x^2}\left(1+\frac{P^*(x)}{\rho^*(x)}\right)\left(1+\frac{4\pi x^3 P^*(x)}{m^*(x)}\right)\left(1-\frac{2m^*(x)}{x}\right)^{-1}, \tag{3.24}$$

the dimensionless EoS (in this case, the Chandrasekhar EoS)

$$\rho^*(x) = \frac{1}{3\pi^2}\frac{m_n}{m_e}\left(\frac{A}{Z}\right)y^3(x)\ , \tag{3.25}$$

$$P^*(x) = \frac{1}{24\pi^2}\left[y(x)\left(2y^2(x)-3\right)\sqrt{1+y^2(x)}+3\ln\left(y(x)+\sqrt{1+y^2(x)}\right)\right] \tag{3.26}$$

and the dimensionless Newtonian and general relativistic exterior gravitational potentials, respectively

$$\varphi^*(x) = -\frac{M^*}{x}, \tag{3.27}$$

$$\varphi^*(x) = \frac{1}{2}\ln\left(1-\frac{2M^*}{x}\right). \tag{3.28}$$

The procedure on how to find the parameter b, and how to nondimensionalize equations of stellar structure and state have been fully demonstrated in our work [86].

3.1.3 Boundary conditions

It is necessary to impose boundary conditions in order to solve the system of differential equations (3.1) and (3.2) or (3.12) and (3.14). The first condition is given at the center of a star, that is, the value of the mass density is constant $\rho^*(0) = \rho_c$ at $x = 0$. The dimensionless Fermi momentum at the center $y(0) = y_c$ is defined by the

expression (3.25) of the central density. Thus, if the central density is given, we find the central pressure through the Fermi momentum in EoS. The second condition is called the regularity condition of the mass which is given as $m^*(0)=0$ at the center of a star. The third condition is given as $P^*(x_s)=0$ on the surface of a star, where $x=x_s$ is the dimensionless radius of a star.

From the technical point of view, the numerical integration of the differential equations is carried out from $x_i=10^{-10}$ to $x_f=10^4$, and this interval includes x_s: $x_i<x_s<x_f$. Because the numerical integration of equations starting from $x_i=0$ leads to uncertainty, for that reason, the lower limit of integration is started from $x_i=10^{-10}$. The density corresponding to the radius of the star x_i is $\rho_c(x_i)=10^k Gb^2/c^2$, where $k=4,5,6,...12$. The regularity condition of the mass for x_i is given by

$$m_c(x_i)=\frac{4}{3}\pi x_i^3\rho_c. \tag{3.29}$$

The central pressure can be found from equation (3.26), as it was shown above, through $\rho^*(x_i)=\rho_c$ and $y(x_i)=y_c$. The upper limit of the numerical integration is given by $x_f=10^4$. The numerical solution of systems of equations (3.21) and (3.22) or (3.23) and (3.24) can be found in the range of $x_i\le x\le x_s$. The numerical integration is terminated when the condition $P^*(x_s)=0$ is satisfied. Also, x_s should always be less than x_f. At the end, by means of the expressions (3.16)-(3.20), we can recover dimensions of physical quantities from dimensionless quantities [86].

3.1.4 Results of numerical calculations

The relation between the pressure and mass density of WDs is given by the EoS which is demonstrated graphically in figure 3.1. As you can see in figure 3.1, the pressure and density are proportional to each other.

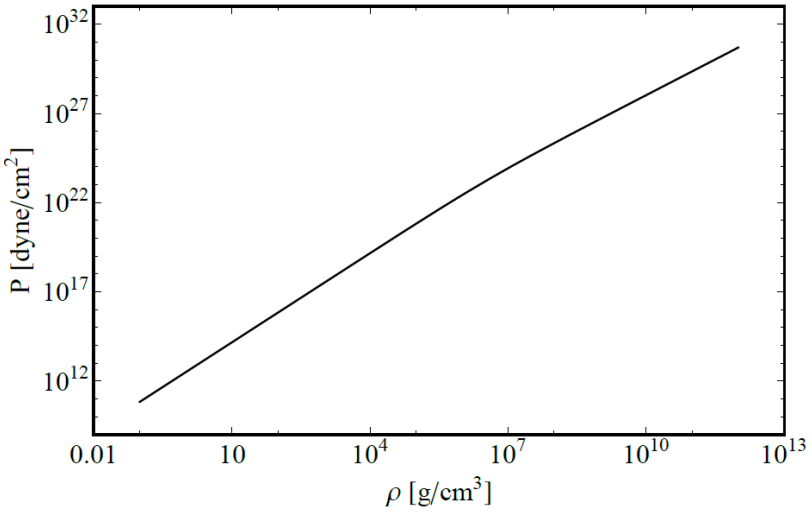


Figure 3.1 – The pressure as a function of the central density for WDs

We can find the relation between the WD mass and its central density by solving the system of equations given in equations (3.21)-(3.22) and (3.23)-(3.24) with the Chandrasekhar EoS given in the equation (3.25)-(3.26) and boundary conditions. This relation is shown in figure 3.2. The mass of the white dwarf star increases with the increasing of the central density, but it cannot increase infinitely. The mass can not exceed the Chandrasekhar limit [7, 104].

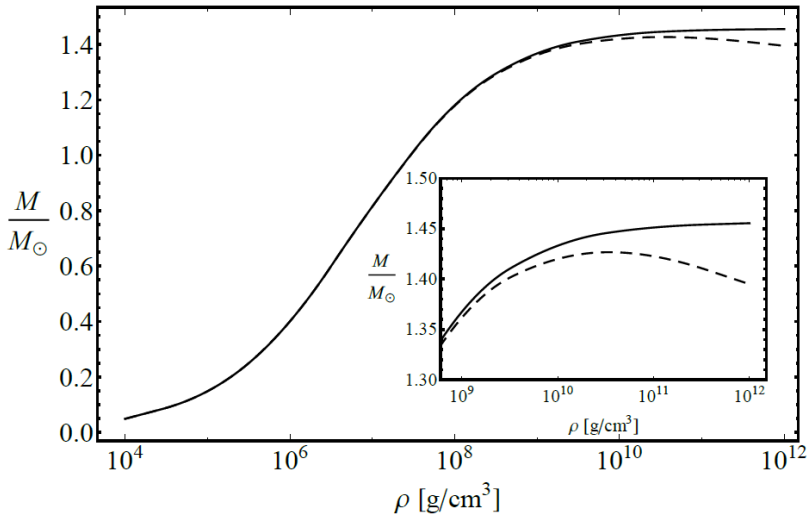


Figure 3.2 – Mass-central density relations of WDs in NG (solid lines) and GR (dashed lines)

Then, we construct the mass-radius relation of WDs in figure 3.3. As one can see from the figure, the main difference of WDs from main sequence stars is the fact that their masses increase when their radii decrease. This feature is explained by the existence of relativistic and quantum corrections in the EoS [105].

The main difference between GR and NG becomes more evident with the increasing of white dwarf mass. The maximum mass in GR is less than the mass in NG and it is associated with the presence of general relativistic corrections in the hydrostatic equilibrium equation. The increase in mass here strengthens the gravitational field. As a consequence, a lower mass is necessary to obtain the required density and pressure in GR compared to NG.

The maximum mass which corresponds to the threshold density in GR is a condition that determines stability. However, in NG, WDs can reach the maximum mass when its radius is zero while the central pressure, the central density and the surface gravitational potential are infinite, but it is not physically possible. There exits a threshold for the central density, hence, central pressure, and this is a condition which determines stability of WDs. If the value of density exceeds this threshold, the white dwarf star becomes a neutron star, otherwise it may explode as a type Ia supernova. Therefore, if one chooses a density of neutronization (inverse beta decay) for WDs composed of ${}^{12}_{6}C$ as a threshold density, and according to this value of the central density one is able to calculate the maximum mass, radius, pressure, and surface gravitational potential both in NG and GR. For example, the maximum mass is 1.447 $M_\odot$ in NG, and 1.425 $M_\odot$ GR.

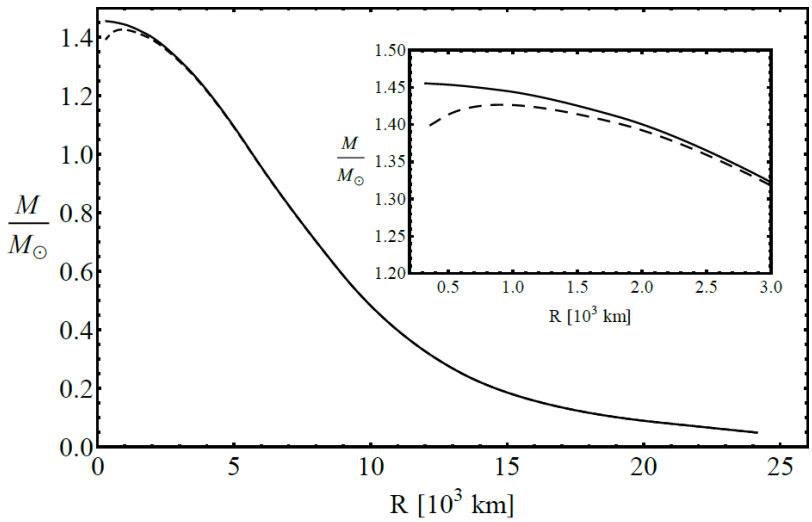


Figure 3.3 – Mass-radius relations of WDs in NG (solid lines) and GR (dashed lines)

An analytical expression for the mass-radius relations of static white dwarf stars has been found. The result of analytical fit is shown in figure 3.4 by the solid line and it is in good agreement with the result of the numerical integrations of stellar structure equations. In figure 3.4 a, the dashed curve denotes the mass-radius relation in NG and the solid one denotes the analytical fit. In figure 3.4 b, the dashed curve denotes the mass-radius relation in GR and the solid one denotes the analytical fit. The analytical expression is given by

$$\frac{M}{M_{\odot}} = \frac{R}{a+dR+eR^2+fR^3+nR^4}, \tag{3.30}$$

where a, d, e, f, n are the constant coefficients. This expression is the same as the expression obtained in [106], but there is a difference in the value of the coefficients. Their values were calculated in NG and GR (table 3.1) and the error is determined to be less than 1%. The form of analytical fit found for static white dwarf stars is the same in NG and GR. The values of coefficients are slightly different from each other [86].

Table 3.1 – The values of coefficients of the analytical expression for mass-radius relation of WDs

Coefficients	Newtonian Gravity	General Relativity
a [km]	6.11	14.65
d [km^0]	0.664	0.665
e [km^{-1}]	$2.26 \cdot 10^{-5}$	$2.17 \cdot 10^{-5}$
f [km^{-2}]	$-1.50 \cdot 10^{-9}$	$-1.38 \cdot 10^{-9}$
n [km^{-3}]	$1.35 \cdot 10^{-12}$	$1.34 \cdot 10^{-12}$

To obtain the solution of stellar structure equations is not a simple task. The analytical fit with an error less than 1 % can be used to save time in order to construct the mass-radius relations in the range of radius from 340 km to 24000 km.

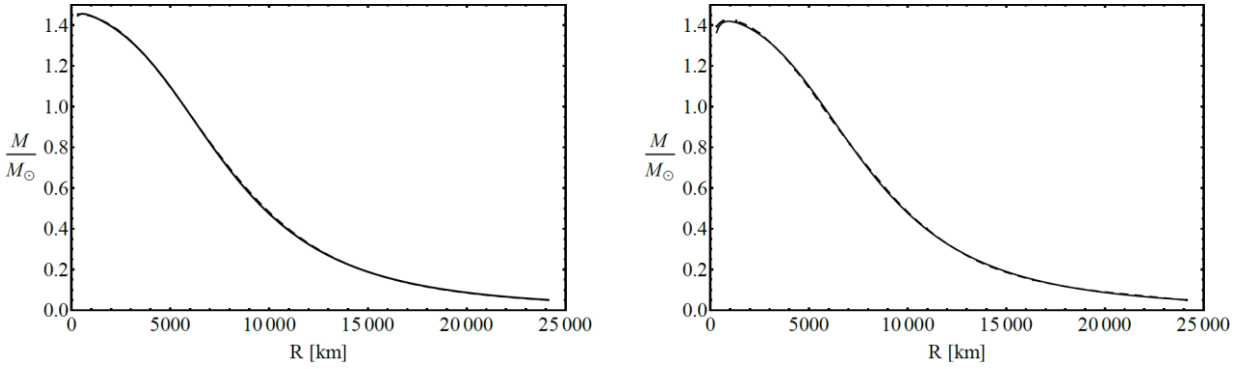


Figure 3.4 – Mass-radius relations of WDs in NG (a) and in GR (b)

The importance of GR for stars can be given by the compactness parameter. The ratio of R_g / R is called the compactness parameter, where $R_g = 2GM/c^2$ is the Schwartzschild radius, R is the radius of a star. As this parameter increases, the gravitational field becomes stronger and, accordingly, the effects of GR become noticeable.

The relation between the compactness parameter and the mass of WD is constructed in figure 3.5. As can be seen from the relation, the smaller a WD is in compactness parameter, the larger it is in mass.

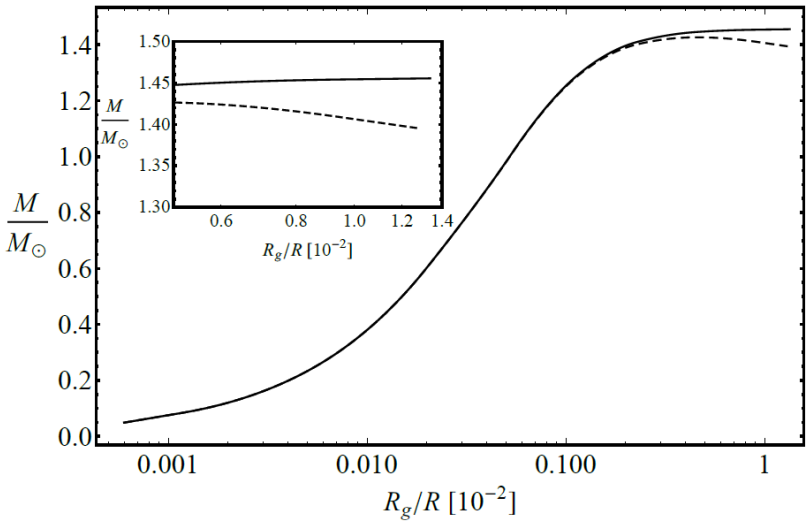


Figure 3.5 – The relation between mass and compactness parameter of WDs in NG (solid lines) and GR (dashed lines)

The relation between the absolute value of the surface gravitational potential of the WD and its radius is shown in figure 3.6. As you can see from formulas (3.27) and (3.28), when the star's radius decreases and its mass increases, as a result, the surface gravitational potential increases. The difference between the surface

gravitational potentials calculated in NG and GR is evident in case of large masses and in small radii [86].

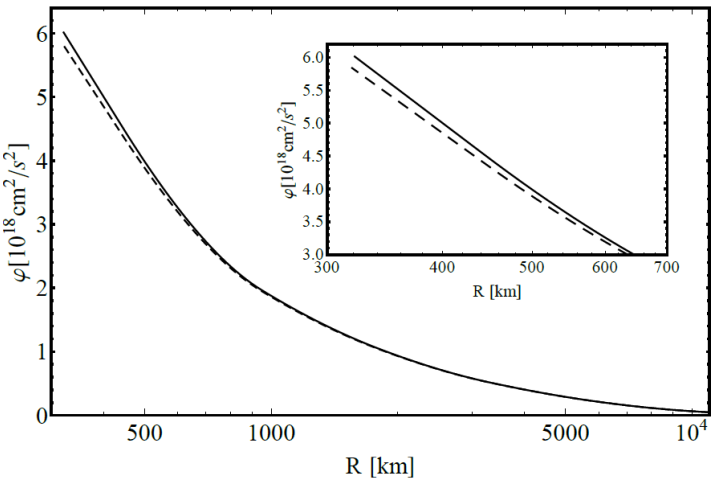


Figure 3.6 – The relation of surface gravitational potential and radius of WDs in NG (dashed curve) and GR (solid curve)

3.2 Static white dwarfs taking into account the effects of finite temperatures and general relativity

3.2.1 Main parameters of white dwarfs and their relations

Figure 3.7 shows the dependence of the total pressure on the total density for selected temperatures T = [0, 10^4, 10^5, 10^6, 10^7, 10^8] K. As can be seen from the figure, the effects of temperature are significant at low densities. The effect of temperature becomes noticeable starting from a temperature of 10^5 K and it goes up with increasing temperature at low densities [27, 90].

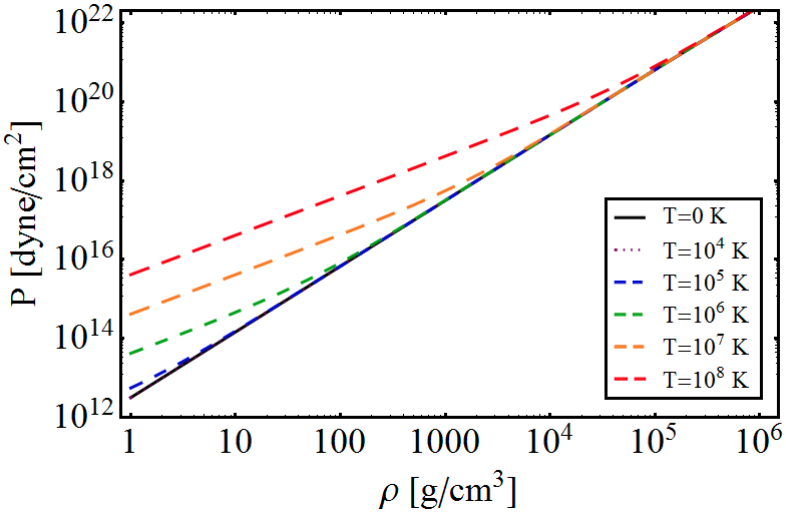


Figure 3.7 – Total pressure as a function of the total mass density for selected temperatures T = (0, 10^4, 10^5, 10^6, 10^7, 10^8) K.

The mass balance and TOV equation completely determines the structure of a spherically symmetric body in hydrostatic equilibrium. By solving the mass balance

and TOV equation for the Chandrasekhar EoS $(\mu = 2)$ at finite temperatures (see subsection 1.2), the mass-radius relation is given in figure 3.8.

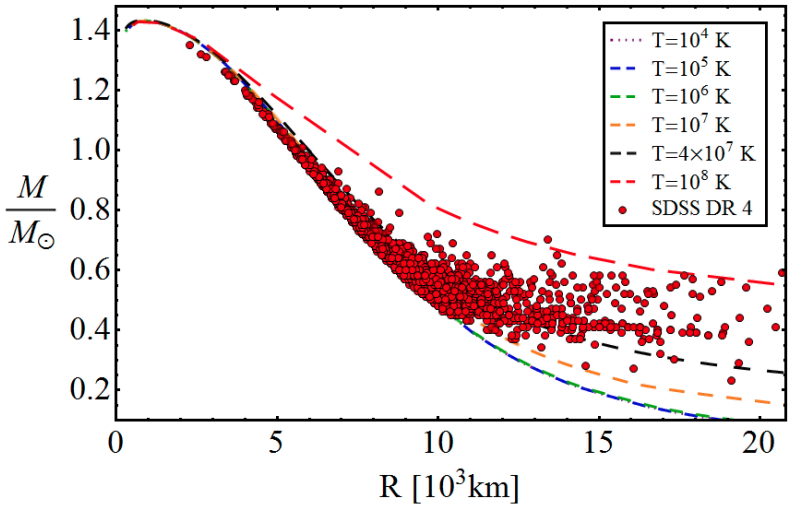


Figure 3.8 – Mass-radius relations at selected temperatures
T = (10^4, 10^5, 10^6, 10^7,10^8) K and data of the SDSS DR 4

It can be seen from figures 3.8 and 3.9 that the effects of finite temperatures are important for low-mass WDs (in figure 3.8, within the mass $M \approx (0.2 - 0.8)M_{\odot}$). Moreover, the role of this effect increases with decreasing mass. This implies that the substance of low-mass WDs cannot be considered completely degenerate.

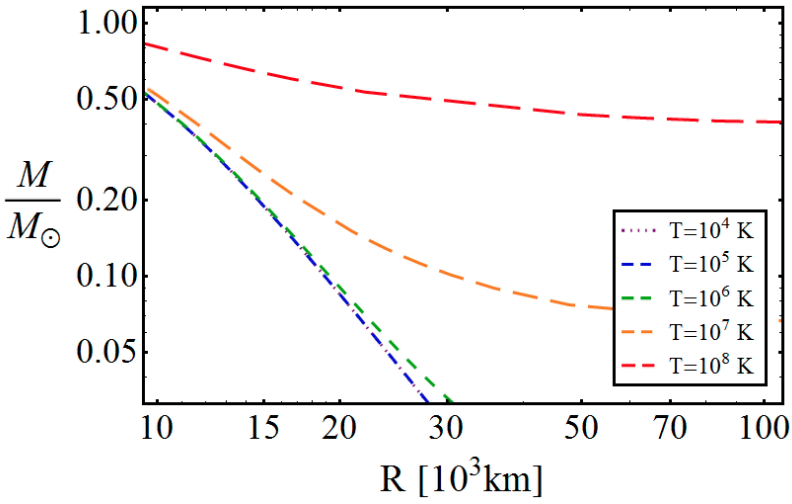


Figure 3.9 – Mass-radius relations at selected temperatures
T = (10^4,10^5,10^6,10^7,10^8) K for the interval of radius R = (10^4-10^5) km

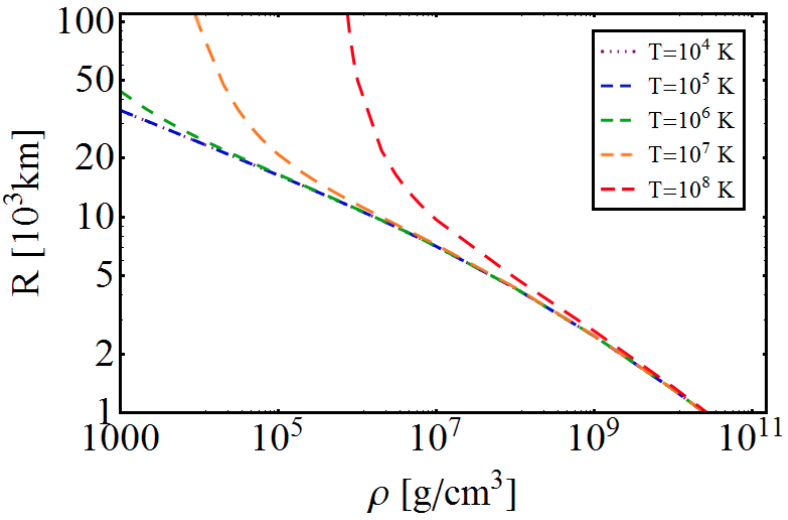


Figure 3.10 – Central density-radius relations at selected temperatures T = (10^4, 10^5, 10^6, 10^7, 10^8) K

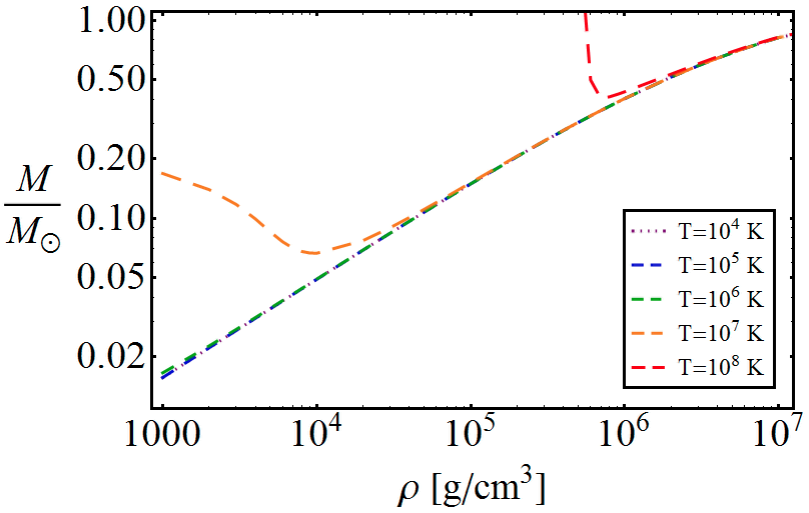


Figure 3.11 – Central density-mass relations at selected temperatures T = (10^4, 10^5, 10^6, 10^7, 10^8) K

As can be seen from figures 3.10 and 3.11, in the relations of the central density-radius and the central density-mass with decreasing central density, the effects of temperatures are more clearly visible, and with an increase in the central density, these effects weaken. That is, temperature effects are especially important for low-mass WDs [27, 90].

3.2.2 Binary systems: white dwarf and millisecond pulsar

A millisecond pulsar is a pulsar with a rotation period in the range of 1 to 10 milliseconds. Similar pulsars were detected in the radio, X-ray and gamma ray ranges (bands) of the electromagnetic spectrum. The theory of the origin of millisecond pulsars has not been fully developed. The most common theory of their formation

states that they begin their life as pulsars with small periods of rotation, but then gradually unwind by accretion. Millisecond pulsars are companions of low-mass X-ray binary systems [107].

For the theoretical estimation of the core temperature, in this work we consider WDs, which are companions of the millisecond pulsars PSR J1738+0333, PSR J1012+5307 and PSR J1911-5958A. In calculations, for simplicity, the core temperature of WDs can be considered isothermal.

a) PSR J1738+0333. In the work of Antoniadis et al. [108], the photometric radius $R = (0.042 \pm 0.004)R_{\odot}$ and the effective surface temperature $T_{eff} = (9130 \pm 150)\,\mathrm{K}$ by using the analysis of the WD atmospheric spectrum and the logarithm of surface gravity $\log_{10}(g) = \log_{10}(GM/R^2) = 6.55 \pm 0.1$ of a WD companion of PSR J1738 + 0333 have been obtained. Details of observation and technical aspects of measurements of the parameters of a binary system can be found in [107].

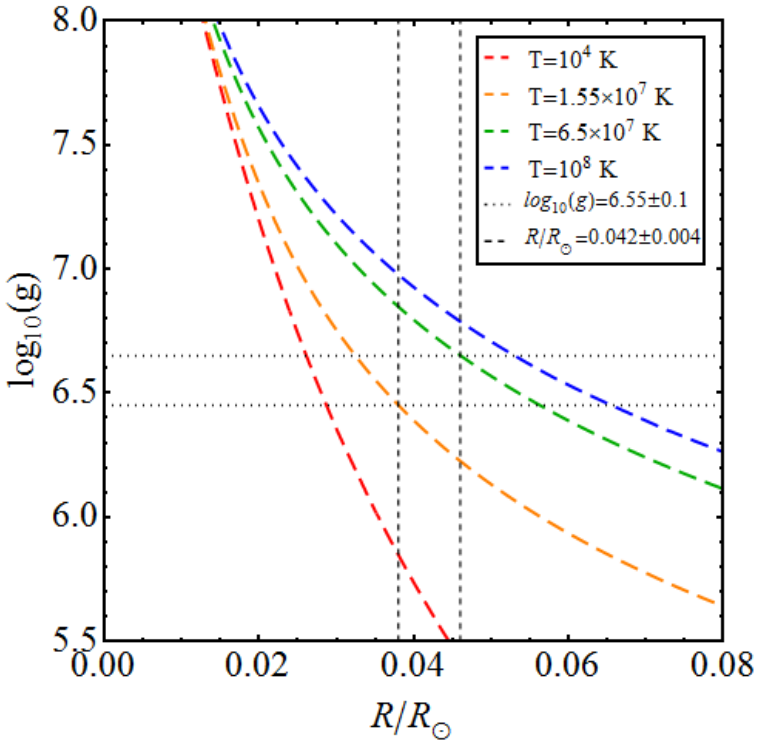


Figure 3.12 – Logarithm of the surface gravity as a function of the radius for selected temperatures T = (10^4, 1.55×10^7, 6.5×10^7, 10^8) K

Figure 6 shows the dependence of the logarithm of surface gravity as a function of the radius of WDs at selected temperatures T = (10^4, 1.55×10^7, 6.5×10^7, 10^8) K of the isothermal core. To estimate the temperature of the isothermal core, observational data for the WD companion of the millisecond pulsar PSR J1738 + 0333 were also plotted. The horizontal dashed and vertical dot-dashed lines in figure 6 show the maximum and minimum values of surface gravity $\log_{10}(g) = 6.55 \pm 0.1$ and photometric radius $R = (0.042 \pm 0.004)R_{\odot}$, respectively. Using these data, it is possible to determine graphically from the figures that the core temperature of the WD

companion of the pulsar PSR J1738+0333 is approximately in the region of $T_c \approx (1.55-6.5)\times 10^7$ K [27].

The obtained theoretical result can be compared with the observation. To do this, we use the Koester formula [109], which relates the surface temperature of a WD to the temperature of its isothermal core

$$\frac{T_{\text{eff}}^4}{g} = 2.05\times 10^{-10} T_c^{2.56}, \tag{3.31}$$

where T_{eff} is the effective surface temperature, T_c is the temperature of the isothermal core, g is the surface gravity (the gravitational acceleration experienced at the surface of an astronomical object). The Koester relation was obtained by solving the heat equation for a degenerate WD matter, taking into account the thickness of the envelope (atmosphere) of WDs and the corrections of the gravitational redshift. For the WD companion of PSR J1738 + 0333, the Koester relation gives the temperature of the isothermal core $T_c = (2.59\pm 0.17)\times 10^7$ K, which, within the margin of error, fully coincides with our theoretical estimation.

b) PSR J1012+5307. In the work of J. A. Panei et al. [110] the parameters of the WD companion of millisecond pulsar PSR J1012+5307, such as a logarithm of the surface gravity $\log_{10}(g) = 6.34\pm 0.2$, mass $M = (0.16 \pm 0.02) M_\odot$ and an effective surface temperature $T_{eff} = (8670\pm 300)$ K are given. In particular, these values of the surface gravity and the mass of the WD companion were used for the graphical estimation of its core temperature.

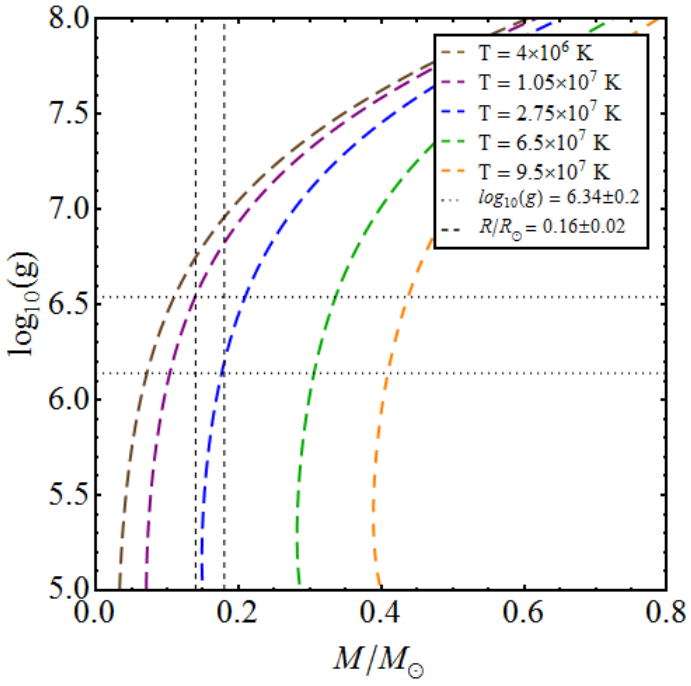


Figure 3.13 – Logarithm of the surface gravity as a function of the mass for selected temperatures T = (10^4, 1.05×10^7, 2.75×10^7, 6.5×10^7, 9.5×10^7) K

The graph of logarithm of the surface gravity $\log_{10}(g)$ as a function of the mass of WDs for selected interior temperatures T = (10^4, 1.05×10^7, 2.75×10^7, 6.5×10^7, 9.5×10^7) K is plotted in figure 3.13. The horizontal dotted lines show the maximum and minimum values of $\log_{10}(g) = 6.34 \pm 0.2$ and the vertical dashed lines are the maximum and minimum values of the mass $M = (0.16 \pm 0.02) M_{\odot}$ of the WD companion of the millisecond pulsar PSR J1012-5307 in the pulsar plus WD binary system.

On the basis of theoretical curves and observational data, the core temperature of the WD companion of the pulsar has been estimated. According to our estimation, it is approximately equal to $T_c = (1{,}05 - 2.75) \times 10^7$ K, while the Koester relation gives $T_c = (2.9 \pm 0.4) \times 10^7$ K. Consequently, the observational and theoretical values of the core temperature T_c correspond in the range $(2.5 - 2.75) \times 10^7$ K.

c) PSR J1911-5958A. In figure 3.14, the mass-radius relation of hot static WDs was obtained at finite temperatures $T = (4\times10^6, 2.75\times10^7, 6.5\times10^7, 9.5\times10^7)$ K. The diagonal dashed and the vertical dot-dashed lines indicate the maximum and minimum values of logarithm of the surface gravity $\log_{10}(g) = 6.44 \pm 0.2$ and photometric radius $R = (0.044 \pm 0.009) R_{\odot}$ of a WD companion of PSR J1911-5958A, respectively.

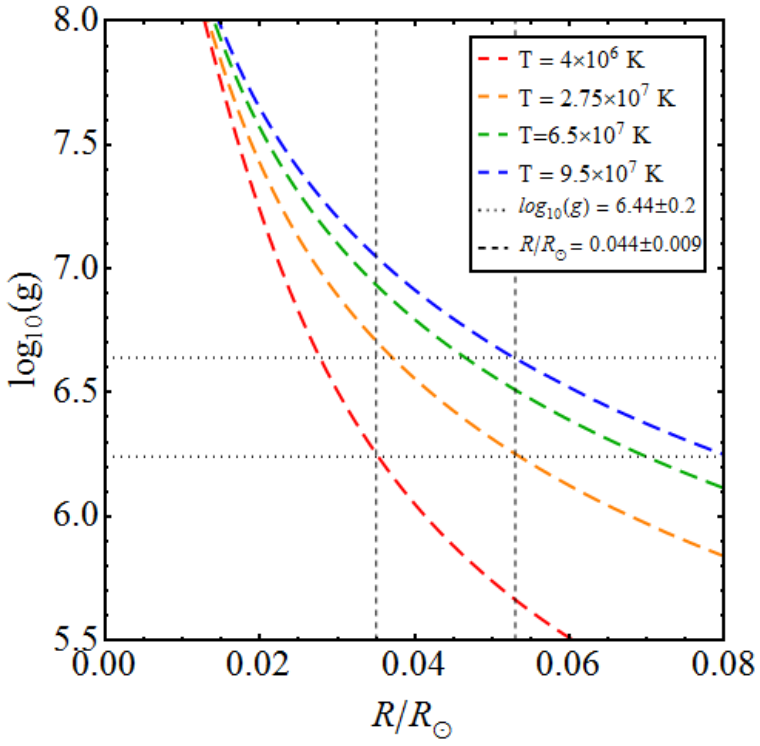


Figure 3.14 – Logarithm of the surface gravity as a function of the radius

From figure 3.14 it is possible to determine graphically the core temperature of a WD in the binary system PSR J1911-5958A as in the previous case. Our estimation

shows that the core temperature of the WD is within the range of $T_c = (2.9 \pm 0.4) \times 10^7$ K. For this WD companion with a logarithm of the surface gravity $\log_{10}(g) = 6.44 \pm 0.2$ and effective surface temperature $T_{eff} = (10090 \pm 150)$ K (see J.A. Panei et al. [110]) the Koester relation gives the core temperature $T_c = (3.35 \pm 0.5) \times 10^7$ K, which, within the error of observation, coincides with our estimation.

Table 3.2 – Parameters of WDs

WD parameters / Sources	Observation				The core temperature of WDs, T_c (10^7 K)	
	T_{eff} (K)	$\log_{10}(g)$	$M/M_\odot$	$R/R_\odot$	Koester relation	Our estimation
PSR J1738+0333	9130±150	6.55±0.1	---	0.042±0.004	2.59±0.17	4.025±2.475
PSR J1012+5307	8670±300	6.34±0.2	0.16±0.02	---	2.9±0.4	1.9±0.5
PSR J1911-5958A	10090±150	6.44±0.2	---	0.044±0.009	3.35±0.5	4.95±4.55

Table 3.2 shows the main observational data and theoretical calculations performed in this work. As can be seen from the table, theoretical calculations within the errors of observation completely correspond [27].

3.3 Static white dwarfs taking into account nuclear composition in general relativity

3.3.1 The catalog of white dwarfs from the Sloan Digital Sky Survey

The first complete catalog of WDs from SDSS was based on the first release of data “Data Release 1”. By analyzing the data from the fourth release of the Data Release 4 catalog [111], the number of spectrally confirmed WDs has approximately doubled. In the seventh version of WD catalog Data Release 7, the total number of WDs has increased more than twice in comparison with the catalog based on the data of DR 4. All the stars from previous releases were also analyzed. More than 8000 new spectrally confirmed WDs were indicated by Kepler and others when analyzing the tenth release of catalog SDSS DR 10 [112, 113].

The criteria for selection of candidates was also improved in comparison with the previous catalogs, as well as, an automated search algorithm was introduced for finding objects which were missed by other selection criteria. It was also the first catalog of WDs on the basis of data fitting of Sloan Digital Sky Survey, stars with hydrogen (DA) and helium (DB) atmospheres, in short, WDs of DA and DB classes. In this section, a detailed analysis was carried out with SDSS DR 10. Although SDSS has increased the number of spectroscopically confirmed WDs by more than an order of magnitude before the start of SDSS, the SDSS catalogs are far from completeness. The procedure for selecting the target of the original SDSS (before DR 8) implied that the choice of a WD for spectroscopy was incomplete. In this subsection we

consider (analyze) the data of new WDs from SDSS DR 4, SDSS DR 10 and SDSS DR 12 [114, 115], which in total were obtained by photometric ways, observing one third of the celestial sphere. This catalog does not contain the stars presented in the previous catalogs, except for corrections in the classification.

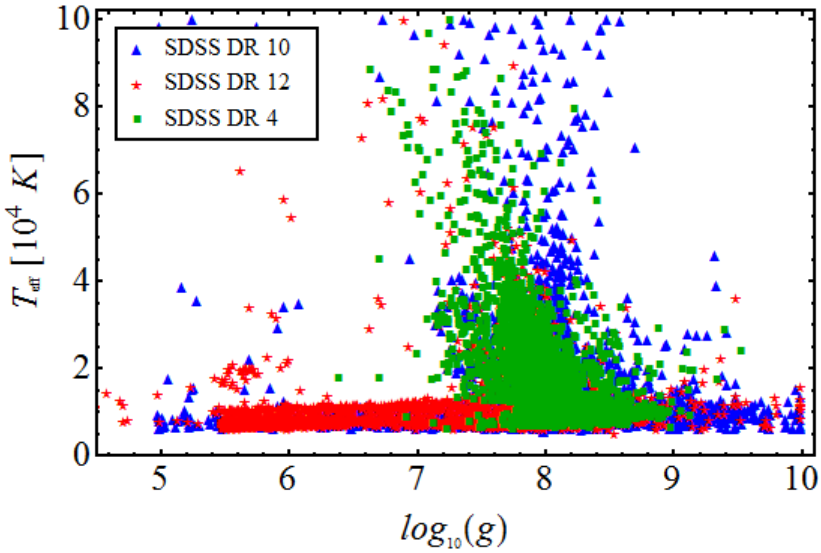


Figure 3.15 – The relationship between the effective temperature and the logarithm of the surface gravity

Figure 3.15 shows the observational data from SDSS DR 4, SDSS DR 10 and SDSS DR 12 of WDs as the relation of the acceleration of gravity on the surface of the star and its effective temperature. Here T_{eff} is the effective surface temperature obtained for all WDs from SDSS DR 4 (green cubes), SDSS DR 10 (blue triangles), SDSS DR 12 (red stars). Hence it can be seen that the majority of WDs has a surface temperature in the range from 5000 K to 40000 K. In turn, the decimal logarithm of the acceleration of gravity on the surface is in the range from 5 to 10 cm/s^2. Observations have shown that there are also hot WDs whose effective temperature can exceed 100,000 K [116]. They are usually young WDs [29].

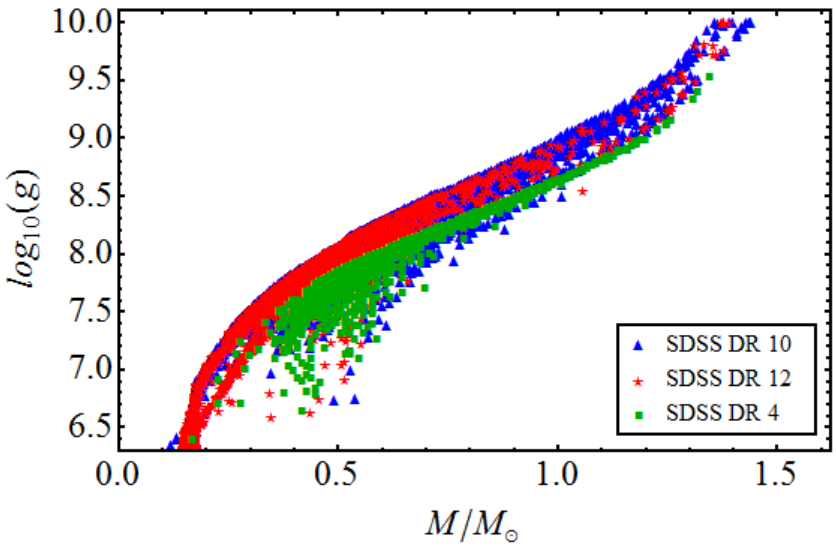


Figure 3.16 – The logarithm of acceleration of gravity and the mass of WDs taken from SDSS DR 4, SDSS DR 10, SDSS DR 12

Figure 3.16 shows the relation between the surface gravity and the mass of WDs in terms of solar mass. From this figure it follows that the larger the mass, the greater the surface gravity or the acceleration of free fall on the surface, and vice versa. The average mass of WDs ranges from 0.3 to 1.0 solar masses. Recall that the mass in this graph was calculated on the basis of various models of equations of state, for example, such as the Salpeter EoS, taking into account the temperature and nuclear composition of matter.

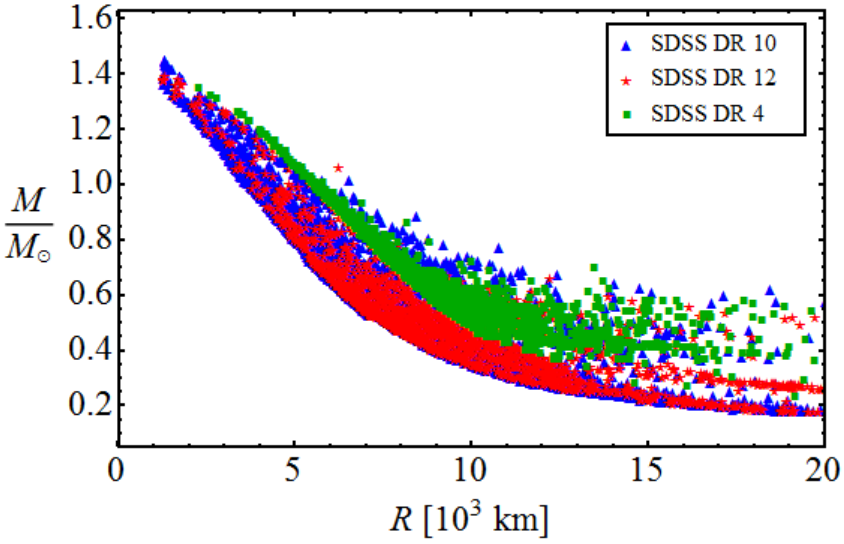


Figure 3.17 – Mass-radius relation of WDs taken from SDSS DR 4, SDSS DR 10, SDSS DR 12

Figure 3.17 shows the values of the mass and radius of WDs of SDSS DR 4, SDSS DR 10, SDSS DR 12 catalogs. The effective temperature and surface gravity were found from the observations. To calculate the radius, as well as the mass,

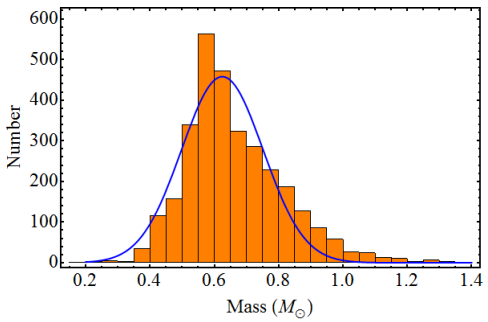
various models are used, taking into account the effects of the finite temperature and the nuclear composition of the WD matter and other parameters.

The maximum, minimum and average observed values of the surface gravity (the acceleration of free fall on the surface) and the surface temperature of WDs are given in table 3.3 [29].

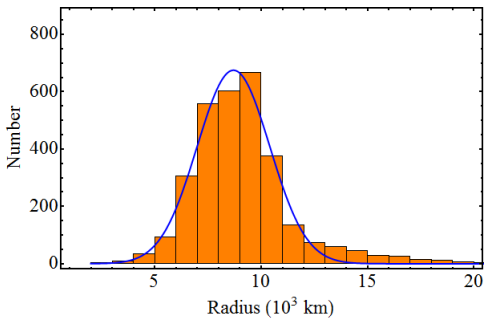
Table 3.3 – The values of the surface gravity and the surface temperature of WDs from SDSS DR 4, SDSS DR 10, SDSS DR 12

Catalogs	$\log_0(g)$			T_{eff}, K		
	Minimum	Average	Maximum	Minimum	Average	Maximum
DR 4	6.4	8.03	9.53	5 910	18 683.8	125 360
DR 10	4	8.05	10	5 327	13 312.1	100 000
DR 12	4.44	6.82	9.99	4 870	10 220.8	99 999

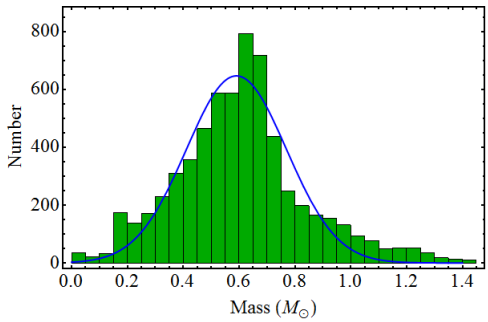
Figure 3.18 shows the histograms of the distribution of masses and radii in the SDSS DR 4, SDSS DR 10 and SDSS DR 12. In the SDSS DR 4, the average mass of WDs is about 0.6 solar masses; in the SDSS DR 10 about 0.6 solar masses and in the SDSS DR 12 about 0.2 solar masses. Most WDs has a radius in the region of 5000-10000 km.



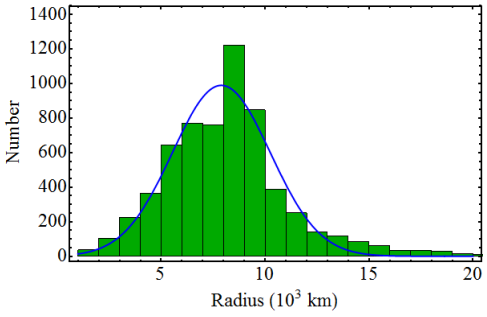
a)



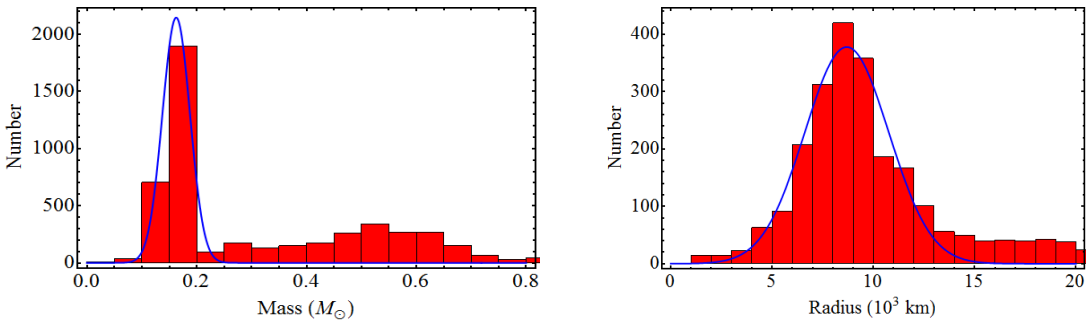
b)



c)



d)



e) f)

a) masses from SDSS DR 4, b) radii from SDSS DR 4, c) masses from SDSS DR 10, d) radii from SDSS DR 10, e) masses from SDSS DR 12, f) radii from SDSS DR 12

Figure 3.18 – Histogram and Gaussian distribution of masses and radii of WDs

The maximum, minimum and average values of the calculated data for mass and radius in the works of Kepler et al. [112-115] are shown in table 3.4.

Table 3.4 – Maximum, minimum and average values of mass and radius of WDs of Sloan Digital Sky Survey Data Releases 4, 10 and 12

Catalogs	Mass ($M_\odot$)			Radius (km)		
	Minimum	Average	Maximum	Minimum	Average	Maximum
DR 4	0.170	0.657	1.35	2 294.28	9 219.84	35 653.7
DR 10	0.041	0.605	1.44	1 340.94	9 384.91	262 361
DR 12	0.042	0.329	1.39	1 061.56	34 259.2	286 249

3.3.2 Results of numerical calculations

The Salpeter EoS allows one to take into account the Coulomb interaction, the Thomas-Fermi correction, and the nuclear composition of the WD. In figures 3.19-3.21, we have constructed the relations between mass M and radius R, mass M and central density ρ, central density ρ and radius R for zero-temperature WDs composed of ^{4}He, ^{12}C, ^{16}O, ^{20}Ne, ^{24}Mg, ^{28}Si and ^{56}Fe (by the Salpeter EoS) and $\mu = 2$ (by the Chandrasekhar EoS) within the framework of GR. It can be seen from the figures that the heavier the element in WDs, the smaller the upper limit of the mass of WDs [29].

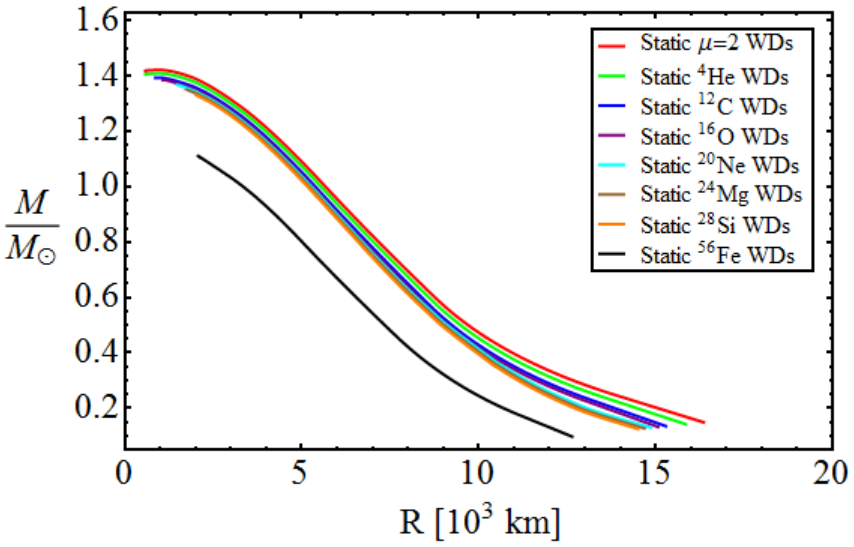


Figure 3.19 – Mass-radius relations of WDs
for the different nuclear compositions

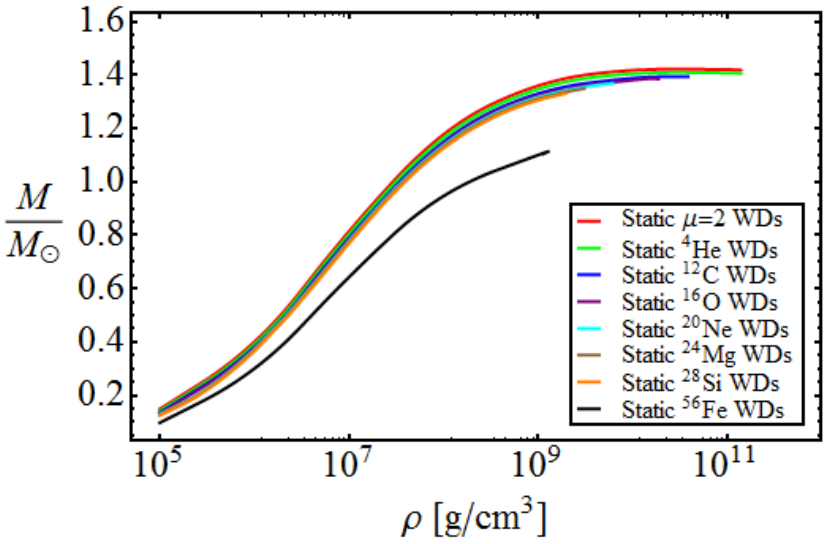


Figure 3.20 – Mass as a function of the central density of WDs
for different nuclear compositions

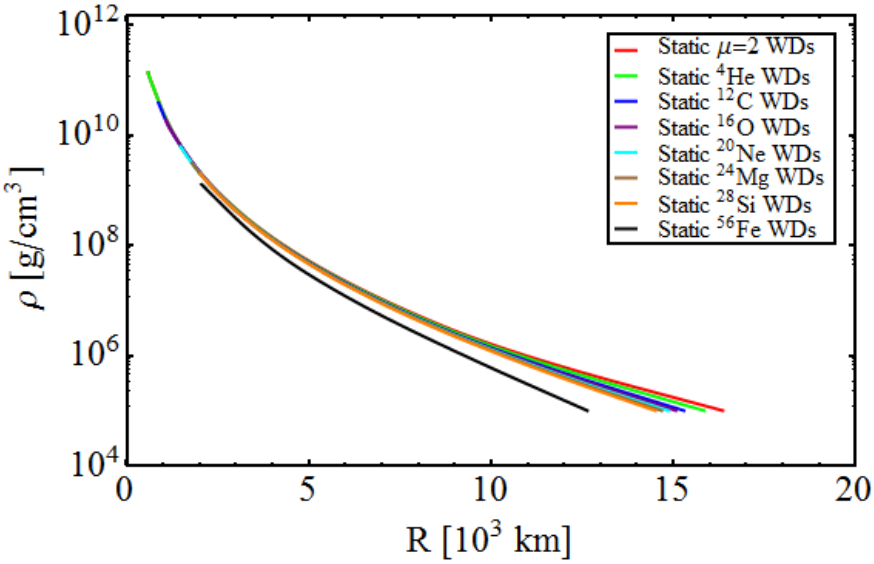


Figure 3.21 – Central density versus radius of WDs
for different nuclear compositions

Moreover, it should be noted that the neutronization threshold (inverse beta decay) for a WD with a uniform nuclear composition has been taken into account in the Salpeter EoS. This effect puts restrictions on the upper value of the central density and, consequently, the mass of WDs. The threshold of inverse beta decay for different compositions is different. The neutronization threshold density is $\rho_C = 1.37 \times 10^{11}\, g/cm^3$ for ${}^{4}_{2}\mathrm{He}$, $\rho_C = 3.90 \times 10^{10}\, g/cm^3$ for ${}^{12}_{6}\mathrm{C}$, $\rho_C = 1.90 \times 10^{10}\, g/cm^3$ for ${}^{16}_{8}\mathrm{O}$, $\rho_C = 6.21 \times 10^{9}\, g/cm^3$ for ${}^{20}_{10}\mathrm{Ne}$, $\rho_C = 3.16 \times 10^{9}\, g/cm^3$ for ${}^{24}_{12}\mathrm{Mg}$, $\rho_C = 1.97 \times 10^{9}\, g/cm^3$ for ${}^{28}_{14}\mathrm{Si}$, $\rho_C = 1.14 \times 10^{9}\, g/cm^3$ for ${}^{56}_{26}\mathrm{Fe}$ [5].

Figure 3.8 demonstrates the mass-radius relations for static WDs in the case of the Chandrasekhar EoS at different temperatures in GR (by the TOV equation); they were compared with data (mass and radius) from the SDSS DR 4. It should be noted that the values of temperature that we have used is the temperature of the isothermal core of a WD. Consequently, the consideration of the finite temperature effects describes almost completely the data from the SDSS DR 4. It is also possible to construct the mass-radius relations at finite temperatures for other equations of state, for example, for the FMT EoS [25, 29].

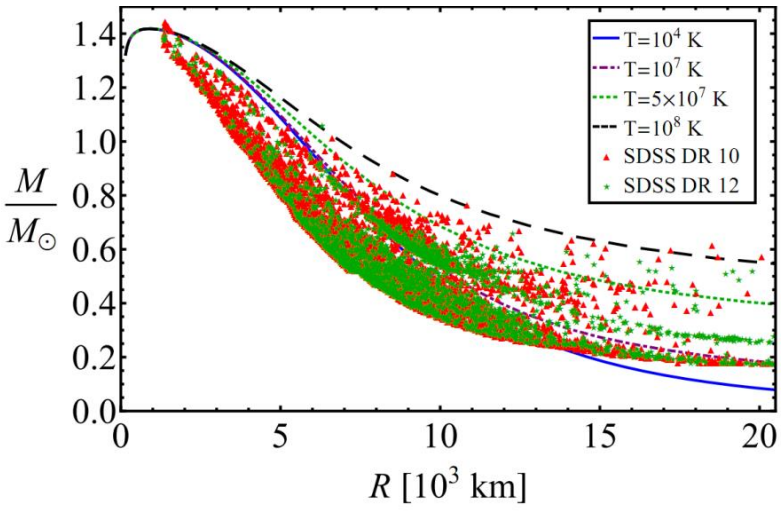


Figure 3.22 – The mass-radius relations of WDs at finite temperatures (the Chandrasekhar EoS) and observational data from the SDSS DR 10 (red triangles) and the SDSS DR 12 (green stars)

But, in the case of SDSS DR 10 and SDSS DR 12, as can be seen from Figure 3.22, even the consideration of finite temperatures in the Chandrasekhar EoS cannot explain some WDs. Because of this, it is necessary to use the EoS of Salpeter, which takes into account the important properties of the WD matter.

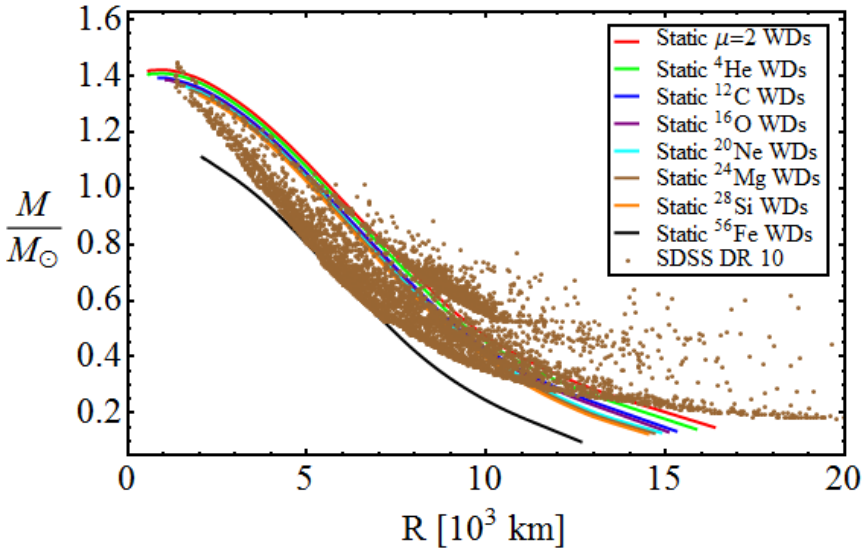


Figure 3.23 – The mass-radius relations of WDs and observational data from SDSS DR 10 (brown dots)

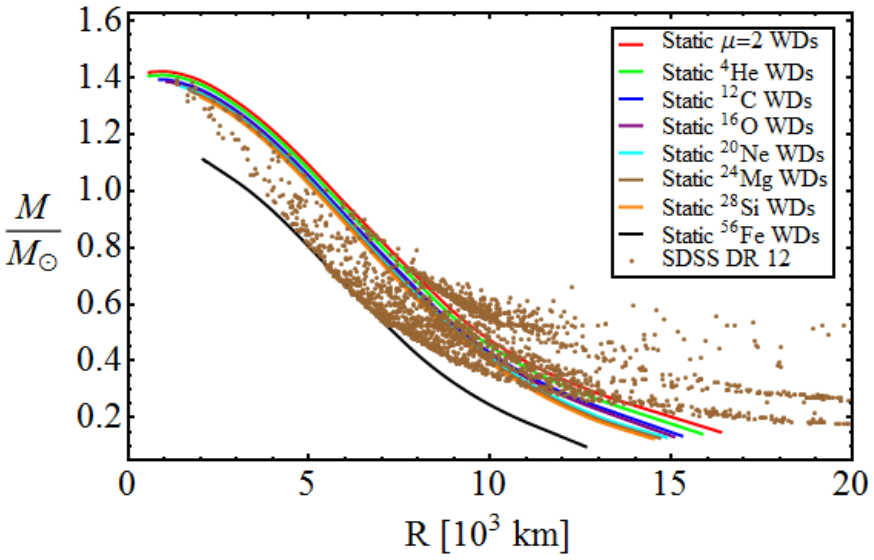


Figure 3.24 – The mass-radius relations of cold WDs and observational data from SDSS DR 12 (brown dots)

As can be seen from the figures 3.23 and 3.24 that the consideration of WDs using the Salpeter EoS can explain the distribution of some WDs. It follows that the consideration of the nuclear composition of the matter of WDs is critically important [29].

3.4 Summary

First, we have calculated the main parameters $(R, M, \rho, P, \varphi, R_g/R)$ of white dwarf stars in NG and GR. Newtonian and relativistic equations of stellar structure and Chandrasekhar EoS have been used to calculate the main parameters. All the differential equations have been nondimensionalized and then numerically solved by predetermined boundary conditions. As a result of computations, pressure-central density, mass-central density, mass-radius, mass-compactness parameter and surface gravitational potential-radius relations have been constructed, and the significance of GR effects in large masses, large densities and small radii have been demonstrated. The analytical expression for the mass-radius relation have been found and its error has been evaluated.

Second, we have studied the properties of non-rotating hot WDs within the framework of the general theory of relativity. For this purpose, the TOV equation together with the mass balance equation has been integrated numerically using the Chandrasekhar EoS at finite temperatures. As a result, the central density-mass, the central density-radius, and the mass-radius relations for hot WDs were obtained. Studies show that effects of finite temperatures significantly affect to the structure of WDs at low densities, that is, they play a key role for low-mass WDs. Apart from this, it has been shown that taking into account the effects of finite temperatures can explain the calculated masses and radii of WDs from the SDSS DR 4. Therefore, in order to construct a realistic model of WDs, the effects of the finite temperatures

must be taken into account properly. Our calculations fully confirm the correctness of the conclusions made in Ref. [25].

The temperatures of isothermal cores of some WD companions of millisecond pulsars PSR J1738+0333, PSR J1012+5307 and PSR J1911-5958A were also estimated in the subsection. In parallel, these estimated temperatures were verified using the Koester relation. The approach used in this subsection can be considered as an alternative way of calculating the core and surface temperatures of a WD.

Third, the observational data from SDSS DR 4, SDSS DR 10 and SDSS DR 12 catalogs were analyzed. It was shown that for SDSS DR 10 and SDSS DR 12 it is not enough to take into account only the finite temperature effects. Therefore, the main parameters of static cold WDs were theoretically calculated using the Salpeter EoS in GR. Mass-radius, mass-central density, central density-radius relations were constructed for different nuclear compositions in GR. It is shown that the consideration of WDs using the Salpeter EoS can explain the distribution of some WDs from SDSS DR 10 and SDSS DR 12 on the plotted graphs, which cannot be interpreted with the inclusion of temperature only as in the case of SDSS DR 4. It was shown that the largest number of WDs has a mass of 0.6 solar masses in SDSS DR 4, SDSS DR 10, and 0.2 solar masses in SDSS DR 12. The radii of most WDs are in the range from 5000 to 10 000 km. The maximum value of the surface temperature is 125360 K in SDSS DR 4, 100 000 K in SDSS DR 10 and ~100000 K in SDSS DR 12. The minimum value of effective temperature is 5 910 K in SDSS DR 4, 5 327 K in SDSS DR 10, and 4 870 K in SDSS DR 12.

As a result of all calculations and analyzes, it was shown that taking into account the nuclear composition, the Coulomb interaction, the Thomas-Fermi correction and the neutronization thresholds (consideration using the Salpeter EoS) in GR are very important for explaining the observed data from the SDSS DR 4, SDSS DR 10, SDSS DR 12 catalogs.

4 EQUILIBRIUM CONFIGURATIONS OF ROTATING WHITE DWARFS

In physics, rotation can be the cause of a lot of changes in the structure of any system. In the case of astronomical objects such as planets and stars, rotation plays a important role. Rotation does not only change the shape of the astronomical objects but also affects to the processes occurring inside stars, for instance, it may decelerate or accelerate thermonuclear reactions under certain conditions, it changes the gravitational field outside the objects and it is one of the main factors that determines the lifetime of all stars (WDs, NSs, giant and main sequence stars, so on) [16, 17, 117-121]. For example, let us consider rotating WDs in the framework of NG (subsection 4.1) [122-126] and GR (subsection 4.2) [91, 127-130].

4.1 Rotating white dwarfs in Newtonian gravity

A static WD has a limiting mass of $1.44\,M_{\odot}$ which is called as the Chandrasekhar mass limit [7]. The central pressure and density corresponding to this limit determine the evolution of WDs. If the WD rotates, then because of the centrifugal forces the central pressure and density decrease [5, 131]. In order to recover the initial values of the central density and pressure of a rotating star one needs to add extra mass. Here we see that a rotating star with the same values for central density and pressure, as those of a static star, possesses a larger mass [48].

In the subsection 4.1, the HF is applied to study equilibrium configurations in the framework of NG. This method allows one to study in a simple manner the properties of the interior gravitational field in the case of non-rotating as well as uniformly rotating stars in hydrostatic equilibrium. It is shown that the gravitational equilibrium conditions reduce to a system of ordinary differential equations which can be solved numerically. All the relevant equations up to the second order in the angular velocity are derived. In addition, the total mass, the equatorial and polar radii, the moment of inertia, the quadrupole moment, the eccentricity and the gravitational binding energy of the rotating body are calculated. The procedure of calculatation the gravitational Love number is also shown. We test the approach in the case of WDs and show its compatibility with the known results in the literature.

In this subsection 4.1, the equations which describe the equilibrium configurations of slowly rotating stars are obtained using the HF [43]. The preeminence of this method is that it allows us to consider in a simple way the influence of the rotation on the interiors properties of the gravitational source. Indeed, we will see that the complexity of the differential equations, which govern the dynamical properties of equilibrium configurations, is reduced to a high degree. When solving this kind of problems in astrophysics, astronomy and celestial mechanics, it is handy to consider the interior structure of planets and stars as being described by a fluid. In the case of slow rotation, we obtain equations that are valid for any fluid up to the second order in the angular velocity [122].

As a result we derive the equations defining the main parameters of the rotating equilibrium configuration such as the radius, mass, gravitational potential, moment of inertia, quadrupole moment and angular momentum as functions of the central

density and angular velocity. Moreover, it is shown how to calculate the ellipticity and by means of it the gravitational Love number [132]. In turn, these parameters are of great importance in defining the evolution of a star.

In order to pursue all these issues in detail we revisit the HF in NG for a slowly rotating configuration as the calculation of its equilibrium properties is much more simpler, because then the rotation can be considered as a small perturbation of an already-known static configuration. We therefore will consider in this section a rotating configuration under the following conditions [43].

– A one-parameter EoS is defined, $p = p(\rho)$, where ρ is the density and p is the pressure of matter [133].

– A non-rotating equilibrium configuration is calculated employing this EoS and the Newtonian equations of hydrostatic equilibrium for spherical symmetry.

– Reflection and axial symmetry. The configuration is symmetric with respect to a plane perpendicular to the axis of rotation.

– A uniform angular velocity is slow enough so that the changes in energy density, pressure and gravitational field are small.

– Slow rotation. This requirement implies that the angular velocity Ω of the star

$$\Omega^2 << \frac{GM}{a^3}, \tag{4.1}$$

where a is the radius of non-rotating configuration, M is its mass, G is the gravitational constant. Hence, the condition in equation (4.1) also means

$$\Omega << \frac{c}{a}, \tag{4.2}$$

where c is the speed of light.

– The Newtonian field equations are expanded in powers of the angular velocity and the perturbations are calculated by retaining only the first- and second-order terms [122-124].

In the present section, the equations necessary to study this problem are obtained explicitly. The issue of describing rotating configurations in NG has been studied in a lot of papers and literatures [9-14, 133-137]. In this section, we will use the HF, which was originally proposed in GR, to consider a non-relativistic Newtonian configuration. No knowledge of relativistic physics is necessary, because only the very intuitive coordinate approach of the HF is utilized in order to handle the NG equation and the corresponding equilibrium condition. It is worth mentioning that the HF has been recently extended for relativistic configurations up to the fourth order terms in angular velocity [67].

In Newtonian gravity the equilibrium configuration of uniformly rotating stars are found by the solution of the three equations of Newtonian hydrostatic equilibrium [5, 43, 131]. They are

1) the Newtonian field equation:

$$\nabla^2\Phi(r,\theta)=4\pi G\rho(r,\theta); \tag{4.3}$$

where ρ is the density and Φ is gravitational potential of a fluid mass rotating with a constant angular velocity Ω;

2) the EoS that shows the relation between density ρ and pressure p is assumed to have a one-parameter form

$$p=p(\rho); \tag{4.4}$$

3) the equation of hydrostatic equilibrium for uniformly rotating configurations which can be written in following form

$$\frac{d\vec{v}}{dt}=-\frac{1}{\rho}\vec{\nabla}p-\vec{\nabla}\Phi, \tag{4.5}$$

where

$$\vec{v}=\frac{d\vec{r}}{dt}=\vec{\Omega}\times\vec{r}. \tag{4.6}$$

For rotation with constant Ω, we obtain that

$$\frac{d\vec{v}}{dt}=\vec{\Omega}\times\vec{v}=\vec{\Omega}\times\left(\vec{\Omega}\times\vec{v}\right)=-\frac{1}{2}\vec{\nabla}\left(\vec{\Omega}\times\vec{v}\right)^2. \tag{4.7}$$

Consequently, inserting this expression in (4.5), we get

$$-\frac{1}{2}\vec{\nabla}\left(\vec{\Omega}\times\vec{v}\right)^2=-\frac{1}{\rho}\vec{\nabla}p-\vec{\nabla}\Phi \tag{4.8}$$

or

$$\frac{dp}{\rho}-\frac{1}{2}d\left(\vec{\Omega}\times\vec{v}\right)^2+d\Phi=0, \tag{4.9}$$

which can be written in terms of its first integral

$$\int_0^p\frac{dp(r,\theta)}{\rho(r,\theta)}-\frac{1}{2}\Omega^2r^2\sin^2\theta+\Phi(r,\theta)=0, \tag{4.10}$$

where θ is the polar coordinate and r is the radial coordinate and of the rotating configuration.

The main task now is to expand the equations of Newtonian hydrostatics in powers of Ω^2. The solution to the first term of the expansion is given by $\Phi^{(0)}$, $p^{(0)}$

and $r^{(0)}$ in the absence of rotation. After that, we need to find the equations which govern the second-order terms. It is expected that the resulting differential equations can be integrated in terms of the known static solution [122-124].

4.1.1 Definition of coordinates

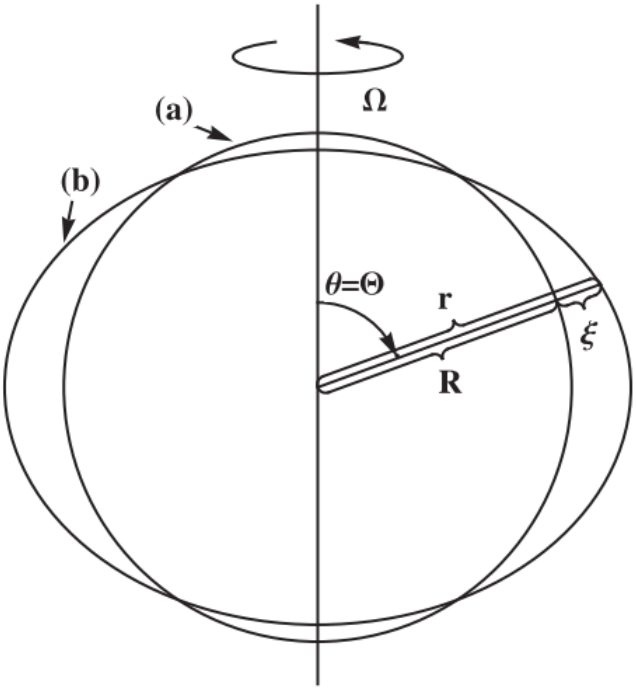
An important point to be considered is the choice of the coordinate system in which the expansions in powers of Ω are carried out. As indicated by Hartle in 1967 [43], one should be very careful when considering perturbation near the surface of the star. Indeed, a simple expansion of the density as a function of the old polar coordinates r, θ is not valid throughout the star as the surface of the configuration will be displaced from its static position and the perturbation in the density may be finite where the unperturbed density vanishes. Thus, following Hartle's formalism [43] we select a coordinate transformation such that the density of the star in terms of the new radial coordinate is the same as in the non-rotating configuration:

$$\rho\left[r\left(R,\Theta\right),\Theta\right]=\rho\left(R\right)\;=\;\rho^{(0)}\left(R\right). \tag{4.11}$$

Therefore, the relation between the old coordinates (r,θ) and the new coordinates $\left(R,\Theta\right)$ are given by

$$\theta=\Theta,\qquad r=R+\xi\left(R,\Theta\right)+O\left(\Omega^{4}\right). \tag{4.12}$$

The function $r\left(R,\Theta\right)$ then replaces the density as a function to be calculated in the rotating configuration. These definitions are clearly demonstrated in figure 4.1.



The surface (a) is the surface of constant density $\rho(R)$ in the non-rotating configuration. The surface (b) is the surface of constant density $\rho(R)$ in the rotating configuration (reproduced from [43]).

Figure 4.1 – Definition of the coordinates R,Θ and the displacement $\xi(R,\Theta)$

According to the HF, we are always free to consider the rotating configuration as a perturbation of a static configuration with the same central density. Hence, in the R, Θ coordinate system, the density (4.11) and pressure are known functions of R

$$p\left[r\left(R,\Theta\right),\Theta\right] = p(R) = p^{(0)}(R) \tag{4.13}$$

related by the one-parametric EoS [122-124].

4.1.2. Spherical harmonics

The expansion of r in terms of Ω^2 is given by equation (4.12) and the expansion of the gravitational potential Φ can be represented as

$$\Phi(R,\Theta) \approx \Phi^{(0)}(R) + \Phi^{(2)}(R,\Theta) + O\left(\Omega^4\right), \tag{4.14}$$

where $\Phi^{(0)}(R)$ is the unperturvated term of the potential and $\Phi^{(2)}(R,\Theta)$ is the perturbed term. Calculating the Taylor expansion in terms of the new the coordinates, on gets

$$\Phi(r,\theta)=\Phi(R+\xi,\Theta)\approx\ \Phi(R,\Theta)+\xi\frac{d\Phi(R,\Theta)}{dR}+O(\Omega^4)\approx$$
$$\approx\Phi^{(0)}(R)+\ \xi\frac{d\Phi^{(0)}(R)}{dR}\ +\Phi^{(2)}(R,\Theta)+O(\Omega^4). \tag{4.15}$$

In order to simplify the equations we take the Taylor series of the functions ξ and $\Phi^{(2)}$ in spherical harmonics

$$\xi(R,\Theta)=\sum_{l=0}^{\infty}\xi_l(R)P_l(\cos\Theta),\qquad \Phi^{(2)}(R,\Theta)=\sum_{l=0}^{\infty}\Phi_l^{(2)}(R)P_l(\cos\Theta), \tag{4.16}$$

where $P_l(\cos\Theta)$ are the Legendre polynomials.

Now let us perform the computations in detail taking the polar axis to be the axis of rotation. Using the expressions for the Legendre polynomials $P_0(\cos\Theta)=1$ and $P_2(\cos\Theta)=\frac{1}{2}(3\cos^2\Theta-1)$, it is easy to show that

$$\sin^2\Theta=\frac{2}{3}[P_0(\cos\Theta)-P_2(\cos\Theta)], \tag{4.17}$$

From here we see that l accepts only two values, namely, 0 and 2. The equations for $\xi_l(R)$, $\Phi_l^{(2)}(R)$, with $l\geq 4$ are thus independent of Ω and their solution is

$$\xi_l=0\ ,\qquad \Phi_l^{(2)}=0\ ,\qquad l\geq 4. \tag{4.18}$$

Rewriting the condition of hydrostatic equilibrium (4.10) in coordinates R,Θ and expanding it in spherical harmonics by using equations (4.11), (4.14), and (4.16), we obtain

$$\int_0^p\frac{dp^{(0)}(R)}{\rho(R)}-\ \frac{1}{3}\Omega^2R^2\ [P_0(\cos\Theta)-P_2(\cos\Theta)]+\ \Phi^{(0)}(R)+$$
$$+\sum_{l=0}^{n}\Phi_l^{(2)}(R)P_l(\cos\Theta)+\sum_{l=0}^{n}\xi_l(R)P_l(\cos\Theta)\frac{d\Phi^{(0)}(R)}{dR}=\text{const}. \tag{4.19}$$

We now gather the terms proportional to $\sim\Omega^0$ and Ω^2 with $l=0,2$ and derive:

$$\int_0^p\frac{dp^{(0)}(R)}{\rho(R)}\ +\ \Phi^{(0)}(R)=\text{const}^{(0)}, \tag{4.20}$$

$$-\frac{1}{3}\Omega^2R^2\ +\ \Phi_0^{(2)}(R)+\xi_0(R)\frac{d\Phi^{(0)}(R)}{dR}=\text{const}_0^{(2)}, \tag{4.21}$$

$$\frac{1}{3}\Omega^2R^2\ +\ \Phi_2^{(2)}(R)+\xi_2(R)\frac{d\Phi^{(0)}(R)}{dR}=0, \tag{4.22}$$

where const is defined as $\text{const}=\text{const}^{(0)}+\text{const}_0^{(2)}P_0(\cos\Theta)$, so that $\text{const}^{(0)}$ and $\text{const}_0^{(2)}$ are found from the sewing between the internal and external solutions. The first of the above equations corresponds to the Newtonian hydrostatic equation for a non-rotating configuration.

Using the same procedure, the Newtonian field equation becomes

$$\nabla^2\Phi(r,\theta)=\frac{1}{r^2}\frac{\partial}{\partial r}\left(r^2\frac{\partial\Phi(r,\theta)}{\partial r}\right)+\frac{1}{r^2\sin\theta}\frac{\partial}{\partial\theta}\left(\sin\theta\frac{\partial\Phi(r,\theta)}{\partial\theta}\right)=$$

$$=\nabla_r^2\Phi(r,\theta)+\frac{1}{r^2}\nabla_\theta^2\Phi(r,\theta)\approx\nabla_r^2\Phi^{(0)}(r)+\nabla_r^2\Phi_0^{(2)}(r)+$$

$$+\nabla_r^2\Phi_2^{(2)}(r)P_2(\cos\theta)+\frac{1}{r^2}\nabla_\theta^2\Phi_2^{(2)}(r)P_2(\cos\theta)=4\pi G\rho(r,\theta). \tag{4.23}$$

Since the functions $\Phi_0^{(2)}(r)$ and $\Phi_2^{(2)}(r)$ are already proportional to Ω^2, we can directly write them in (R,Θ) coordinates. But $\nabla_r^2\Phi^{(0)}(r)\approx\nabla_R^2\Phi^{(0)}(R)+\xi(R,\Theta)\frac{d}{dR}\nabla_R^2\Phi^{(0)}(R)$ (see [122]). Therefore

$$\nabla^2\Phi(r,\theta)=\nabla_R^2\Phi^{(0)}(R)+\xi(R,\Theta)\frac{d}{dR}\nabla_R^2\Phi^{(0)}(R)+$$
$$+\nabla_R^2\Phi_0^{(2)}(R)+\nabla_R^2\Phi_2^{(2)}(R)P_2(\cos\Theta)+\frac{1}{R^2}\nabla_\Theta^2\Phi_2^{(2)}(R)P_2(\cos\Theta)=4\pi G\rho(R). \tag{4.24}$$

Considering that $\xi(R,\Theta)=\xi_0(R)+\xi_2(R)P_2(\cos\Theta)$ and gathering the corresponding parts, we derive the Newtonian field equations of both non-rotating and rotating configurations:

$$\nabla_R^2\Phi^{(0)}(R)=4\pi G\rho(R), \tag{4.25}$$

$$\xi_0(R)\frac{d}{dR}\nabla_R^2\Phi^{(0)}(R)+\nabla_R^2\Phi_0^{(2)}(R)=0, \tag{4.26}$$

$$\xi_2(R)\frac{d}{dR}\nabla_R^2\Phi^{(0)}(R)+\nabla_R^2\Phi_2^{(2)}(R)-\frac{6}{R^2}\Phi_2^{(2)}(R)=0. \tag{4.27}$$

The differential equations for $\Phi_0^{(2)}(R)$, $\Phi_2^{(2)}(R)$, $\xi_0(R)$ and $\xi_2(R)$, which establish the relationship between mass and central density for rotating star and define the shape of the star, will now be given in forms suitable for solving these problems.

The above description of the rotating equilibrium configuration allows us to obtain all the main quantities that are necessary for establishing the physical significance and determining the physical properties of the rotating source. In this section, we will obtain all the equations that must be solved in order to find the values of all the relevant quantities [122-124].

4.1.3 Mass and central density

The total mass of the rotating configuration is given by the integral of the density over the volume

$$M_{tot} = \int_V \rho(r, \theta) dV = \int_V \rho(r, \theta) r^2 \, dr \sin\theta \, d\theta \, d\phi.$$

To proceed with the computation of the integral, we use formula (4.12) and derive the relation

$$r^2 \, dr = (R + \xi)^2 (dR + d\xi) \approx R^2 \left(1 + \frac{2\xi}{R}\right)\left(1 + \frac{d\xi}{dR}\right) dR \approx \left(1 + \frac{2\xi}{R} + \frac{d\xi}{dR}\right) R^2 dR, \qquad (4.28)$$

which means that

$$M_{tot} = \int_V \rho(R) R^2 \, dR \sin\Theta \, d\Theta \, d\phi + \int_V \rho(R) R^2 \left(\frac{2\xi(R,\Theta)}{R} + \frac{d\xi(R,\Theta)}{dR}\right) dR \sin\Theta d\Theta \, d\phi. \qquad (4.29)$$

Performing the integration within the range of angles $0 < \Theta < \pi$ and $0 < \phi < 2\pi$ and using the identities

$$\int_0^\pi \sin\Theta d\Theta = 2, \qquad \int_0^\pi P_2(\cos\Theta) \sin\Theta d\Theta = 0, \qquad (4.30)$$

one finds that the change in mass $M^{(2)}$ of the rotating configuration from the static one can be written as

$$M_{tot}(R) = M^{(0)}(R) + M^{(2)}(R), \qquad (4.31)$$

$$M^{(0)}(R) = 4\pi \int_0^R \rho(R) R^2 \, dR, \qquad (4.32)$$

$$\begin{aligned} M^{(2)}(R) &= 4\pi \int_0^R \rho(R) R^2 \left(\frac{2\xi_0(R)}{R} + \frac{d\xi_0(R)}{dR}\right) dR = \\ &= 4\pi \, \xi_0(R) \rho(R) R^2 \Big|_0^R + 4\pi \int_0^R \left(-\xi_0(R) \frac{d\rho(R)}{dR}\right) R^2 \, dR. \end{aligned} \qquad (4.33)$$

The last integral is calculated via integration by parts. On the surface of the star $R = a$ the density vanishes and the first term in the last integral $\xi_0(R)\rho(R)R^2\Big|_0^a$ vanishes too. So

$$M^{(2)}(a) = 4\pi \int_0^a \left(-\xi_0(R) \frac{d\rho(R)}{dR}\right) R^2 \, dR. \qquad (4.34)$$

Here we have used the following expressions that follow from the field equations and definitions of the masses

$$\nabla^2\Phi^{(0)}(R) = 4\pi G\rho(R), \tag{4.35}$$

$$\frac{d}{dR}\nabla^2\,\Phi^{(0)}(R) = 4\pi G\frac{d\rho(R)}{dR}, \tag{4.36}$$

$$\frac{dM^{(0)}(R)}{dR} = 4\pi R^2\rho(R), \tag{4.37}$$

$$\frac{dM^{(2)}(R)}{dR} = 4\pi\left(-\xi_0(R)\frac{d\rho(R)}{dR}\right)R^2. \tag{4.38}$$

Using the condition that $\Phi^{(0)}(R)\to const^{(0)}$ and $\Phi_0^{(2)}(R)\to const_0^{(2)}$, as $R\to 0$, and taking into account (4.26) the masses of both configurations can be expressed as

$$\frac{G\,M^{(0)}(R)}{R^2} = \frac{d\,\Phi^{(0)}(R)}{dR}, \tag{4.39}$$

$$\frac{G\,M^{(2)}(R)}{R^2} = \frac{d\,\Phi_0^{(2)}(R)}{dR}. \tag{4.40}$$

It is convenient to display the $l = 0$ equation in a form in which it resembles the equation of hydrostatic equilibrium. To do this, we define

$$p_0^*(R) = \xi_0(R)\,\frac{d\,\Phi^{(0)}(R)}{dR}. \tag{4.41}$$

Furthermore, taking derivative of (4.21) and taking into account (4.40), we derive

$$-\frac{dp_0^*(R)}{dR} + \frac{2}{3}\Omega^2 R = \frac{GM^{(2)}(R)}{R^2}. \tag{4.42}$$

The above equation along with

$$\frac{dM^{(2)}(R)}{dR} = 4\pi R^2\rho(R)\frac{d\rho(R)}{dp(R)}\,p_0^*(R), \tag{4.43}$$

show the balance between the gravitational, pressure and centrifugal forces per unit mass in the rotating star. The latter expression was derived by using (4.20).

4.1.4 The shape of the star and numerical integration

If the surface of the static star has radius a, then equations (4.11) and (4.16) show that the equation for the surface of the rotating star has the form

$$r(a,\Theta) = a + \xi_0(a) + \xi_2(a) P_2(\cos\Theta). \tag{4.44}$$

The value of $\xi_0(a)$ is already defined in the $l = 0$ calculation

$$\xi_0(a) = \frac{a^2}{GM}\, p_0^*(a), \tag{4.45}$$

where $M = M^{(0)}(a)$ is the mass of the static configuration. But, the determination of $\xi_2(R)$ from $l = 2$ equations is not straightforward. So far, we have the $l = 2$ equations (4.22) and (4.27) representing the hydrostatic equilibrium and the field equation, respectively. From (4.22) we derive the expression

$$\xi_2(R) = -\frac{R^2}{GM(R)}\left\{\frac{1}{3}\Omega^2 R^2 + \Phi_2^{(2)}(R)\right\}, \tag{4.46}$$

which we insert into (4.27) and get

$$\nabla_R^2 \Phi_2^{(2)}(R) - \frac{6}{R^2}\Phi_2^{(2)}(R) = \frac{4\pi R^2}{M(R)}\left\{\frac{1}{3}\Omega^2 R^2 + \Phi_2^{(2)}(R)\right\}\frac{d\rho(R)}{dR}, \tag{4.47}$$

where $M(R) = M^{(0)}(R)$ denotes the static mass. In order to solve the latter equation numerically, one needs to rewrite it as first-order linear differential equations. For this purpose, we introduce new functions $\varphi = \Phi_2^{(2)}$ and χ so that equation (4.47) generates the system

$$\frac{d\chi(R)}{dR} = -\frac{2GM(R)}{R^2}\varphi(R) + \frac{8\pi}{3}\Omega^2 R^3 G\rho(R), \tag{4.48}$$

$$\frac{d\varphi(R)}{dR} = \left(\frac{4\pi R^2\rho(R)}{M(R)} - \frac{2}{R}\right)\varphi(R) - \frac{2\chi(R)}{GM(R)} + \frac{4\pi}{3M(R)}\rho(R)\Omega^2 R^4. \tag{4.49}$$

The above equations can be solved by quadratures. The computation of the solution can be performed numerically by integrating outward from the origin. At the origin the solution must be regular. An examination of the equations shows that, as $R \to 0$,

$$\varphi(R) \to AR^2, \qquad \chi(R) \to BR^4, \tag{4.50}$$

where *A* and *B* are any constants related by

$$B + \frac{2\pi}{3} G \rho_c A = \frac{2\pi}{3} G \rho_c \Omega^2 \tag{4.51}$$

and ρ_c is the value of the density in the centre of the star. The remaining constant in the solution is determined by the boundary condition that $\varphi(R) \to AR^2$ at large values of *R*. The constant is thus determined by sewing the internal solution with the external solution which satisfies this boundary condition [122-124].

In the exterior region, the solutions of the equations (4.48) and (4.49) are

$$\varphi_{ex}(R) = \frac{K_1}{R^3}, \qquad \chi_{ex}(R) = \frac{K_1 G M^{(0)}}{2R^4}. \tag{4.52}$$

The internal solution to the equations (4.48) and (4.49) may be written as the sum of a particular solution and a homogeneous solution. The particular solution may be found by integrating the equations outward from the centre with any values of *A* and *B* which satisfy (4.51). The homogeneous solution is then found by integrating the equations

$$\frac{d\chi_h(R)}{dR} = -\frac{2GM(R)}{R^2} \varphi_h(R), \tag{4.53}$$

$$\frac{d\varphi_h(R)}{dR} = \left(\frac{4\pi R^2 \rho(R)}{M(R)} - \frac{2}{R} \right) \varphi_h(R) - \frac{2\chi_h(R)}{GM(R)}, \tag{4.54}$$

with *A* and *B* related now by

$$B + \frac{2\pi}{3} G \rho_c A = 0. \tag{4.55}$$

The general solution may then be written as

$$\varphi_{in}(R) = \varphi_p(R) + K_2 \varphi_h(R), \qquad \chi_{in}(R) = \chi_p(R) + K_2 \chi_h(R). \tag{4.56}$$

By sewing (4.52) and (4.56) at $R = a$, the constants K_1 and K_2 can be found. Consequently, $\varphi_{in}(R)$ is found and $\xi_2(R)$ can be easily calculated from

$$\xi_2(R) = -\frac{R^2}{GM(R)} \left\{ \frac{1}{3} \Omega^2 R^2 + \varphi_{in}(R) \right\}. \tag{4.57}$$

4.1.5 Moment of inertia

Similarly to the total mass of the star, the total moment of inertia can be

calculated as

$$I_{tot} = \int_V \rho(r,\,\theta)(r\sin\theta)^2\, dV = \int_V \rho(r,\theta)\, r^4 dr \sin^3\theta\, d\theta\, d\varphi. \tag{4.58}$$

Using the definition of the radial coordinate r, we find the expression

$$r^4\, dr = (R+\xi)^4\,(dR + d\xi) \approx R^4\left(1+\frac{4\xi}{R}\right)\left(1+\frac{d\xi}{dR}\right)dR \approx \left(1+\frac{4\xi}{R}+\frac{d\xi}{dR}\right)R^4\, dR, \tag{4.59}$$

which allows us to rewrite the moment of inertia as

$$I_{tot} = \int_V \rho(R)\, R^4 dR \sin^3\Theta d\Theta\, d\phi + \int_V \rho(R)\, R^4\left(\frac{4\xi(R,\Theta)}{R} + \frac{d\xi(R,\Theta)}{dR}\right)dR\sin^3\Theta d\Theta\, d\phi. \tag{4.60}$$

Performing the integration within the range $0 < \Theta < \pi$ and $0 < \phi < 2\pi$, we derive

$$I_{tot}(R) = I^{(0)}(R) + I^{(2)}(R), \tag{4.61}$$

$$I^{(0)}(R) = \frac{8\pi}{3}\int_0^R \rho(R) R^4\, dR, \tag{4.62}$$

$$\begin{aligned} I^{(2)}(R) &= \frac{8\pi}{3}\int_0^R \rho(R) R^4\left(\frac{d\xi_0(R)}{dR} - \frac{1}{5}\frac{d\xi_2(R)}{dR} + \frac{4}{R}\left[\xi_0(R) - \frac{1}{5}\xi_2(R)\right]\right)dR = \\ &= \frac{8\pi}{3}\left[\xi_0(R) - \frac{1}{5}\xi_2(R)\right]\rho(R)R^4\Big|_0^R + \frac{8\pi}{3}\int_0^R\left(-\left[\xi_0(R) - \frac{1}{5}\xi_2(R)\right]\frac{d\rho(R)}{dR}\right)R^4 dR, \end{aligned} \tag{4.63}$$

where the last expression has been derived via integration by parts and we have used the integrals

$$\int_0^\pi \sin^3\Theta\; d\Theta = \frac{4}{3}, \qquad \int_0^\pi P_2(\cos\Theta)\sin^3\Theta\; d\Theta = -\frac{4}{15}. \tag{4.64}$$

When $R = a$ the expression for the change in moment of inertia due to rotation becomes

$$I^{(2)}(a) = \frac{8\pi}{3}\int_0^a\left(-\left[\xi_0(R) - \frac{1}{5}\xi_2(R)\right]\frac{d\rho(R)}{dR}\right)R^4 dR. \tag{4.65}$$

In the corresponding limit, our results coincide with the definition of the moment of inertia for slowly rotating relativistic stars as given in [138]. Notice that, knowing the value of the moment of inertia, one can easily calculate the total angular momentum of the rotating stars

$$J_{tot} = J^{(0)} + J^{(2)}, \tag{4.66}$$

where $J^{(0)} = I^{(0)}\Omega$ is the angular momentum of the spherical configuration and $J^{(2)} = I^{(2)}\Omega$ is the change of the angular momentum due to rotation and deformation.

4.1.6 Gravitational binding energy and rotational kinetic energy

The total gravitational binding energy of a rotating configuration can be calculated in analogy to the total mass and moment of inertia as

$$W_{tot} = \frac{1}{2}\int_V \Phi(r,\theta)\rho(r,\theta)dV = \int_V \Phi(r,\theta)\rho(r,\theta)\, r^4 dr \sin\theta\, d\theta\, d\phi\,, \tag{4.67}$$

where the radial coordinate r can be expressed in coordinates R, Θ by using equation (4.12), the density is simply given by equation (4.11) and the gravitational potential by equation (4.15). Then, we rewrite equation (4.67) as

$$\begin{aligned} W_{tot} = {} & \frac{1}{2}\int_V \left[\Phi^{(0)}(R) + \Phi^{(0)}(R)\left(\frac{2\xi(R,\Theta)}{R} + \frac{d\xi(R,\Theta)}{dR}\right)\right]\rho(R)\, R^2 dR \sin\Theta\, d\Theta\, d\phi + \\ & + \frac{1}{2}\int_V \left(\xi(R,\Theta)\frac{d\Phi^{(0)}(R)}{dR} + \Phi^{(2)}(R,\Theta)\right)\rho(R)\, R^2 dR \sin\Theta\, d\Theta\, d\phi + O(\Omega^4). \end{aligned} \tag{4.68}$$

Expanding the functions $\Phi^{(2)}(R,\Theta)$ and $\xi(R,\Theta)$ in spherical harmonics, according to equation (4.16), and integrating the above expression in the range $0 < \Theta < \pi,\ 0 < \phi < 2\pi$, taking into account equation (4.30), we obtain

$$W_{tot}(R) = W^{(0)}(R) + W^{(2)}(R), \tag{4.69}$$

$$W^{(0)}(R) = 2\pi\int_0^R \Phi^{(0)}(R)\,\rho(R)R^2 dR\,, \tag{4.70}$$

$$\begin{aligned} W^{(2)}(R) = {} & 2\pi\int_0^R \left[\xi_0(R)\frac{d\Phi^{(0)}(R)}{dR} + \Phi_0^{(2)}(R) + \Phi^{(0)}(R)\left(\frac{2\xi_0(R)}{R} + \frac{d\xi_0(R)}{dR}\right)\right]\rho(R)R^2 dR = \\ = {} & 2\pi\xi_0(R)\Phi^{(0)}(R)\rho(R)R^2\Big|_0^R - 2\pi\int_0^R \left(\xi_0(R)\Phi^{(0)}(R)\frac{d\rho(R)}{dR} - \Phi_0^{(2)}(R)\rho(R)\right)R^2 dR, \end{aligned} \tag{4.71}$$

where $W^{(0)}$ is the gravitational binding energy of the non-rotating configuration and $W^{(2)}$ is the change in the gravitational binding energy because of rotation. On the surface $W^{(2)}$ becomes

$$W^{(2)}(a) = -2\pi\int_0^a \left(\xi_0(R)\Phi^{(0)}(R)\frac{d\rho(R)}{dR} - \Phi_0^{(2)}(R)\rho(R)\right)R^2 dR. \tag{4.72}$$

In the second-order approximation in Ω, the rotational kinetic energy can be written as

$$T = \frac{J_{tot}\Omega}{2} \approx \frac{J^{(0)}\Omega}{2} + O\left(\Omega^4\right) = \frac{I^{(0)}\Omega^2}{2} + O\left(\Omega^4\right). \tag{4.73}$$

The ratio of the rotational kinetic energy to the binding energy allows one to investigate the stability of rotating configurations [122].

4.1.7 Quadrupole moment

The Newtonian potential $\Phi(R,\Theta)$ outside the star will be written as before as (see equation (4.14))

$$\Phi(R,\Theta) = \Phi^{(0)}(R) + \Phi_0^{(2)}(R) + \Phi_2^{(2)}(R)P_2(\cos\Theta), \tag{4.74}$$

where

$$\Phi^{(0)}(R) = -\frac{GM^{(0)}}{R}, \tag{4.75}$$

$$\Phi_0^{(2)}(R) = -\frac{GM^{(2)}}{R}, \tag{4.76}$$

$$\Phi_2^{(2)}(R) = \frac{K_1}{R^3}. \tag{4.77}$$

In view of (4.31), equation (4.74) can be written as follows

$$\Phi(R,\Theta) = -\frac{GM_{tot}}{R} + \frac{K_1}{R^3}P_2(\cos\Theta), \tag{4.78}$$

It follows that the constant K_1 determines the mass quadrupole moment Q of the star as $K_1 = GQ$. For a vanishing K_1 we recover the static configuration. Moreover, according to Hartle's definition $Q > 0$ represents an oblate object and $Q < 0$ corresponds to a prolate object.

4.1.8 Ellipticity and gravitational Love number

The quantity defined by

$$\varsigma(R) = -\frac{3}{2R}\xi_2(R), \tag{4.79}$$

is the ellipticity of the surface of constant density labelled by *R*. We use this expression and (46), and eliminate $\Phi_2^{(2)}$ from (4.47), to derive the following equation for $\varsigma(R)$:

$$\frac{M(R)}{R}\frac{d^2\varsigma(R)}{dR^2}+\frac{2}{R}\frac{dM(R)}{dR}\frac{\varsigma(R)}{dR}+\frac{2dM(R)}{dR}\frac{\varsigma(R)}{R^2}-\frac{6M(R)\varsigma(R)}{R^3}=0, \tag{4.80}$$

or equivalently in a compact form

$$\frac{d}{dR}\frac{1}{R^4}\frac{d}{dR}\left[\varsigma(R)M(R)R^2\right]=4\pi\varsigma(R)\frac{d\rho(R)}{dR}. \tag{4.81}$$

This equation is equivalent to Clairaut's equation. Here both $M(R)$ and $\rho(R)$ are known functions of R. The ellipticity must be regular at small values of R, and equation (4.81) shows that it approaches a constant at $R=0$. With this boundary condition, equation (4.81) may be integrated to find the shape of $\varsigma(R)$. To find the magnitude of $\varsigma(R)$ one needs to use (4.57). The procedure for considering the boundary condition at the surface given in the previous section, together with the condition of regularity at the origin and the differential equation (4.81), uniquely determine the ellipticity of the surfaces of constant density as a function of the coordinate R.

It is easy to show that equation (4.80) can be written in the form given in [135]

$$R^2\frac{d^2\varsigma(R)}{dR^2}+6\frac{\rho(R)}{\rho_m(R)}\left[R\frac{d\varsigma(R)}{dR}+\varsigma(R)\right]=6\varsigma(R), \tag{4.82}$$

where

$$\rho_m(R)=\frac{3M(R)}{4\pi R^3} \tag{4.83}$$

is the average mass density. By introducing a new function as

$$\eta_2(R)=\frac{R}{\varsigma(R)}\frac{d\varsigma(R)}{dR}. \tag{4.84}$$

Equation (4.82) reduces to the well known Clairaut-Radau equation [132]

$$R\frac{d\eta_2(R)}{dR}+6D(R)\left[\eta_2(R)+1\right]+\eta_2(R)\left[\eta_2(R)-1\right]=6, \tag{4.85}$$

where

$$D(R) = \frac{\rho(R)}{\rho_m(R)} \tag{4.86}$$

encodes the relevant information about the structure of the body. The differential equation is integrated outward from $R=0$, with the boundary conditions $D(0)=1$ and $\eta(R=0)=0$, up to $R=a$, obtaining the value $\eta_2(R=a)$. The Love number is then given by

$$k_2 = \frac{3-\eta_2(a)}{2[2+\eta_2(a)]}. \tag{4.87}$$

In the celestial mechanics and astronomical works, the dimensionless quantity k_2 is called 'apsidal constant', because it controls the size of tidal and rotational deformations of stars in close binary systems, which lead to observable perturbations in the 'line of apsides'. Sometimes, the quantity defined as $\lambda = 2k_2 a^5/(3G)$ is called the Love number. In this section, however, we use k_2 as the Love number; it is named after the British geophysicist Augustus E. H. Love (1863–1940), who introduced it early in the 20th century [132]. The Love number characterizes the rigidity and the susceptibility of the body's shape to changes in response to a rotational deformation or to a tidal potential. For a rigid object $k_2 = 0$, meaning that a rigid object cannot change its shape. In Newtonian gravity, the tidal and rotational Love numbers coincide with each other. But, in GR because of the Lense-Thirring effect they are different. The knowledge of the Love numbers has a wide range of applications in the astrophysical context. Namely, using the Love numbers, one can simulate the motion of binary systems with tidal interactions, and estimate the correct values of the orbital parameters. The Love numbers are directly related to the quadrupole moment and the moment of inertia of a deformed object; hence, knowing the Love numbers, one can establish the relation between the quadrupole moment and the moment of inertia through the I-Love-Q relations [139, 140]. Finally, Love numbers are involved in the expansions of the exterior gravitational potential for deformed objects. Consequently, whenever one considers gravitational interactions between celestial objects, the Love numbers play a key role in these processes [132].

Note that once $\xi_2(R)$ is known, then $\varsigma(R)$ is also known from equation (4.79), and we have

$$\eta_2(a) = \frac{a}{\varepsilon(a)}\frac{d\varepsilon(R)}{dR}\bigg|_{R=a} = \frac{a}{\xi_2(a)}\frac{d\xi_2(R)}{dR}\bigg|_{R=a} - 1. \tag{4.88}$$

One can see from here that $\eta_2(a)$ does not depend on the angular velocity of the star, neither does the Love number.

4.1.9 Equations of structure

Our results show that it is possible to write explicitly all the differential equations that define the behaviour of a slowly rotating compact object. For a better presentation of the results obtained in preceding sections, we summarise the steps that must be followed to integrate the resulting equations.

a) The non-rotating case. To determine the relation between mass and central density, one must proceed as follows. (1) Specify the EoS $p = p(\rho)$ (polytrope, tabulated, etc). (2) Choose the value of the central density $\rho(R=0)=\rho_c$. Calculate the mass and pressure from the Newtonian field equation and the equation of hydrostatic equilibrium with the regularity condition at the center $M^{(0)}(R=0)=0$

$$\begin{cases} \dfrac{dM^{(0)}(R)}{dR} = 4\pi R^2 \rho(R), \\ \dfrac{dp^{(0)}(R)}{dR} = -\rho(R)\dfrac{GM^{(0)}(R)}{R^2}. \end{cases} \tag{4.89}$$

The gravitational potential of the static star is obtained as

$$\frac{d\Phi^{(0)}(R)}{dR} = \frac{GM^{(0)}(R)}{R^2} = -\frac{1}{\rho(R)}\frac{dp^{(0)}(R)}{dR}. \tag{4.90}$$

On the surface, the pressure must vanish $p^{(0)}(R=a)=0$.

The solution of equation (4.89) gives the mass, pressure and density profile inside the star and, in turn, the density profile allows us to calculate the moment of inertia from equation (4.63).

In order to determine the correct value of the interior gravitational potential for the static configuration $\Phi^{(0)}(R)$, one should calculate $const^{(0)}$ by sewing the potential with its exterior counterpart on the spherical surface. The external potential is given by equation (4.75). By using the sewing condition

$$\Phi^{(0)}_{in}(R)\big|_{R=a} = \Phi^{(0)}_{ex}(R)\big|_{R=a}, \tag{4.91}$$

along with equation (4.20), one can determine $const^{(0)}$ as

$$const^{(0)} = \int_0^a \frac{1}{\rho(R)}\frac{dp^{(0)}(R)}{dR}dR + \Phi^{(0)}_{ex}(a). \tag{4.92}$$

Knowing the value of $const^{(0)}$, the correct expression for the internal potential is

$$\Phi^{(0)}(R) = \Phi^{(0)}_{in}(R) = const^{(0)} - \int_0^R \frac{1}{\rho(R)}\frac{dp^{(0)}(R)}{dR}dR. \tag{4.93}$$

b) The rotating case: $l = 0$ equations. Select the value of the angular velocity of the star. For example, take as a test value the Keplerian orbit with

$$\Omega_{test} = \Omega = \sqrt{\frac{GM^{(0)}(a)}{a^3}}. \tag{4.94}$$

Then, integrate the system of equations

$$\begin{cases} \dfrac{dp_0^*(R)}{dR} = \dfrac{2}{3}\Omega^2 R - \dfrac{GM^{(2)}(R)}{R^2}, \\ \dfrac{dM^{(2)}(R)}{dR} = 4\pi R^2 \rho(R) \dfrac{d\rho(R)}{dp(R)} p_0^*(R), \end{cases} \tag{4.95}$$

out from the origin with boundary conditions

$$p_0^*(R) \to \frac{1}{3}\Omega^2 R^2, \qquad M^{(2)}(R) \to 0. \tag{4.96}$$

These boundary conditions guarantee that the central density of the static and rotating configurations are the same.

Additionally, to compute $const_0^{(2)}$ from equation (4.21), one makes use of the sewing condition for $\Phi_0^{(2)}(R)$

$$\Phi_{0in}^{(2)}(R)\Big|_{R=a} = \Phi_{0ex}^{(2)}(R)\Big|_{R=a}, \tag{4.97}$$

where $\Phi_{0ex}^{(2)}(R)$ is given by equation (4.76). Hence

$$const_0^{(2)} = -\frac{1}{3}\Omega^2 a^2 + \Phi_{0ex}^{(2)}(a) + p_0^*(a) \tag{4.98}$$

and finally

$$\Phi_0^{(2)}(R) = \Phi_{0in}^{(2)}(R) = const_0^{(2)} + \frac{1}{3}\Omega^2 R^2 - p_0^*(R). \tag{4.99}$$

To compute the gravitational binding energy and its correction because of rotation, one should integrate equations (4.70) and (4.71) by using equations (4.93) and (4.99).

c) The rotating case: $l = 2$ equations. 1) Particular solution. Integrate the equations

$$\begin{cases} \dfrac{d\chi(R)}{dR} = -\dfrac{2GM(R)}{R^2}\,\varphi(R) + \dfrac{8\pi}{3}\Omega^2 R^3 G\,\rho(R) \\ \dfrac{d\varphi(R)}{dR} = \left(\dfrac{4\pi R^2\rho(R)}{M(R)} - \dfrac{2}{R}\right)\varphi(R) - \dfrac{2\chi(R)}{GM(R)} + \dfrac{4\pi}{3M(R)}\rho(R)\Omega^2 R^4 \end{cases}$$

outward from the centre with arbitrary initial conditions satisfying the equations, as $R \to 0$

$$\varphi(R) \to AR^2\,, \quad \chi(R) \to BR^4\,, \quad B + \frac{2\pi}{3}G\rho_c A = \frac{2\pi}{3}G\rho_c\Omega^2\,, \tag{4.100}$$

where A and B are constants subject to the above algebraic relation. Therefore, we can freely select only one of the constants. Set, for instance, $A=1$ and define B from the above equation. This determines a particular solution $\varphi_p(R)$ and $\chi_p(R)$.

2) Homogeneous solution. Integrate the homogeneous equations

$$\begin{cases} \dfrac{d\chi_h(R)}{dR} = -\dfrac{2GM(R)}{R^2}\,\varphi_h(R) \\ \dfrac{d\varphi_h(R)}{dR} = \left(\dfrac{4\pi R^2\rho(R)}{M(R)} - \dfrac{2}{R}\right)\varphi_h(R) - \dfrac{2\chi_h(R)}{GM(R)} \end{cases}$$

outward from the centre with arbitrary initial conditions satisfying the equations, as $R \to 0$

$$\varphi_h(R) \to AR^2\,, \quad \chi_h(R) \to BR^4\,, \quad B + \frac{2\pi}{3}G\rho_c A = 0\,, \tag{4.101}$$

This determines a homogeneous solution $\varphi_h(R)$ and $\chi_h(R)$. Thus, the interior solution is

$$\varphi_{in}(R) = \varphi_p(R) + K_2\,\varphi_h(R), \qquad \chi_{in}(R) = \chi_p(R) + K_2\,\varphi_h(R). \tag{4.102}$$

3) Sewing with an exterior solution. The external solution is given as

$$\varphi_{ex}(R) = \frac{K_1}{R^3}, \qquad \chi_{ex}(R) = \frac{K_1 GM^{(0)}}{2R^4}. \tag{4.103}$$

By sewing (4.103) and (4.102) at $R = a$,

$$\varphi_{ex}(R=a) = \varphi_{in}(R=a), \qquad \chi_{ex}(R=a) = \chi_{in}(R=a), \tag{4.104}$$

the constants K_1 and K_2 can be obtained.

4) Relations among moment of inertia, eccentricity and love number. Once functions $\xi_0(R)$ and $\xi_2(R)$ are known from

$$\xi_0(R) = \frac{R^2}{GM(R)} p_0^*(R),$$
$$\xi_2(R) = -\frac{R^2}{GM(R)}\left\{\frac{1}{3}\Omega^2 R^2 + \varphi_{in}(R)\right\}. \tag{4.105}$$

One can easily calculate the perturbation of the moment of inertia and other important quantities.

The surface of the rotating configuration is described by the polar r_p and equatorial r_e radii that are determined from the relations

$$r(a, \Theta) = a + \xi_0(a) + \xi_2(a) P_2(\cos\Theta), \tag{4.106}$$

$$r_p = r(a, 0) = a + \xi_0(a) + \xi_2(a), \tag{4.107}$$

$$r_e = r(a, \pi/2) = a + \xi_0(a) - \xi_2(a)/2. \tag{4.108}$$

Moreover, the eccentricity is defined as

$$eccentricity = \sqrt{1 - \frac{r_p^2}{r_e^2}} \tag{4.109}$$

and determines completely the sewing surface.

In terms of function $\xi_2(R)$ one can easily compute ellipticity $\varsigma(R)$, function $\eta_2(R)$, hence the gravitational Love number k_2.

4.1.10 An example: white dwarfs

In this section, we investigate an example of the formalism introduced in the preceding sections to test the applicability of the approach. To appreciate the validity of our results, we consider a very realistic case, namely, WDs whose EoS at zero temperature is given by the Chandrasekhar EoS [105]. The behaviour of the EoS is illustrated in figure 4.2 for the case of a degenerate electron gas [122].

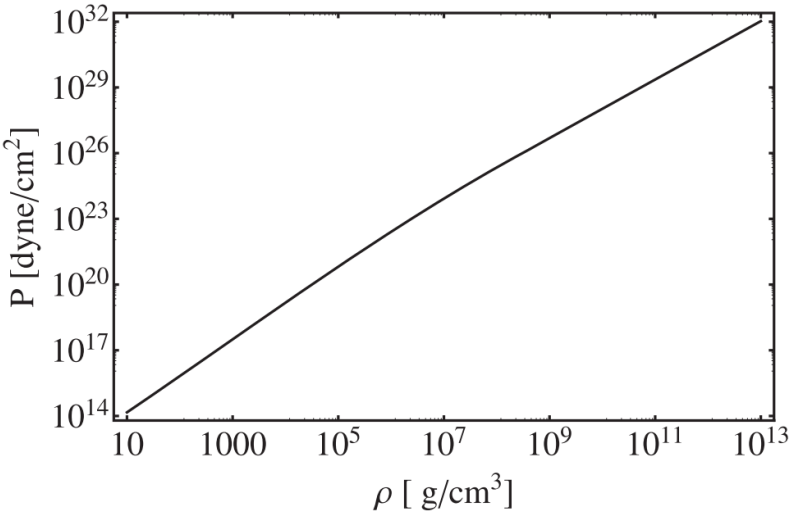


Figure 4.2 – Pressure versus density for the Chandrasekhar EoS

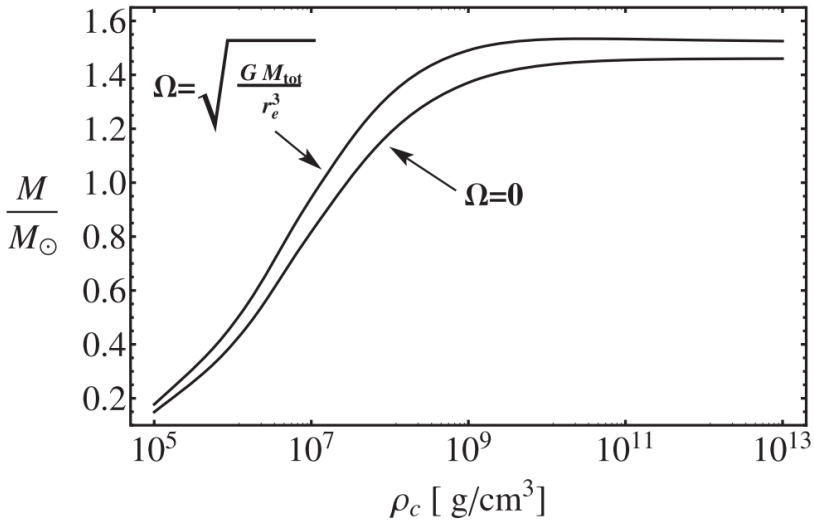


Figure 4.3 – Total mass and central density relation obtained from the Chandrasekhar EoS

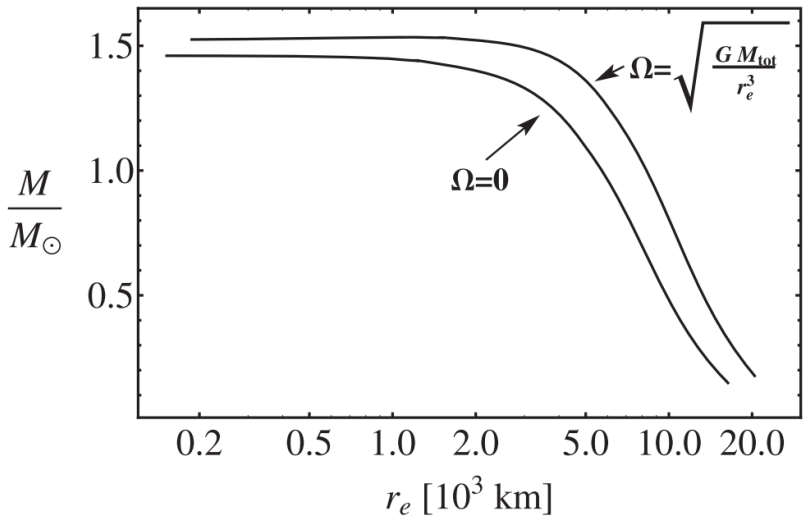


Figure 4.4 – Total mass and equatorial radius relation for Chandrasekhar EoS

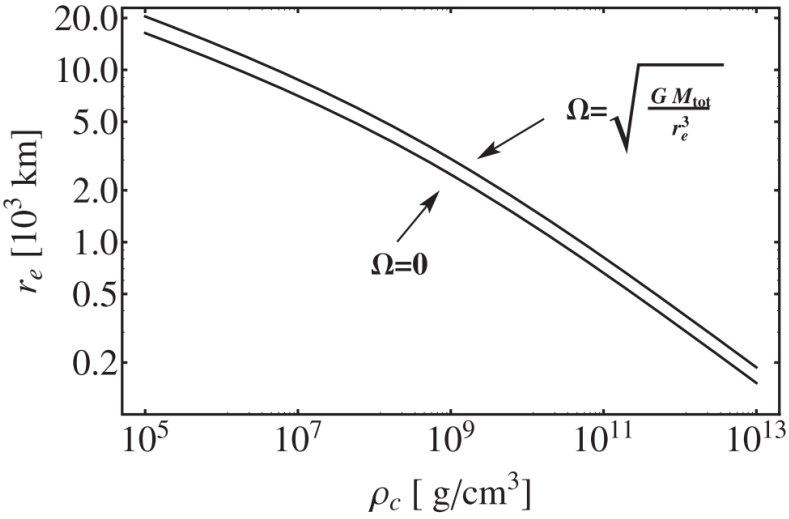


Figure 4.5 – Equatorial radius versus central density. Note that $\Omega \to 0$ as $r_e \to a$

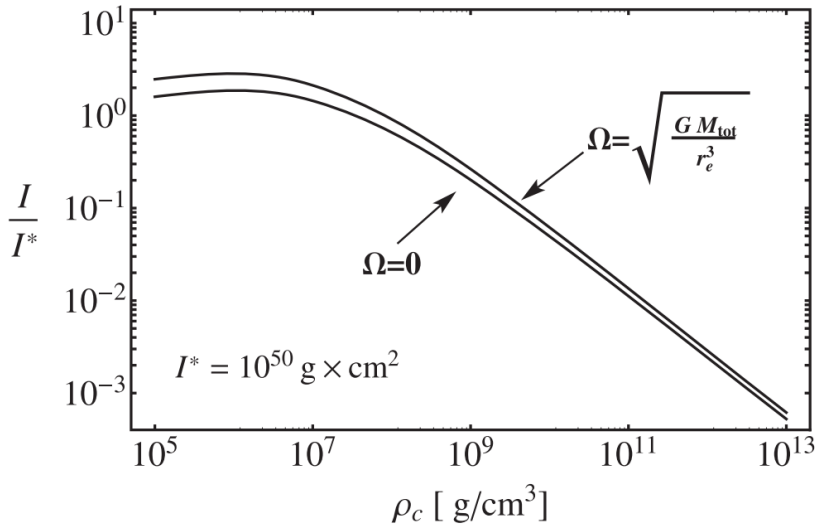


Figure 4.6 – Total moment of inertia versus central density

In figure 4.3, we plot the behaviour of the total mass as a function of the central density for a static star and for a rotating star with our test angular velocity. It is clear that for a given central density the value of the total mass is larger in the case of a rotating object than for a static body. This is in accordance with the physical expectations based upon other alternative studies [9-14, 136, 137]. A similar behaviour takes place when we explore the mass as a function of the equatorial radius, as shown in figure 4.4.

The relationship between the central density and the equatorial radius is illustrated in figure 4.5. As expected, the equatorial radius diminishes as the density increases, and it is larger in the case of a rotating body. In the limit of vanishing angular velocity, the equatorial radius approaches the value of the static radius *a* [122].

The moment of inertia depends also on the central density and on the value of the angular velocity, as illustrated in figure 4.6. For each value of the angular velocity, there is particular value of the central density at which the moment of inertia acquires a maximum. The value of the moment of inertia at the maxima increases as the angular velocity increases. For very large values of the central density, the gap between the moment of inertia of static and rotating configurations is narrowing. Notice, however, that this happens for values close to or larger than $10^{11}\, g/cm^{-3}$ which should be considered as unphysical because they are larger than the critical value $\rho_c \sim 1.37\times10^{11}\, g/cm^{-3}$ at which the EoS under consideration can no longer be applied because of the inverse β-decay process for WDs consisting of helium ions. It should be mentioned that, in general, the inverse β-decay instability is affected by the rotation indirectly, since the main ingredient for the onset of the β-instability is the value of the density at the centre of the WD. Rotation affects the central density and,

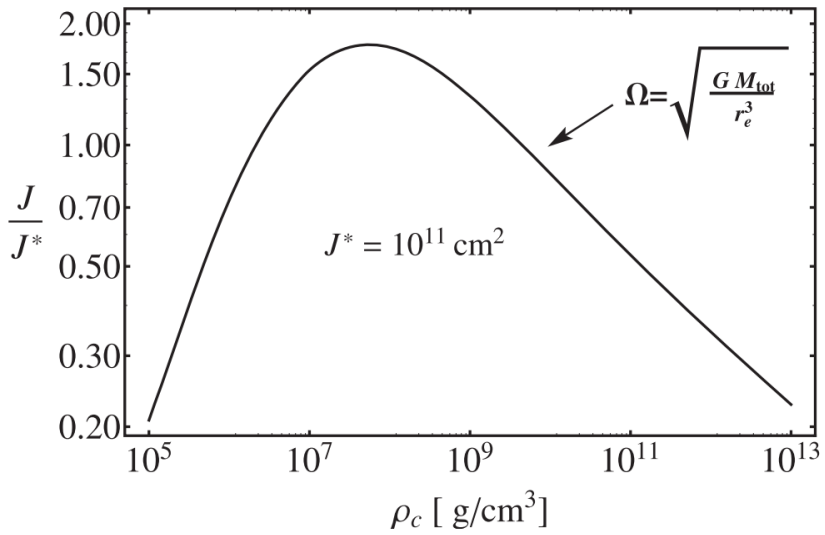


Figure 4.7 – Angular momentum versus central density

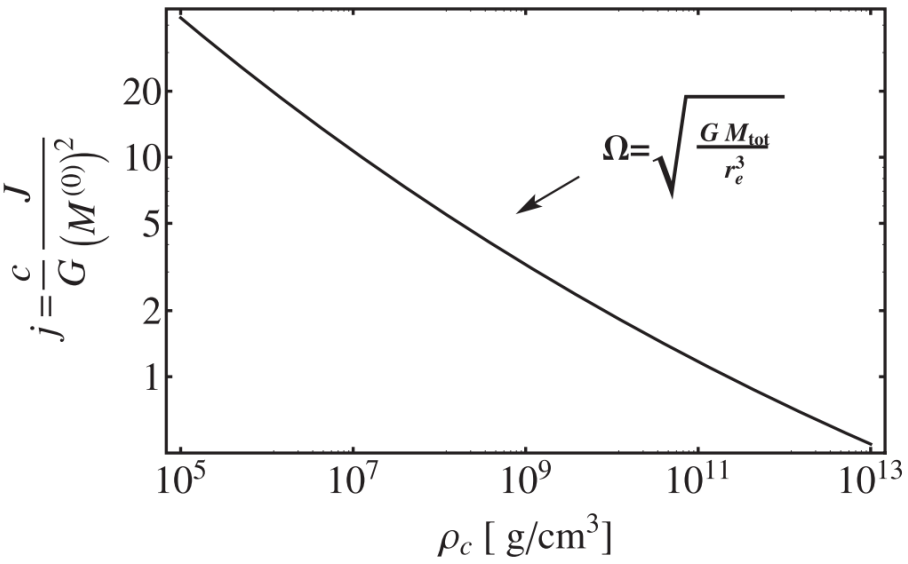


Figure 4.8 – Dimensionless angular momentum $j=(cJ)/(GM^2)$ versus central density

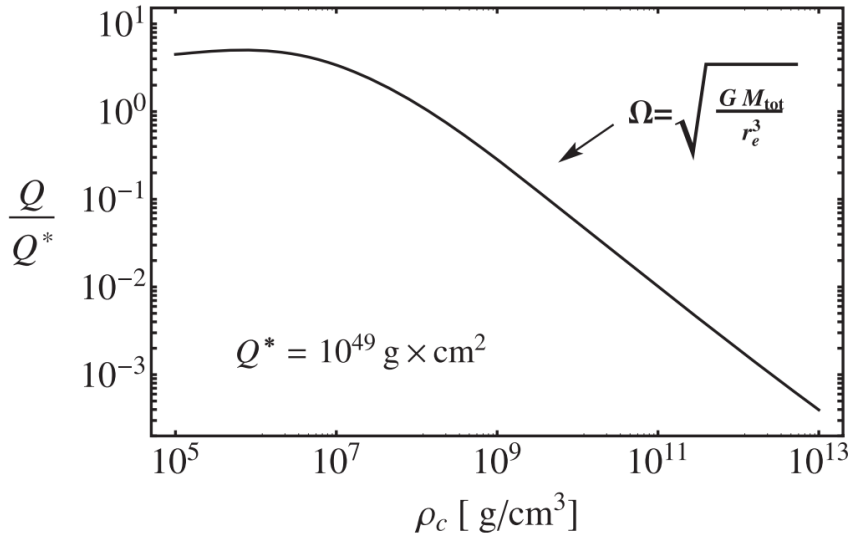


Figure 4.9 – Mass quadrupole moment versus central density

in turn, it affects the β-instability. Nevertheless, we are considering in all our plots the interval $(10^5-10^{13})g\,cm^{-3}$ for the sake of generality. The total angular momentum as a function of the central density is given in figure 4.7.With increasing central density, first, it increases up to its maximum value and then it decreases. The dimensionless angular momentum or the spin parameter is shown in figure 4.8. It turns out that for WDs the spin parameter is quite large for small central densities and it is less than unity for central densities larger than the inverse β-decay density for helium WDs [122]. Thus, if we assume that a WD collapses into a neutron star at the inverse β-decay

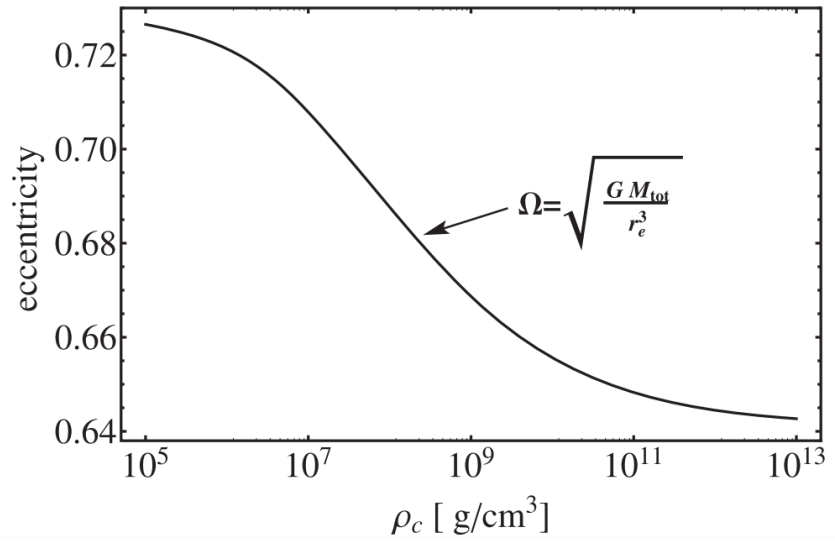


Figure 4.10 – Eccentricity versus central density of rotating configurations

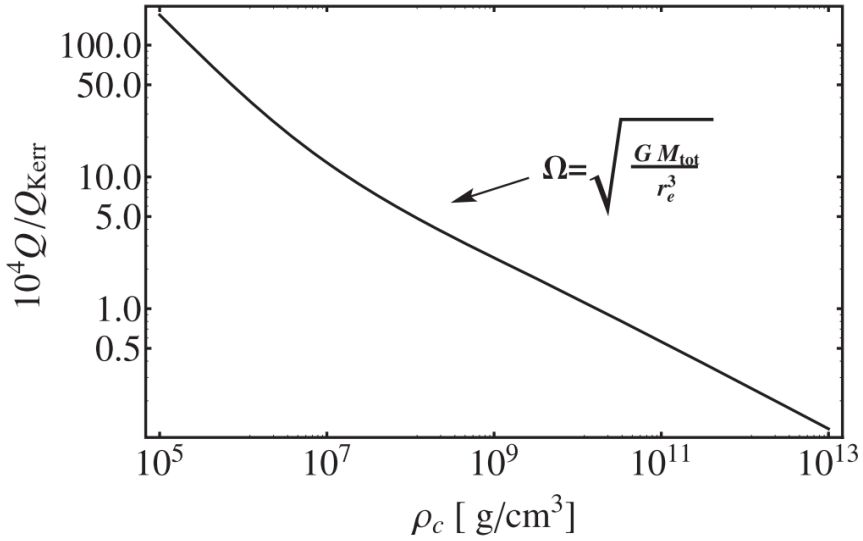


Figure 4.11 – Mass quadrupole moment over the Kerr quadrupole moment $Q_{Kerr} = J^2/(c^2 M)$ versus central density

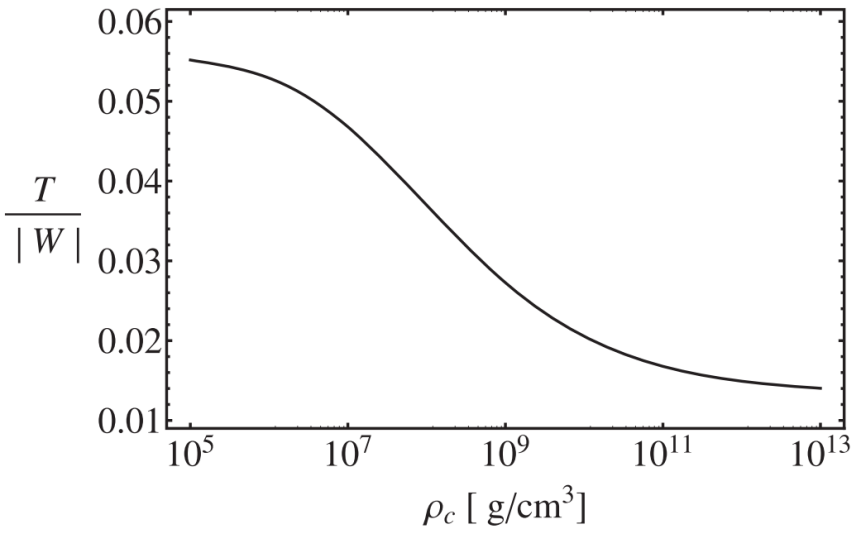


Figure 4.12 – Rotational kinetic energy over gravitational binding energy $T/|W|$ versus central density of rotating configurations

instability density and the spin parameter is conserved, then the spin parameter will be in agreement with the theoretical upper limits for NSs [141-144].

In figures 4.9 and 4.10 we plot the quantities which determine the shape of the surface where the interior solution is matched with the exterior one, namely, the quadrupole moment and the eccentricity. Obviously, both quantities vanish in the limiting case of vanishing rotation. The quadrupole possesses a maximum at a certain value of the central density which coincides with the position of the maximum of the moment of inertia.

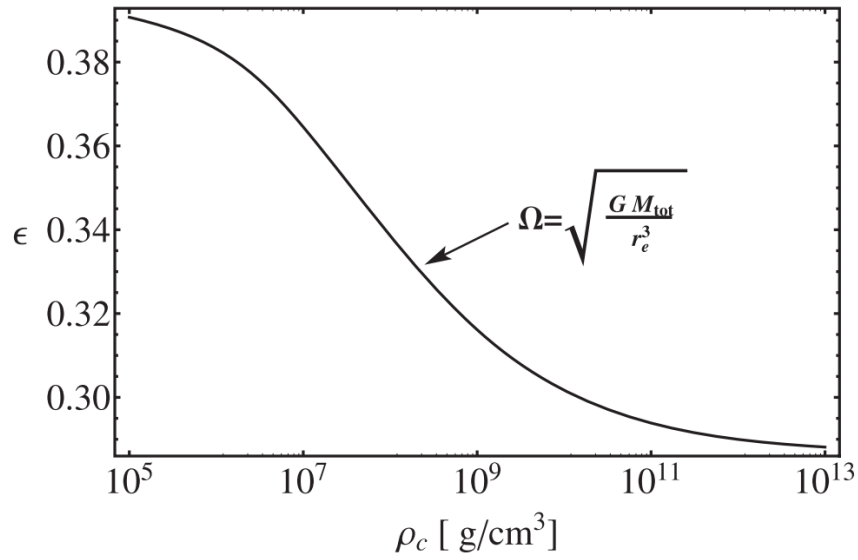


Figure 4.13 – Ellipticity versus central density of rotating configurations

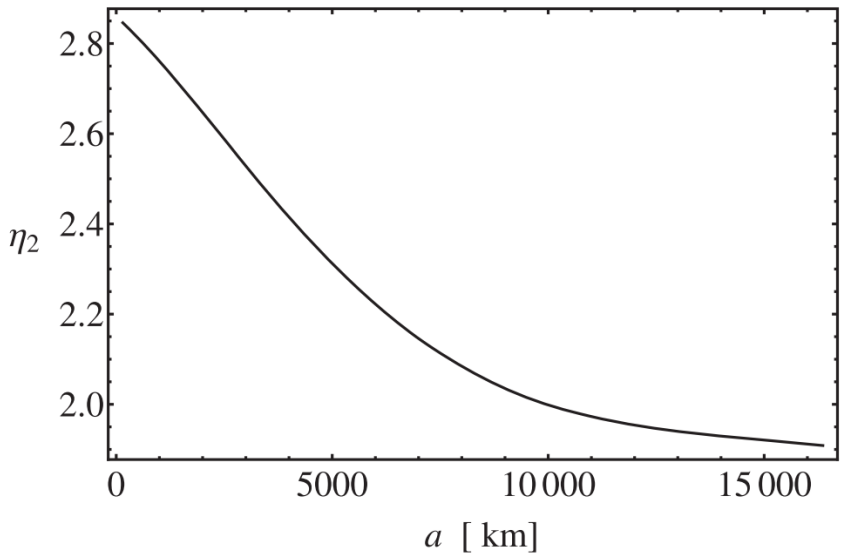


Figure 4.14 – Function η_2 versus spherical radius a of static configurations

The quadrupole moment normalized by the Kerr quadrupole moment as a function of the central density is illustrated in figure 4.11. One can see here that the quadrupole moment for WDs is always larger than the Kerr quadrupole.

The ratio of the rotational kinetic energy to the gravitational binding energy as a function of the central density is shown in figure 4.12. The values of the ratio and the eccentricity are well below the upper limits for secular and dynamical instabilities. According to [65], the conditions (values) $T/|W| = 0.14$, $e = 0.81$ and $T/|W| = 0.25$, $e = 0.95$, for rigidly rotating fluids (liquids) with uniform density the so-called Maclaurin spheroids, are considered to be the upper limits for secular and dynamical instabilities, respectively.

The secular instability determines the instability of rotating configurations with respect to small perturbations. In fact, in order to investigate the secular instability of realistic objects Friedman et al [145] formulated the method of turning points. According to this method, one needs to calculate constant angular momentum sequences, compute the mass-central density relations, and estimate the maximum mass. The maximum mass is the indicator (turning point) for the onset of the secular instability. For different values of the angular momentum there are different maximum masses and by joining all the points for the maxima one obtains the secular instability curve. In the mass-central density diagram the configurations on the left-hand side of the maxima are considered to be secularly stable, and the configurations on the right-hand side are unstable configurations.

We constructed the constant angular momentum sequences and found that the maximum mass is reached for configurations with central densities beyond our range of consideration [122].

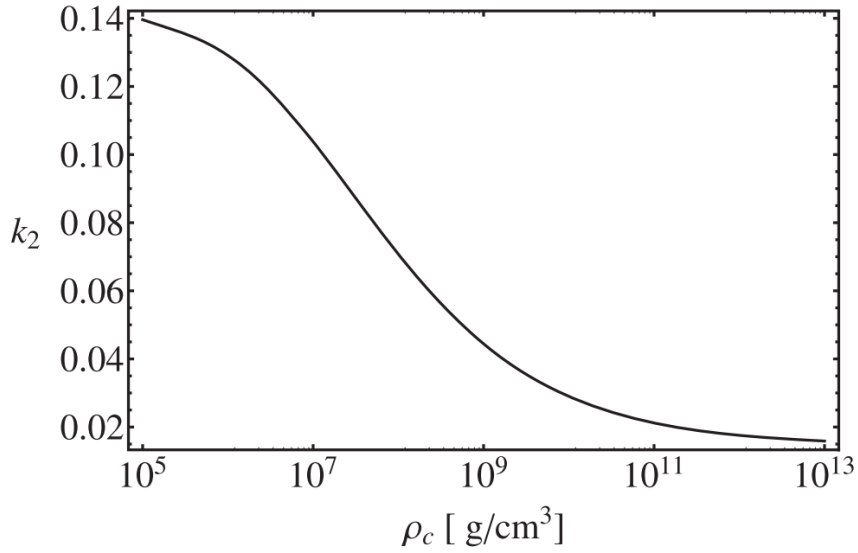


Figure 4.15 – Love number versus central density of static configurations

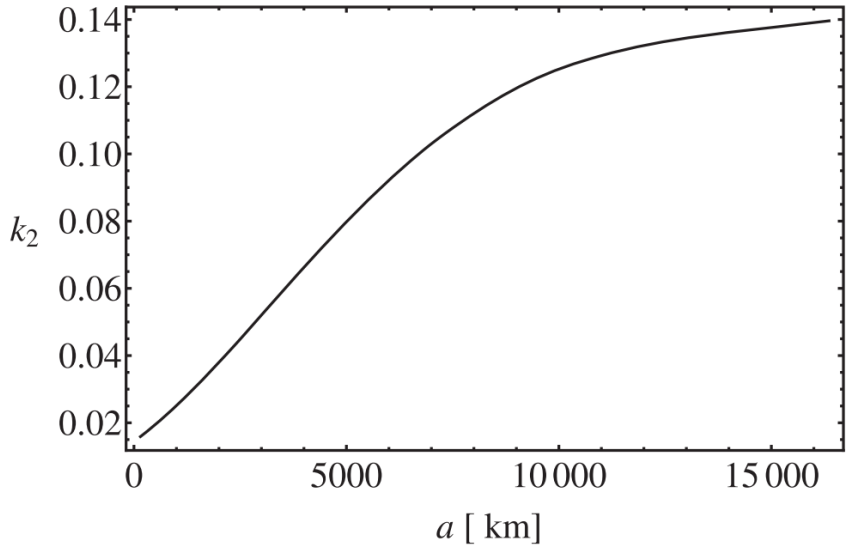


Figure 4.16 – Love number versus spherical radius of static configurations

This fact allows us to state that, unlike their relativistic counterparts, the Newtonian uniformly rotating WDs are secularly stable [16, 17].

The ellipticity of the rotating deformed star is illustrated as a function of the central density in figure 4.13. On the surface of the star the ellipticity shows similar behaviour as the eccentricity and as density increases it decreases. Thus, the star becomes more compact and more spherical.

The dependence of function η_2 is shown as a function of the spherical radius a in figure 4.14. As the radius increases the function decreases. The function η_2 is necessary to calculate the Love number. Finally, in figures 4.15 and 4.16 we depict the gravitational Love number as a function of the central density and spherical radius, respectively. For increasing central density the Love number decreases. This implies that with the increasing central density or decreasing radius WDs become less

susceptible to rotational and tidal deformations, since $k_2 = 0$ for a rigid body. It should be mentioned that the values for the Love number in agreement with those presented in [146].

Notice that in all the plots, the selected values for the central mass and the equatorial radius are in accordance with the expected values for WDs. We conclude that the results obtained from the numerical integration of the differential equations derived by using the approach proposed in this work are consistent with the physical expectations, when restricted to the region in which the formalism can be applied [9-14, 137, 147-149].

Table 4.1 – The values of multiplicative factor κ for different values of the central density

ρ(g cm^{-3})	10^5	10^6	10^7	10^8	10^9	10^{10}	5×10^{10}	10^{11}	1.37×10^{11}	10^{12}	10^{13}
κ	0.781	0.780	0.777	0.770	0.762	0.755	0.752	0.751	0.750	0.748	0.747

Table 4.2 – Maximum static and rotating masses of WDs. NG stands for Newtonian gravity, PN stands for Post-Newtonian weak field ($1/c^2$ approximation), GR stands for general relativity, $\mu = 2$ indicates the average molecular weight in the Chandrasekhar EoS and $n = 3$ stands for the polytrope index

Treatment / EoS	$M_{max}^{J=0}/M_\odot$	$M_{max}^{J\neq0}/M_\odot$	Approximation	Formalism	References
NG/μ=2	1.437	1.474	Slow rotation ~Ω^2	Chandrasekhar	Anand (1965) [9]
NG/n=3	1.437	1.487	Rapid rotation	Monaghan-Roxburgh	Roxburgh (1965) [10]
PN/μ=2	1.417	1.482	Slow rotation ~Ω^2	Durney-Roxburgh	Roxburgh and Durney (1966) [11]
NG/μ=2	1.435	1.513	Slow rotation ~Ω^2	Sedrakyan-Chubaryan	Papoyan et al (1971) [12]
NG/μ=2	1.437	1.516	Rapid rotation	Chandrasekhar	Geroyannis et al (1989,1994) [13, 14]
NG/μ=2	1.459	1.534	Slow rotation ~Ω^2	Hartle	This work
GR/μ=2	1.405	1.478	Slow rotation ~Ω^2	Sedrakyan-Chubaryan	Arutyunyan et al (1971) [15]
GR/μ=2	1.429	1.516	Slow rotation ~Ω^2	Hartle	Boshkayev et al (2013, 2015) [16, 17]

4.1.11 The mass-shedding limit and scaling law

In this section we will discuss about some technical details related to the computation of the Keplerian mass-shedding limit of any rotating configurations and the scaling law for physical quantities that can be rescaled without additional numerical integrations for various objectives [122].

a) The mass-shedding limit. It is well known that the velocity of particles on the equator of the star cannot exceed the Keplerian velocity of free particles, computed at the same location. At this limit, particles on the star's surface remain bound to the star only because of a balance between gravitational and centrifugal forces. The evolution of a star rotating at the Keplerian rate is accompanied by a loss of mass, thus becoming unstable. The Keplerian angular velocity in NG is determined as follows

$$\Omega_{Kep} = \sqrt{\frac{GM_{tot}}{r_e^3}}, \tag{4.110}$$

where G is the gravitational constant, M_{tot} is the total mass of the rotating configuration and r_e is the equatorial radius. This is the critical angular velocity at which rotational shedding will occur, and it is thus an upper bound on those angular velocities for which the assumption of slow rotation could be valid.

In order to estimate this quantity correctly, one needs to select a test value of the angular velocity, for example, in our computations we used $\Omega_{test} = \sqrt{GM^{(0)}/a^3}$. Usually $\Omega_{test} > \Omega_{Kep}$, hence one needs to decrease the values of Ω_{test} gradually and estimate Ω_{Kep} successively, until $\Omega_{test} = \Omega_{Kep}$ with a given precision. For that purpose, in practice, it is convenient to use the shooting method.

If we express $\Omega_{Kep} = \kappa \Omega_{test}$, then the value of multiplicative factor κ can be estimated from the above procedure by numerical integration and the results are shown in table 4.1.

As one can see from the table, indeed $\Omega_{test} > \Omega_{Kep}$ and this results are in agreement with the ones in the literature [9-14, 137]. It should be stressed that the Keplerian angular velocity allows one to estimate the maximum rotation rate (the minimum rotation period) and the maximum rotating mass of stars. Moreover it allows us to determine the stability region of a rotating star, inside which all rotating configurations can exist (see [16] for details).

Although the data presented in table 4.1 seem to indicate that the value of κ is close to 0.75, it is important to note that this multiplicative factor is not the same at any density. In fact, it depends on the EoS of the WD matter and for different central densities with different nuclear compositions, it accepts distinct values. Even in the case of NSs the parameter κ possesses various values for a variety of the models used to construct the equations of state. For example, in [150], this parameter has been calculated for a particular EoS and a fixed range of values for the central density, leading to the result that the parameter varies in the range $0.63-0.67$. So, in general, there is no reason for this parameter to be independent of the density in the case of WDs, as well.

In all our computations, we used the value $\Omega_{Kep} = \sqrt{GM_{tot}/r_e^3}$. Of course, this is a rough approximation. Nevertheless, as it was pointed out by Berti et al [46] (see also

[151]), Hartle's approach with Ω_{Kep} gives only small differences (errors) with respect to the exact numerical methods used in GR for NSs. In the case of WDs, the errors should be even smaller than for neutron stars since WDs rotate more slowly than neutron stars (see appendix D of [16]). Moreover, we compare in table 4.2 our results with other more sophisticated approaches used in the literature; our results are in good agreement with other works.

b) Scaling law. The scaling procedure is used in order to rescale all the known values of physical quantities for different objectives. For instance, the angular momentum J is directly proportional to Ω, hence there is always the possibility for the following scaling law $J_{new}/\Omega_{new} = J_{old}/\Omega_{old}$ to be held. This means that knowing the old value of the angular momentum J_{old} for the given angular velocity Ω_{old}, one can easily evaluate a new value of the angular momentum J_{new} for a given new angular velocity Ω_{old} without reintegrating the structure equations. The same is true for all the physical quantities which are directly proportional to the second order of the angular velocity Ω^2. The following quantities are subject to scaling: $M^{(2)}_{new}/\Omega^2_{new} = M^{(2)}_{old}/\Omega^2_{old}$, $Q_{new}/\Omega^2_{new} = Q_{old}/\Omega^2_{old}$, $I^{(2)}_{new}/\Omega^2_{new} = I^{(2)}_{old}/\Omega^2_{old}$ and $W^{(2)}_{new}/\Omega^2_{new} = W^{(2)}_{old}/\Omega^2_{old}$. From a practical point of view it is very convenient to make use of the scaling law for various computational goals.

On the other hand, a careful examination of the scaling law for the quadrupole moment shows some resemblance with the I-Love-Q relations. Indeed, Q/Ω^2 is a constant quantity which is a function of the central density only, and it can be identified with the gravitational Love number λ. In the Ω^2 approximation, expressing Ω in terms of $I^{(0)}$ through $J^{(0)} = I^{(0)}\Omega$ and normalizing Q to the Kerr quadrupole moment, one obtains an approximate universal relation among the stellar moment of inertia, gravitational Love number and quadrupole moment as shown in [139], that do not depend strongly on the EoS. Of course, it would be interesting to check these relations also for WDs. In this case, in accordance to the generally accepted theoretical models for WDs, one needs to analyze at least two different equations of state with several nuclear compositions. This requires a detailed analysis which is beyond the scope of the present work. A more detailed study of these relations for WDs will be presented elsewhere.

4.1.12 Comparison with other results in the literature

In this section, we compare and contrast our results with other known results. The configurations of uniformly rotating WDs have been intensively investigated since their first theoretical descriptions. Here we present previous results obtained in this context. For example, in table 4.2, we show some results for the maximum static and rotating masses computed by several authors in NG, the post-Newtonian approximation and in GR. Regardless of the approximation, approach, treatment, theory and numerical codes, the results are very similar. These maximum masses for rotating WDs are to be compared with the ones found in this work using the Chandrasekhar EoS with μ=2. In NG, the maximum static mass is $1.459\,M_{\odot}$ and for a

rotating mass we obtain $1.534\,M_{\odot}$. The difference appears already at the level of the static configuration and this, in turn, translates to the rotating configurations.

For the sake of clarity, it should be mentioned that the structure equations describing uniformly rotating configurations, as derived in GR by Hartle in [43], reduce identically to the equations shown in this work for $c \to \infty$. Correspondingly, the structure equations formulated by Sedrakyan and Chubaryan [80] in GR also reduce to their Newtonian counterparts in the corresponding limiting case [12]. The mathematical and physical equivalence of these two formalisms has been recently shown in [35] by comparing the exterior Hartle-Thorne [44] and the Sedrakyan-Chubaryan [80] solutions. Thus, the difference in numbers of these two approaches in table 4.2 can be due to the numerical integrations, only.

4.2 Rotating white dwarfs in general relativity

4.2.1 Equations of structure

In section 3, we have considered the non-rotating configurations of WDs in the framework of general relativity. We consider now the effects of a slow rotation on these configurations. The stationary, axially symmetric metric may be written in the form (see, e.g. [43])

$$ds^2 = -H^2 dt^2 + Q dr^2 + r^2 K^2 \left[d\theta^2 + \sin^2\theta (d\varphi - L dt)^2 \right], \tag{4.111}$$

where $H = H(r,\theta)$, $Q = Q(r,\theta)$, $K = K(r,\theta)$, and $L = L(r,\theta)$. In order to describe the structure of slowly rotating objects, up to second order terms in the angular velocity of Ω, the metric (4.111) is defined by the following expression

$$\begin{aligned} ds^2 = &-e^{\nu(r)}\left(1 + 2h(r,\theta)\right) dt^2 + e^{\lambda(r)} \left[1 + 2m(r,\theta)/(r - 2M)\right] dr^2 + \\ &+ r^2 \left(1 + 2k(r,\theta)\right) \left[d\theta^2 + \sin^2\theta (d\varphi - \omega(r,\theta) dt)^2 \right], \end{aligned} \tag{4.112}$$

where $e^{\nu(r)}$ and $e^{\lambda(r)}$ are the metric functions of the static solution, M is the mass of the corresponding static (non-rotating) configuration with the same central density as the rotating one. The functions h, m, k may be expanded in spherical harmonics as

$$h(r,\theta) = h_0(r) + h_2(r) P_2(\theta) + \ldots, \tag{4.113}$$

$$m(r,\theta) = m_0(r) + m_2(r) P_2(\theta) + \ldots, \tag{4.114}$$

$$k(r,\theta) = k_0(r) + k_2(r) P_2(\theta) + \ldots, \tag{4.115}$$

where $P_2(\cos\theta)$ is the Legendre polynomial of second order. The angular velocity of local inertial frames ω is proportional to Ω, as well as the functions h_0, h_2, m_0, m_2, and k_2 are proportional to Ω^2. They can be found from the Einstein equations [43].

To be more precise, h_0, m_0 can be found from the $l=0$ components of two $(\Delta G_t^t)_{l=0} = 8\pi(\Delta T_t^t)_{l=0}$ and $(\Delta G_r^r)_{l=0} = 8\pi(\Delta T_r^r)_{l=0}$ Einstein equations in the form

$$\frac{dm_0}{dR} = 4\pi R^2 \frac{dE}{dP}(E+P)p_0^* + \frac{1}{12} j^2 R^4 (\bar{\omega}_R)^2 - \frac{1}{3} R^3 (j^2)_R (\bar{\omega})^2, \tag{4.116}$$

$$\frac{dh_0}{dR} = -\frac{m_0 R^2}{(R-2M)^2}\left(8\pi P + \frac{1}{R^2}\right) - \frac{4\pi(E+P)R^2}{(R-2M)} p_0^* + \frac{1}{12}\frac{R^4}{(R-2M)} j^2 (\bar{\omega}_R)^2, \tag{4.117}$$

and h_2, m_2, and k_2 from the $l=2$ components of gravitational field equations in the form

$$h_2 + \frac{m_2}{r-2M} = -\frac{1}{3} R^3 (j^2)_R \bar{\omega}^2 + \frac{1}{6} j^2 R^4 (\bar{\omega}_R)^2, \tag{4.118}$$

$$\frac{d}{dR}(h_2 + k_2) = h_2\left(\frac{1}{R} - \frac{\nu_R}{2}\right) + \frac{m_2}{R-2M}\left(\frac{1}{R} + \frac{\nu_R}{2}\right), \tag{4.119}$$

$$\frac{2}{R}\left(1-\frac{2M}{R}\right)\frac{dh_2}{dR} + \left(1-\frac{2M}{R}\right)\left(\nu_R + \frac{2}{R}\right)\frac{dk_2}{dR} - \frac{2m_2}{R}\left(\nu_R + \frac{1}{R}\right) - \\ - \frac{6h_2}{R} - \frac{4k_2}{R} + 8\pi\xi_2 \frac{dP}{dR} - \frac{1}{6} R^2 j^2 (\bar{\omega}_R)^2 = 0. \tag{4.120}$$

By introducing $\upsilon = h_2 + k_2$ and using $l=2$ part of the integral of the equation of hydrostatic equilibrium one finds the resulting equations in the form [43, 44]

$$\frac{d\upsilon}{dR} = -\nu_R h_2 + \left(\frac{1}{R} + \frac{\nu_R}{2}\right) + \left[-\frac{1}{3} R^3 (j^2)_R \bar{\omega}^2 + \frac{1}{6} j^2 R^4 (\bar{\omega}_R)^2\right], \tag{4.121}$$

$$\frac{dh_2}{dR} = \left\{-\nu_R + \frac{R}{(R-2M)\nu_R}\left[8\pi(E+P) - \frac{4M}{R^3}\right]\right\} h_2 - \frac{4\vartheta}{R\nu_R(R-2M)} + \\ + \frac{1}{6}\left[\frac{1}{2}\nu_R R - \frac{1}{(R-2M)\nu_R}\right] R^3 j^2 (\bar{\omega}_R)^2 - \frac{1}{3}\left[\frac{1}{2}\nu_R R - \frac{1}{(R-2M)\nu_R}\right] R^2 (j^2)_R (\bar{\omega}_R)^2. \tag{4.122}$$

The quantities $p^*{}_0$ and ν_R are given by $p^*{}_0 = -\xi_0/(E+P)dP/dR$ and $\nu_R = (8\pi R^3 + 2M)/R(R-2M)$, M is the mass of the non-rotating configuration. It is convenient to introduce $\upsilon = h_2 + k_2$ for the purpose of numerical computation of these equations.

By using $l=0$ part of the integral of the equation of hydrostatic equilibrium expanded in powers of Ω^2 we can rewrite the equation (4.117)

$$-\frac{dp_0^*}{dR}+\frac{1}{12}\frac{R^4}{(R-2M)}j^2(\bar{\omega}_R)^2+\frac{1}{3}\frac{d}{dR}\left(\frac{R^3j^3\bar{\omega}^2}{R-2M}\right)=\frac{4\pi(E+P)R^2}{(R-2M)}p_0^*+\frac{m_0R^2}{(R-2M)^2}\left(8\pi P+\frac{1}{R^2}\right). \quad (4.123)$$

The equation (4.123) is the relativistic equation of hydrostatic equilibrium for slowly rotating configurations. This equation demonstrates the balance of gravitational, pressure and centrifugal forces and together with the of (4.116) completely solve $l=0$ problem, find the unknown functions m_0, h_0. In turn, the unknown functions m_2, h_2, k_2 and ξ_2 may be calculated from the system of equations (4.118-4.120), together with $l=2$ part of the integral of the equation of hydrostatic equilibrium. It completely determines the $l=2$ problem. By expanding all quantities in powers of $1/c^2$, one can obtain the corresponding equations for slowly rotating configurations in NG, which has been already discussed in subsection 4.2 and 4.3 [43, 44].

4.2.2 Rotating white dwarfs at zero temperature

In this subsection we construct equilibrium configurations of static and uniformly rotating WDs using the Chandrasekhar EoS and the relativistic FMT EoS within GR for the sake of completeness [91, 105]. First we perform computations for zero temperature uniformly rotating WDs at the mass shedding limit by utilizing the relativistic FMT EoS within the HF [43, 44, 91, 127]. Afterwards, we investigate static WDs at finite temperatures by employing the Chandrasekhar EoS. Finally, we superpose these theoretical results with the estimated data obtained from the SDSS DR 4 by Tremblay et al [111].

In figure 4.17 we constructed the mass-radius relation of uniformly rotating WDs using both the Chandrasekhar and relativistic FMT EoS in GR by fulfilling their stability criteria [105, 91]. The radius of the WDs in this plot is defined as the average spherical radius $\langle R\rangle=(1/3)(R_p+2R_e)$, where R_p is the polar radius, R_e is the equatorial radius. For the sake of generality, we accounted for the nuclear composition of the WD matter in the relativistic FMT EoS. As one can see from figure 4.17 the consideration of the nuclear composition along with rotation at the Keplerian limit is not sufficient to explain all the observational data.

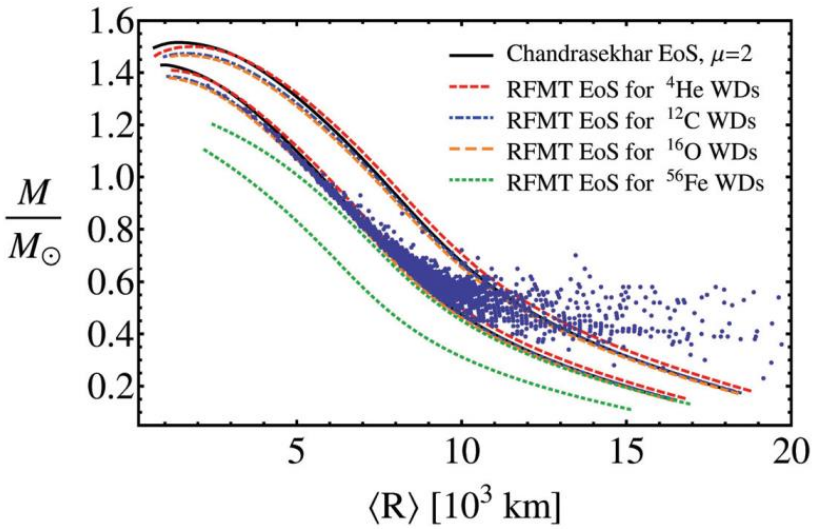


Figure 4.17 – Mass-radius relation of uniformly rotating WDs obtained with the Chandrasekhar EoS and the RFMT EoS for T = 0 K case and their superposition with the estimated masses and radii of WDs taken from the SDSS DR 4 (blue dots). Upper curves indicate rotating WDs and lower curves indicate static WDs.

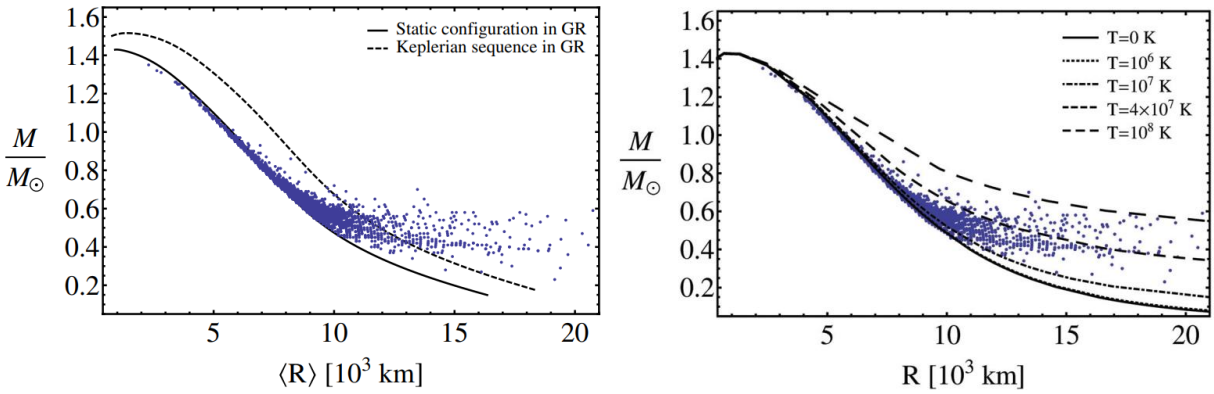


Figure 4.18 – Mass-radius relation of uniformly rotating WDs obtained with the Chandrasekhar EoS for T=0 K case (left panel) and mass-radius relation of static WDs for selected finite temperatures from T = [0, 10^6, 10^7, 4×10^7, 10^8] K (right panel) and their superposition with the estimated masses and radii of WDs taken from the SDSS DR 4 (blue dots)

In order to tackle this relevant issue S.M. de Carvalho et al [25] proposed to include the finite-temperature effects in the EoS. Following this idea we performed a similar analysis for static WDs at finite-temperatures with the simplest Chandrasekhar EoS by solving the TOV equation (see [90] for details). The results of [90, 91] are illustrated in figure 4.18. As one can see here in analogy to [25] the only inclusion of the finite-temperature effects in the Chandrasekhar EoS leads to the mass-radius relation in better agreement with the observational data [91, 127].

It should be noted, that from the astronomical observations of isolated WDs one infers the effective surface temperature and the surface gravity but not the mass-radius relation. All main parameters are inferred and estimated by using certain

models. However for WDs in close eclipsing binaries there exist techniques to measure their masses. The data obtained from these binaries are considered to be more reliable and model-independent. Therefore to perform more realistic computations one needs to take into account the effects of rotation, chemical composition and temperature together for selected WDs with known parameters. Only after one can perform more precise analyses and make further predictions.

4.2.3 Rotating white dwarfs at finite temperatures

In this subsection the influence of the effects of GR, rotation and finite-temperatures on the structure of WDs is considered. Accounting for such effects and physical parameters make the theory of WD be more realistic. The HF [43, 44, 127] was invoked to calculate the main parameters of rotating WDs employing the Chandrasekhar EoS at finite temperatures. The main results are depicted in figures 4.19 and 4.20.

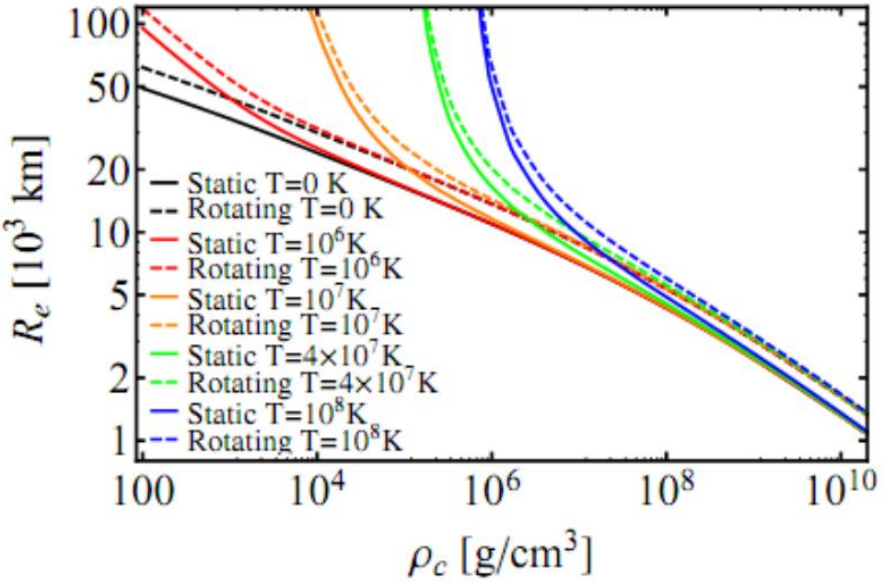


Figure 4.19 – The equatorial radius-central density relation for rotating hot WDs

Figure 4.19 shows the dependence of the equatorial radius on the central density and temperature for static and rotating WDs in GR. From the figure one can see that the hot WDs possess larger radii than the cold ones with the same central densities. By examining only static WDs one can show that easily by calculating the thickness of a hot non-degenerate layer on top the cold degenerate one. Consequently, this effect translates also to rotating WDs [129].

From the astrophysical context it is also important to construct the mass-radius relations for hot WDs. As one can see from figure 4.20 for the fixed mass the radius of a WD can be various depending on the values of rotation period and temperature. From observations, unlike the radius of stars, it is relatively easy to measure the mass. Therefore, the calculation of radius is a very delicate problem as the small corrections

of GR and the effects of finite temperatures become more dominant in radius not in mass.

In figures 4.19 and 4.20 all WDs rotate at the Keplerian rate (mass shedding limit). All realistic uniformly rotating WDs will be in between the static and mass shedding limit. It should be noted, that here we consider only the core temperatures. The interrelation of the core temperature and the observed effective surface temperature is given via the Koester relation. By employing the Koester formula one can show easily that our calculations are compatible and consisted with the observational data for WDs [25].

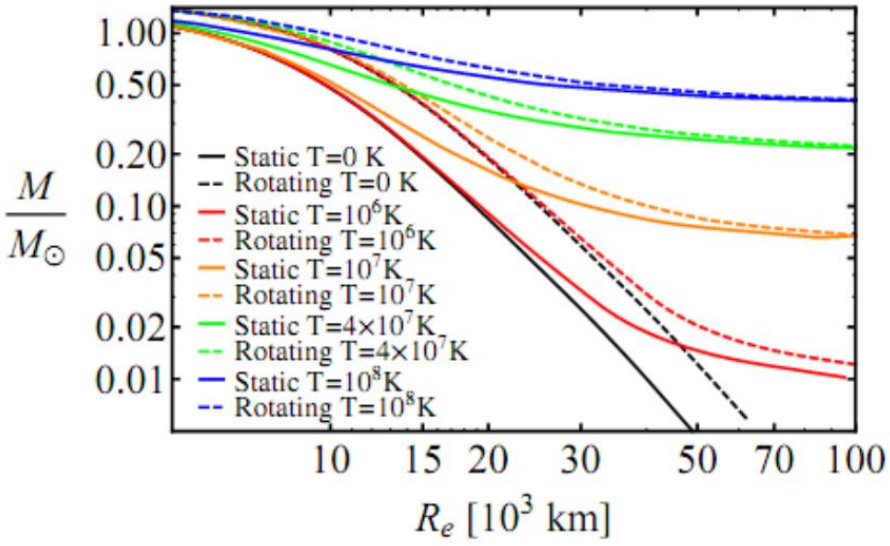


Figure 4.20 – The total mass-equatorial radius relation for rotating hot WDs

Figure 4.20 shows the mass-radius relation for hot static and rotating WDs in GR. It is evident that this relation is very different from the degenerate case, in particular, for small masses and large radii, depending on the temperature of the isothermal core. These results can be used to explain a wider range of observations of WDs [129].

4.3 Summary

In subsection 4.1, we have revisited the Hartle formalism to describe in Newtonian gravity the structure of rotating compact objects under the condition of hydrostatic equilibrium. We use a particular set of polar coordinates that is especially constructed to take into account the deformation of the source under rotation. Moreover, we use an expansion in terms of spherical harmonics and consider all the equations only up to the second order in the angular velocity. The main point is that these assumptions allow us to reduce the problem to a system of ordinary differential equations, instead of partial differential equations. As a consequence, we derive all the equations explicitly and show how to perform their numerical integration. In addition, the formalism developed here allows us to find explicit expressions for the

main physical quantities that determine the properties of the rotating configuration. In particular, we derived the equation which determines the relation between mass and central density, and showed that it takes the form of an equation of hydrostatic equilibrium. It enforces the balance of pressure, gravitational, and centrifugal forces correctly to order Ω^2. In this approximation, the surfaces of constant density are spheroids whose ellipticity varies from zero at the centre of the star up to the values which describe the shape of the star at the surface. The ellipticity, as a function of the radius, turns out to be determined by Clairaut's differential equation. The equations which determine the relation between mass and central density and those which determine the ellipticity are systems of ordinary differential equations whose solution may be obtained by numerical integration. Furthermore, we also derived analytic expressions for the quadrupole moment and moment of inertia of the source. In addition we derived and integrated the expressions for the rotational kinetic energy and gravitational binding energy. We constructed $T/|W|$ ratio versus central density and checked its consistency with the instability criteria for secular and dynamical instabilities of the Maclaurin spheroids. Finally, we obtained the Clairaut-Radau equation from the Clairaut equation and calculated the gravitational Love number, which indicates rotational or tidal response to the exterior field. We have tested the formalism developed here by using the Chandrasekhar equation of state for white dwarfs. All the derived physical quantities are in accordance with the results in the literature. This result reinforces the validity of the assumptions and approximations applied in this work to formulate a method that takes into account the rotation in the context of hydrostatic equilibrium in Newtonian gravity. Eventually, on top of everything the procedure of computing the Keplerian mass-shedding angular velocity along with the scaling law of physical quantities have been presented for rotating configurations. In view of recent works [139, 140] on the so-called I-Love-Q relations in neutron stars and quark stars, it would be interesting to investigate these relations in white dwarf stars. This is considered in the section 5.

In subsection 4.2, at first, we calculated the mass-radius relations for cold uniformly rotating WDs within the HF in GR using both the Chandrasekhar and RFMT EoS. We superposed our results with the estimated values of masses and radii obtained by Tremblay et al [111]. As a result we showed that the rotation along with the chemical composition are not sufficiently enough to explain all the observational data. Furthermore, to investigate WDs at finite-temperatures we considered a static case and solved the TOV equation numerically by using the Chandrasekhar EoS.

We compared and contrasted our results with the estimated data from the observations and showed that the data, including the range of low masses, can be covered and described by taking into account the effect of finite temperatures alone. We have considered the effects of finite-temperatures and rotation separately.

In all our computations we used the uniform temperature of the WDs core. To link this temperature with a real surface temperature of a WD we exploited the Koester formula [109] which establishes the relationship between the effective surface temperature and the core temperature. We found that most of the observed WDs core temperatures are lower than 10^8 K (Fig. 4.18). More data are still needed to

confirm and extend our results. In view of recent discoveries of WDs by Koester and Kepler et al. [114] the theoretical study of these objects become more fascinating and overwhelming then ever before.

Second, mass-radius and radius-central density relations of static and rotating, cold and hot WDs were calculated using the Chandrasekhar EoS in GR. The effects of finite temperatures were accounted for in the EoS. The effects of GR were involved the structure equations. The effects of rotation (deformation of a star, extra mass due to the balance of the centrifugal force and gravity) were investigated within the HF. It was shown that in the construction of a realistic model of WDs the effects of finite temperatures, GR and rotation must be accounted for properly. It was demonstrated that for low-mass WDs the effects of temperature are more prominent while the general relativistic effects are more important for massive WDs. Instead the rotation affects the structure of WDs in all mass ranges. Consequently, rotation gives an additional degree of freedom for cold and hot WDs, as expected. The mass-radius relations obtained in this work are consistent with observations [127]. Moreover, the effects of rotation and finite temperatures were considered together in all our calculations. Namely, we considered the temperatures of the isothermal cores of WDs. For comparison with the observed surface temperatures of WDs, the Koester formula must be used, which establishes the interrelation between the effective surface temperature and the temperature of the isothermal cores.

5 I-LOVE-Q RELATIONS FOR WHITE DWARF STARS

As compared to Newtonian stars, the conditions determining the hydrostatic equilibrium of a star changes drastically when the full system of Einstein's equations is taken into account. In fact, in GR, the Newtonian equation of hydrostatic equilibrium for compact stars becomes modified to what is known as TOV equation. A general analysis of spherically symmetric compact stars, taking into account general relativistic effects, was performed in [152]. By considering an EoS valid for both non-relativistic and ultra-relativistic electron velocities, it was found that in the case of WDs, general relativistic effects lead only to small perturbations of the values obtained in NG. It follows that it is justified to use Newton's theory to investigate the essential part of the physical properties of WDs. In this section, we will follow this hypothesis.

Although many approaches can be used to investigate the properties of compact stars in NG, a particularly useful method was proposed recently [120, 122] in which the relativistic HF is applied explicitly to solve the corresponding set of differential equations. The HF has been widely used in the scientific community to describe relativistic objects such as neutron stars, quark stars, and other exotic objects [43, 44, 48]. One of the advantages of its application is that it is very intuitive from a geometric and a physical point of view, because it uses coordinates that are especially adapted to the shape and dynamics of rotating bodies. When applied to describe equilibrium configurations in NG, the HF transforms the dynamic equations to be solved into a system of ordinary differential equations. Moreover, it allows us to derive in detail all physically relevant quantities such as the total rotating mass M_{tot}, equatorial r_e and polar r_p radii, angular momentum J, eccentricity e, ellipticity ϵ, rotational Love number λ, moment of inertia I, and the quadrupole moment Q. All these parameters play a pivotal role in the investigation of the stability and the lifespan of WDs [147, 148, 16, 153, 17, 149].

In this section [154], we investigate the effects that rotation causes in the structure of WDs; namely, we construct the I-Q, I-e, Q-e, I-Love and Love-Q relations, and show that they are universal and independent of the equations of state for WDs. We focus on the case of slow and rigid rotation. We integrate the equations of structure for slowly rotating WDs numerically by using the Chandrasekhar and Salpeter equations of state [7, 133, 20, 155, 105]. In addition, we analyze the stability properties of WDs against the mass-shedding limit, the inverse β-decay instability, and the secular instabilities [16].

5.1 Equations of structure

The method used to construct models for uniformly and slowly rotating relativistic stars is summarized briefly here. For details and derivations the reader may refer to [122, 120, 43], the notation of which we follow. The main idea consists in considering a spherically symmetric non-rotating compact object as starting point. Then, the rotation is considered up to the second order as a small perturbation of the non-rotating model [154].

5.2 Stability criteria for rotatingwhite dwarfs

5.2.1 Inverse β-decay instability

The inverse β-decay instability allows us to determine the critical density which in turn defines the onset of instability for a WD to collapse into a neutron star. The inverse β-decay instability is crucial both for static and rotating configurations. It represents one of the boundaries of the stability region in rotating WDs [16].

In WDs, when the central density increases, the electrons become ultra-relativistic and start interacting with protons in nuclei, thus forming neutrons and neutrinos as a byproduct. In order for this process to take place, the electron Fermi energy without the rest mass must be larger than the mass difference between the initial (Z, A) and the final (Z – 1, A) nucleus (see e.g. [20, 5]). This threshold energy is denoted as ε_Z^β and the corresponding central density as ρ_{crit}^β for the Salpeter EoS. The empirical threshold energies along with possible decay channels are presented in Table 4.1 (see also [105] for more details). Since the internal pressure of the WD is determined by the pressure of the degenerate electron gas, configurations with $\rho > \rho_{crit}^\beta$ become unstable, as a result of the electron capture process (see [156], [20] for details).

Table 5.1 – Onset for the inverse β-decay of ^{4}He, ^{12}C, ^{16}O and ^{56}Fe. The experimental values of the threshold energies ε_Z^β have been taken from Table 1 of [157]; see also [158], [5]; [105]

Decay	ε_Z^β (MeV)	ρ_{crit}^β (g/cm^3)
$^4\mathrm{He} \rightarrow {}^3\mathrm{H} + \mathrm{n} \rightarrow 4\mathrm{n}$	20.596	1.37×10^{11}
$^{12}\mathrm{C} \rightarrow {}^{12}\mathrm{B} \rightarrow {}^{12}\mathrm{Be}$	13.370	3.88×10^{10}
$^{16}\mathrm{O} \rightarrow {}^{16}\mathrm{N} \rightarrow {}^{16}\mathrm{C}$	10.419	1.89×10^{10}
$^{56}\mathrm{Fe} \rightarrow {}^{56}\mathrm{Mn} \rightarrow {}^{56}\mathrm{Cr}$	3.695	1.14×10^{9}

5.2.2 Mass-shedding limit

The balance between the gravitational and centrifugal forces determines the maximum angular velocity of any astrophysical object. In addition, the deformation of the object must be also taken into account. Though for any rigidly rotating object the angular velocity is uniform throughout the object, the linear velocity reaches its maximum at the equator. Thus the equatorial plane will be first subjected to the mass-loss or mass-shedding, making the star unstable. The Keplerian angular velocity also known as the mass-shedding velocity is determined as follows

$$\Omega_{Kep} = \sqrt{\frac{G M_{tot}}{r_e^3}}. \tag{5.1}$$

In order to compute this quantity correctly, one needs to select a test value for the angular velocity, for example $\Omega_{test} = \sqrt{G M^{(0)} / a^3}$. Usually, $\Omega_{test} > \Omega_{Kep}$, hence one needs

to decrease gradually the values of Ω_{test} and estimate Ω_{Kep} successively, until $\Omega_{test} = \Omega_{Kep}$ with a given precision. For that purpose, in practice it is convenient to use the shooting method.

The Keplerian angular velocity allows us to estimate the maximum angular velocity, mass, moment of inertia, and other parameters of the star. Moreover, it allows us to determine the stability region inside which rotating configurations can exist [16].

5.2.3 The turning-point criterion and secular axisymmetric instability

In order to investigate the secular instability that emerges due to small perturbations, a turning point method was proposed in [145] for uniformly rotating relativistic stars. According to this method, the points where the secular instability sets in are located along a sequence of rotating stars with constant angular momentum and increasing central density. The condition

$$\left(\frac{\partial M(\rho_c, J)}{\partial \rho_c}\right)_J = 0 \tag{5.2}$$

defines the onset of the secular axisymmetric instability. In the mass-central density diagram, the maximum mass of a constant J sequence is a turning point. The configurations on the right-hand side of the turning point are secularly unstable and the configurations on the left-hand side are stable. Thus the boundary made of the turning points for different values of fixed J separate stable from unstable stars (see [48]). It should be emphasized that the turning point of a constant J sequence is a sufficient but not a necessary condition for secular instability. Consequently, for a constant angular momentum sequence it establishes an absolute upper bound for the mass [16].

5.3 Results and discussion

In equilibrium, a rotating star attains a balance between pressure, gravitational and centrifugal forces. In classical physics, the magnitude of the centrifugal force is determined by the angular velocity Ω of the fluid relative to a distant observer. We adopt this angular velocity Ω as the mass shedding or the Keplerian angular velocity for the sake of generality [154].

In Fig. 5.1, the mass of a WD is shown as a function of the central density. The mass is given in units of one solar mass and the central density is given in g/cm^3. We have selected two equations of state: the Chandrasekhar EoS with average molecular weight $\mu=2$, and the Salpeter EoS for pure helium ^{4}He, carbon ^{12}C, oxygen ^{16}O and iron ^{56}Fe WDs, as limiting cases. All solid curves indicate non-rotating (static) WDs, whereas all dashed curves indicate rotating WDs at the mass shedding rate. As expected, rotating WDs have larger masses with respect to their static counterparts. In all our computations we restricted the maximum values of the central density to the values of inverse β-decay density to fulfill the stability condition of WDs [105, 16].

In addition, by using the turning point method, we investigated secular instability of the WDs. It turned out that in classical physics all uniformly rotating WDs are stable against axisymmetric secular instabilities.

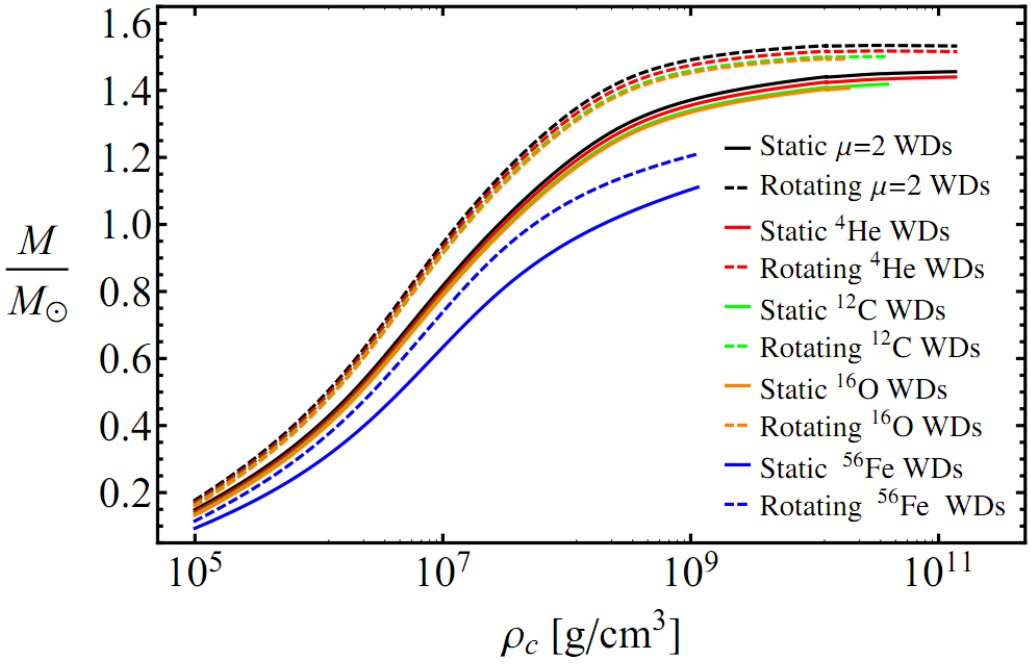


Figure 5.1 – Mass versus central density

Fig. 5.2 shows the mass and equatorial radius relation. The equatorial radius for a static case reduces to the static radius. All legends in the plot are the same as in Fig. 5.1 and hereafter we keep these legends in all our plots. Depending on the EoS and nuclear composition, WDs display different mass-radius relations. This explains the variety of observed WDs. Nowadays, we have data for more than thirty two thousand WDs and all of them have diverse characteristics [159, 160, 111, 161, 114].

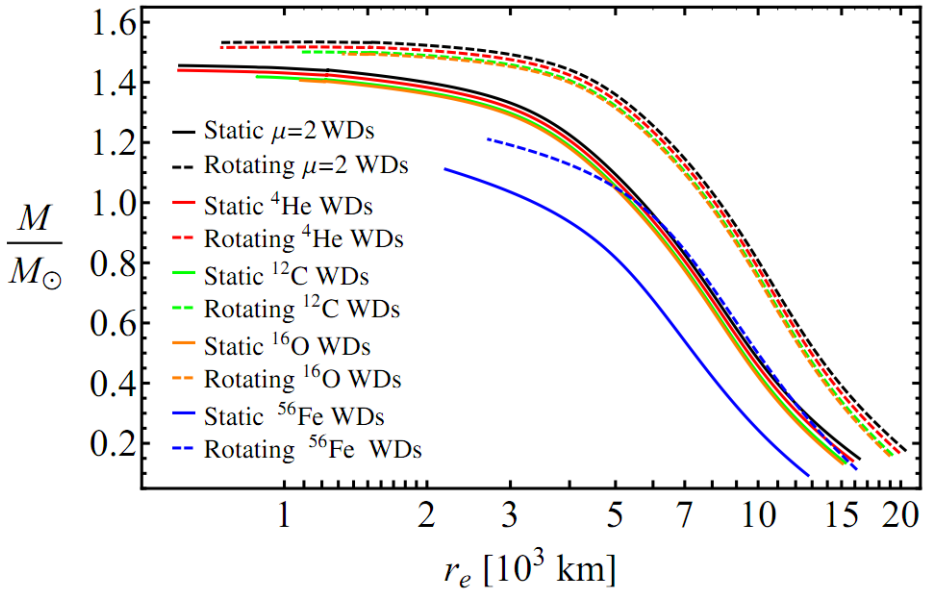


Figure 5.2 – Mass versus radius

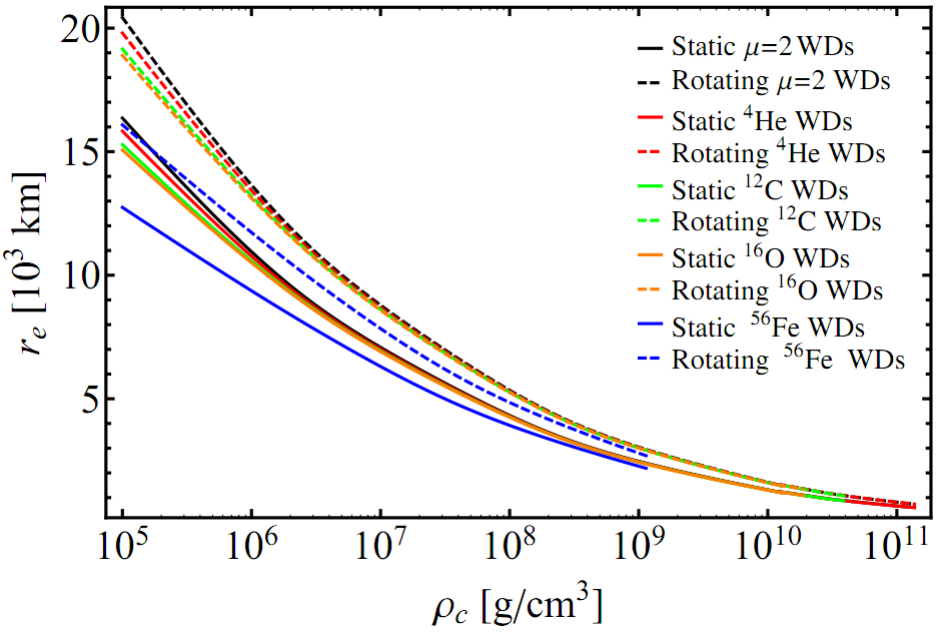


Figure 5.3 – Radius versus central density

Fig. 5.3 shows the radius and central density relations of both rotating (equatorial radius) and non-rotating (static radius) WDs. For increasing central densities, the gap between equatorial and static radii is narrowed. Thus, WDs become more gravitationally bound and spherical.

Fig. 5.4 illustrates the behavior of the normalized moment of inertia in terms of the static mass and the square of the static radius as a function of the central density. For lower densities, the difference in the moment of inertia between rotating and static WDs is quite large. However, for higher densities the difference becomes smaller. A different representation of the moment of inertia in terms of the total mass is given in Fig. 5.5, where one can see a similar behavior [154].

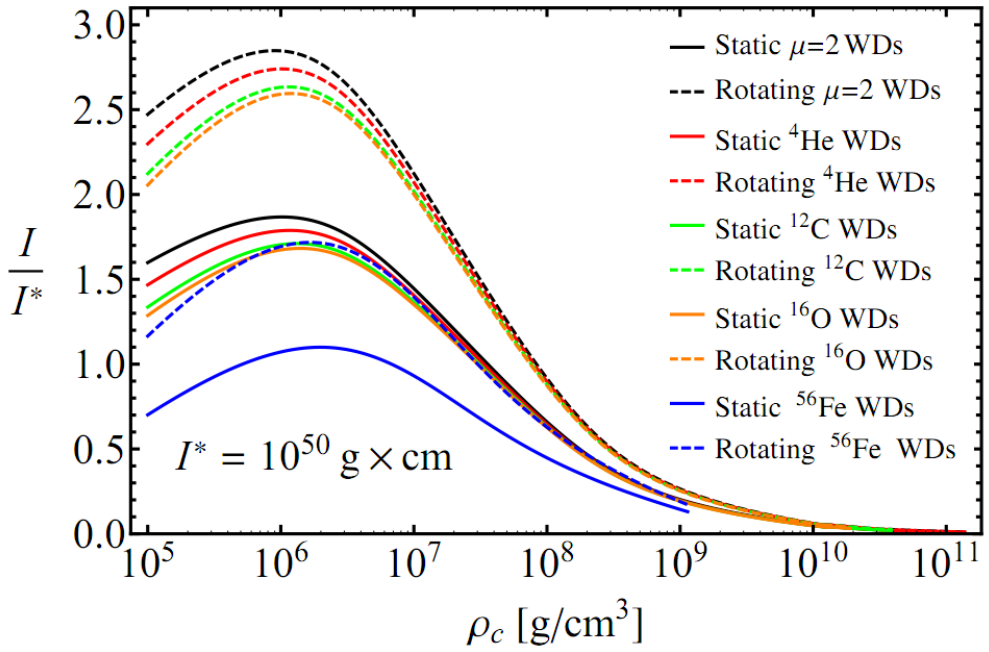


Figure 5.4 – Moment of inertia versus central density

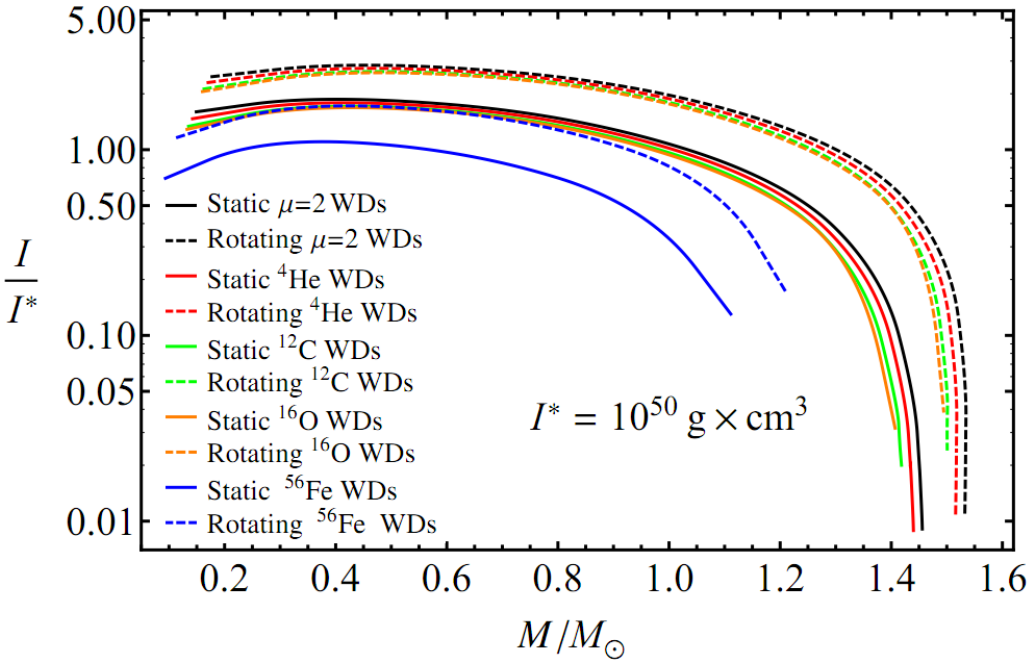


Figure 5.5 – Moment of inertia versus mass

The total mass as a function of the angular momentum for rotating WDs is presented in Fig. 5.6. The dependence between mass and angular momentum is nonlinear. This is obvious for large values of the angular momentum. This is a very important fact, especially when one deals with its astrophysical implications.

The rotating mass as a function of the angular velocity is presented in Fig. 5.7. As one can see, due to their compactness, massive WDs can reach higher values for the angular velocity than less massive stars. In addition, Fig. 5.7 shows the maximum rotation rate for a given mass [154].

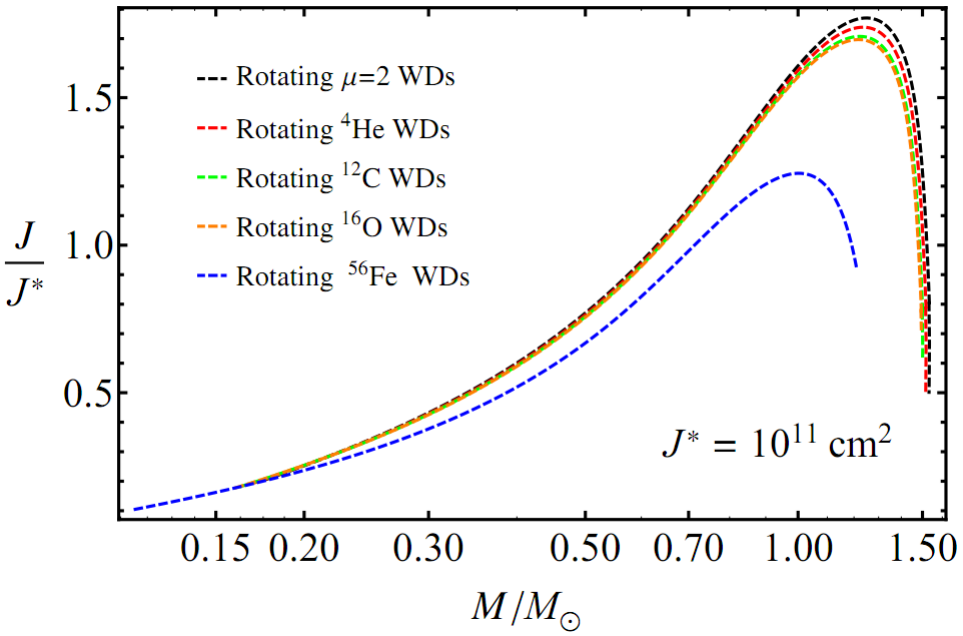


Figure 5.6 – Mass versus angular momentum

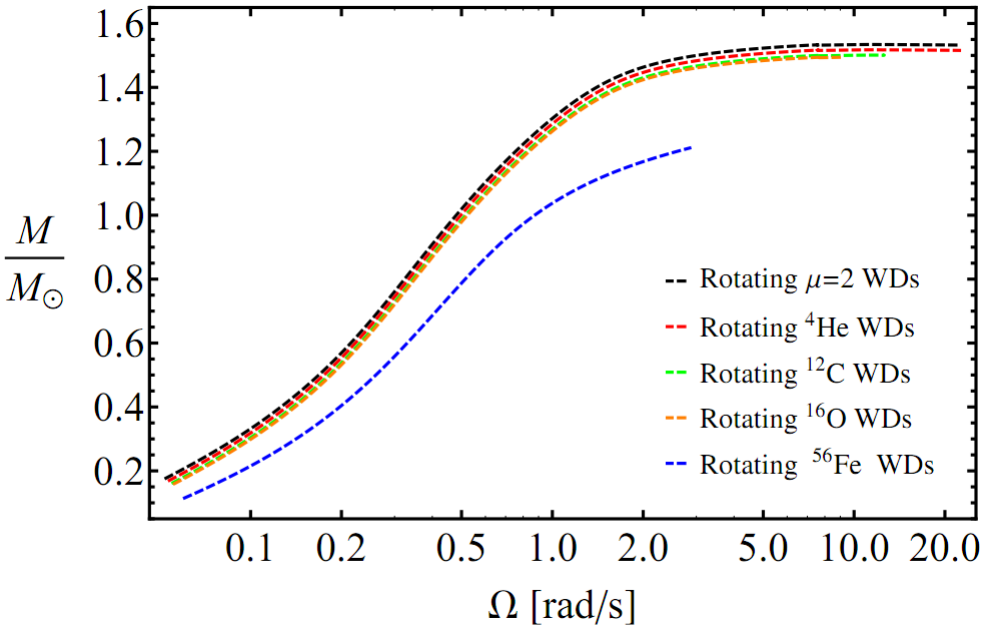


Figure 5.7 – Mass in units of solar mass versus maximal angular velocity

The angular momentum as a function of the angular velocity along the Keplerian sequence is given in Fig. 5.8. It should be noted that the angular momentum is not always directly proportional to the angular velocity. Depending on the mass, one can observe either spin-up or spin-down effects. WDs having mass close to the Chandrasekhar mass limit can experience both spin-up and spin-down effects [16, 120 or 153].

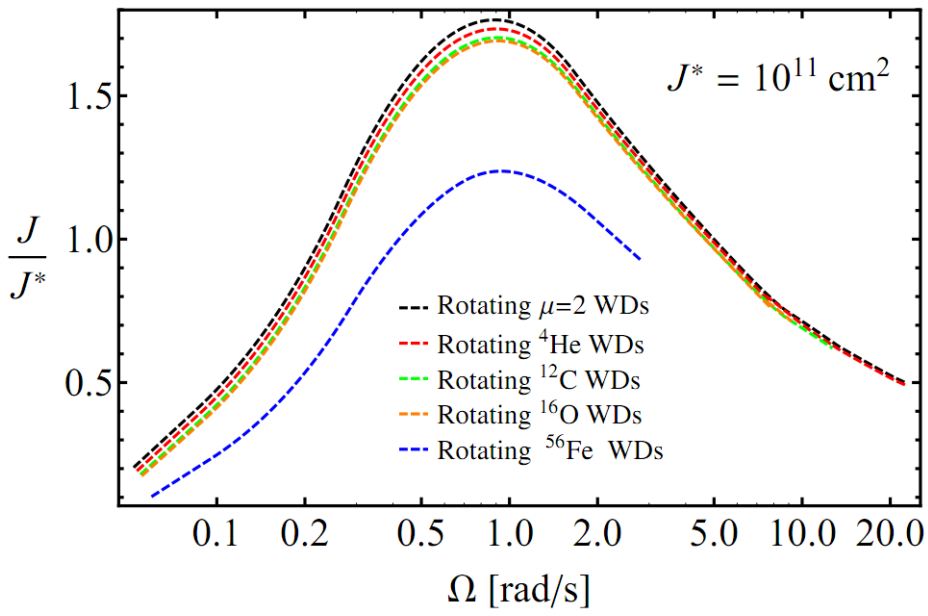


Figure 5.8 – Angular momentum versus maximal angular velocity

The eccentricity of rotating WDs as a function of the central density is shown in Fig. 5.9. For higher densities, the eccentricity decreases and vice versa. Thus, WDs with increasing central density become more spherical as they approach their maximum mass.

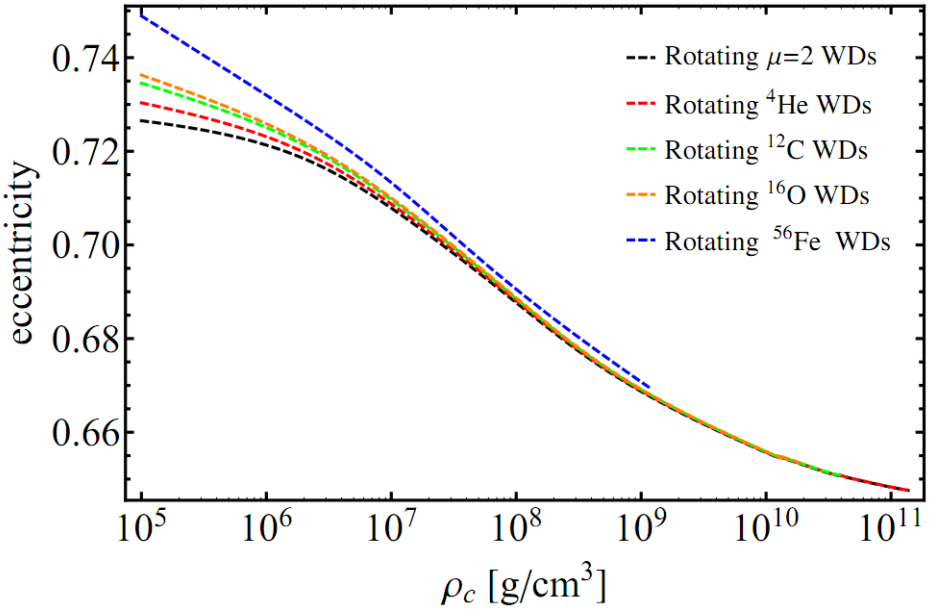


Figure 5.9 – Eccentricity versus central density

The normalized moment of inertia is shown as a function of the central density in Fig. 5.10. The behavior of both rotating and static moments of inertia is similar to the eccentricity.

The normalized quadrupole moment as a function of the central density is shown in Fig. 5.11. Here the normalized quadrupole moment shows the same behavior as the

eccentricity and the moment of inertia. So, for more massive WDs it decreases as the radius decreases.

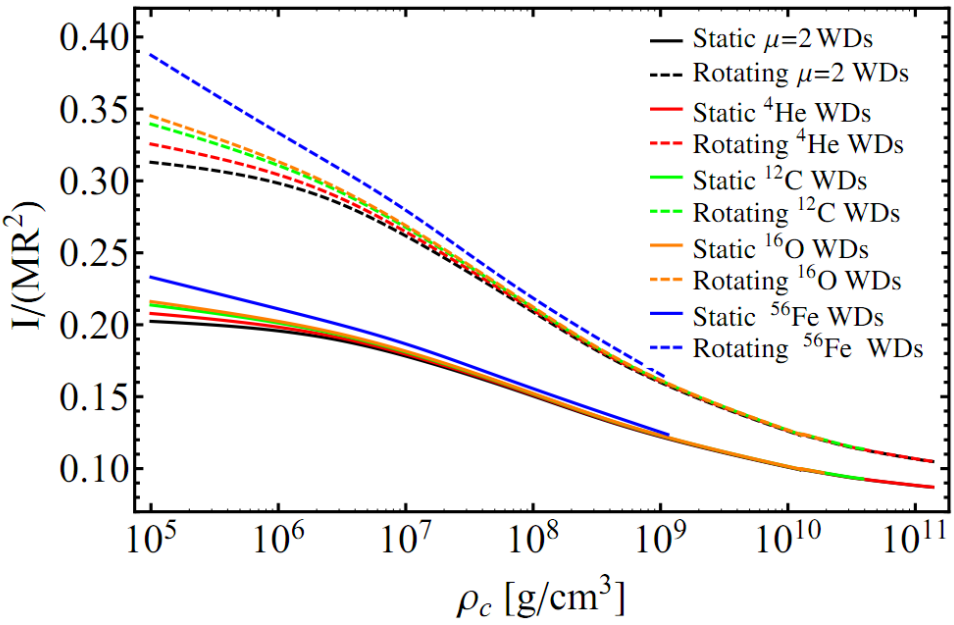


Figure 5.10 – Normalized moment of inertia versus central density

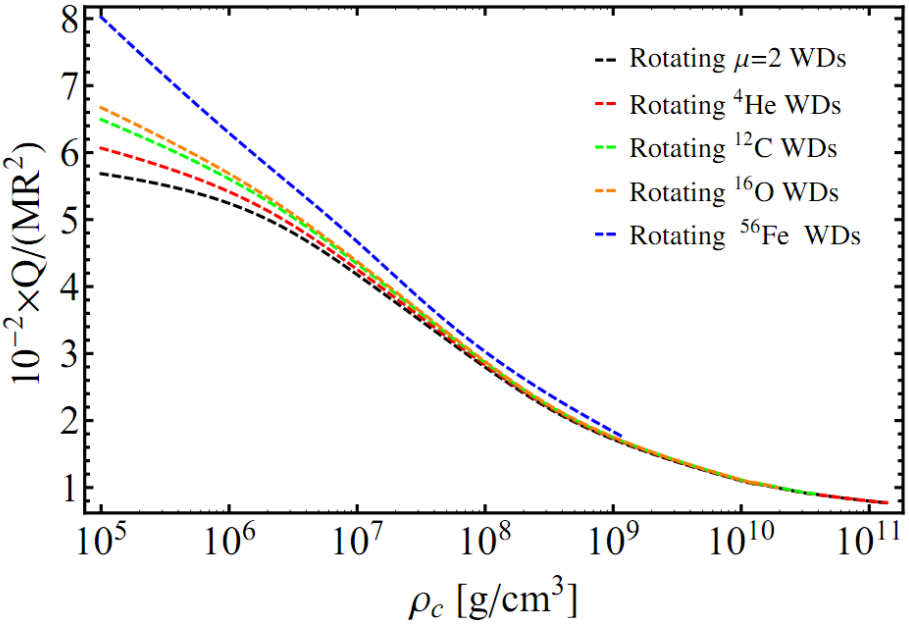


Figure 5.11 – Normalized quadrupole moment versus central density

5.4 I-LOVE-Q and I-Q-e relations for white dwarfs

First, we notice that an inspection of Figs. 5.9, 5.10 and 5.11 shows an intriguing correlation between the moment of inertia and the quadrupole moment as functions of the eccentricity of rotating WDs. We therefore analyze the behavior of the moment of inertia as a function of the eccentricity in Fig. 5.12, where the moment of inertia is

divided by 10^{22} cm^3 for the sake of convenience. As expected, the moment of inertia increases with the eccentricity until it reaches a maximum value which depends on the angular velocity and composition of the star. This graphic does not present any especial peculiarities. However, the situation changes completely, if instead we consider the normalized moment of inertia $I/(10MR^2)$ with respect to the static configuration. The result is presented in Fig. 5.13 for static and rotating stars. It shows an universal behavior for the I-e relation, independently of the EoS and nuclear composition of the WD.

Note that in Figs. 5.12, 5.13, 5.16, 5.17 etc. we plot both static and rotating configurations together. This is because Hartle's approach allows one to calculate rotating configurations with the same central densities as the static ones. Hence it is always possible to display both static and rotating configurations in one diagram indirectly in terms of the central density.

Consider now the quadrupole moment; in Fig. 5.14, we show its behavior as a function of the eccentricity. The value of the quadrupole is bounded, reaching a maximum value which depends on the nuclear composition of the star. Furthermore, in Fig. 5.15, we consider the normalized quadrupole $Q/(100MR^2)$, where M and R correspond to the static configuration. The universality of this Q-e relation is evident because no dependence can be observed neither from the EoS nor from the nuclear composition of the WD.

We now consider the quadrupole moment as a function of the moment of inertia. This behavior is illustrated in Figs. 5.16 and 5.17. Similar to the previous cases for the I-e and Q-e relations, the Q-I relation displays the same trend, i.e., only for the normalized quantities one can establish the same universality, independently of the EoS.

Finally, we investigate the I-Love-Q relations in Figs. 5.18, 5.19 and 5.20 which represent the dependence of the dimensionless moment of inertia $\bar{I}$, the dimensionless Love number $\bar{\lambda}$, and the dimensionless quadrupole moment $\bar{Q}$ on each other. We see that the I-Love-Q relations proposed by Yagi and Yunes [139] for relativistic objects are also true for white dwarf stars in classical physics.

It should be stressed that it is always possible to display both static and rotating configurations for the moment of inertia in one plot in terms of the central density. However, if we display them as in Figs. 5.18, 5.19 and 5.20 they will overlap with each other and one cannot distinguish them; hence, we plot them using a different representation (see [154]for details).

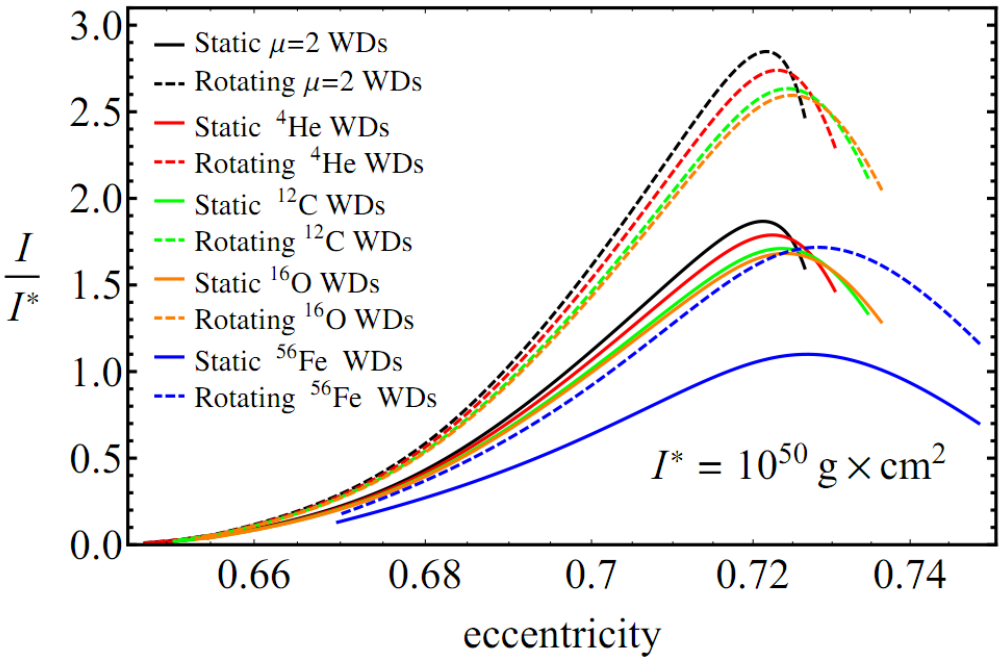


Figure 5.12 – Moment of inertia versus eccentricity

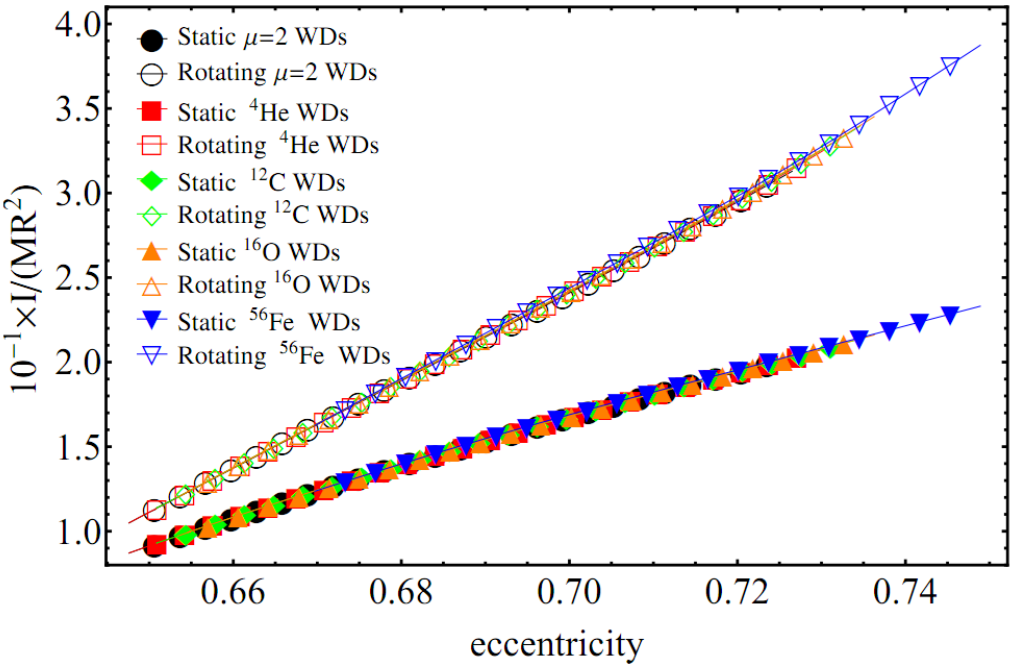


Figure 5.13 – Normalized moment of inertia versus eccentricity.

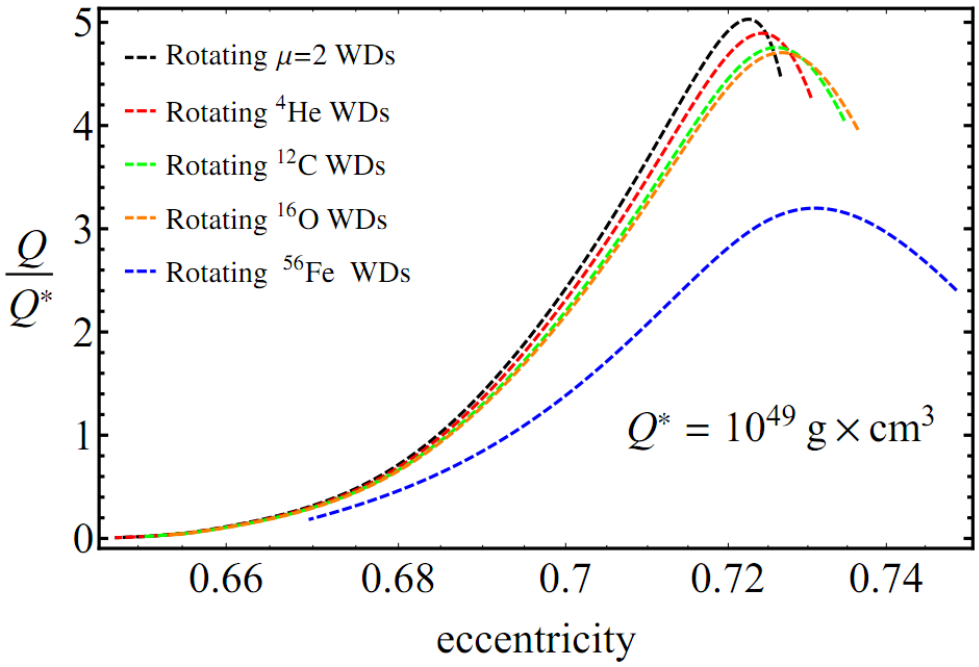


Figure 5.14 – Quadrupole moment versus eccentricity

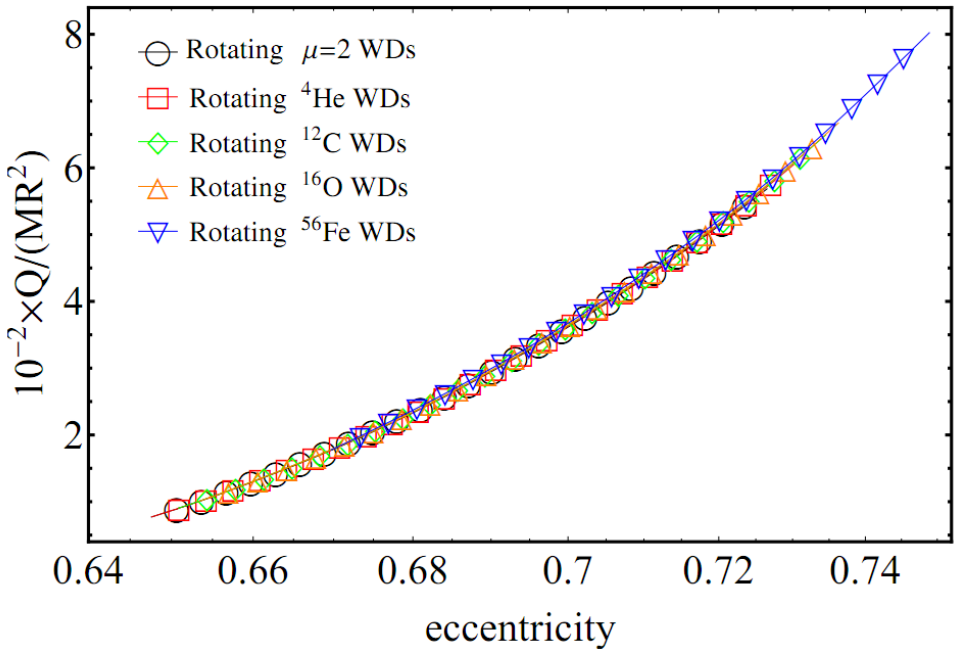


Figure 5.15 – Quadrupole moment normalized to the static mass and corresponding radius squared versus eccentricity

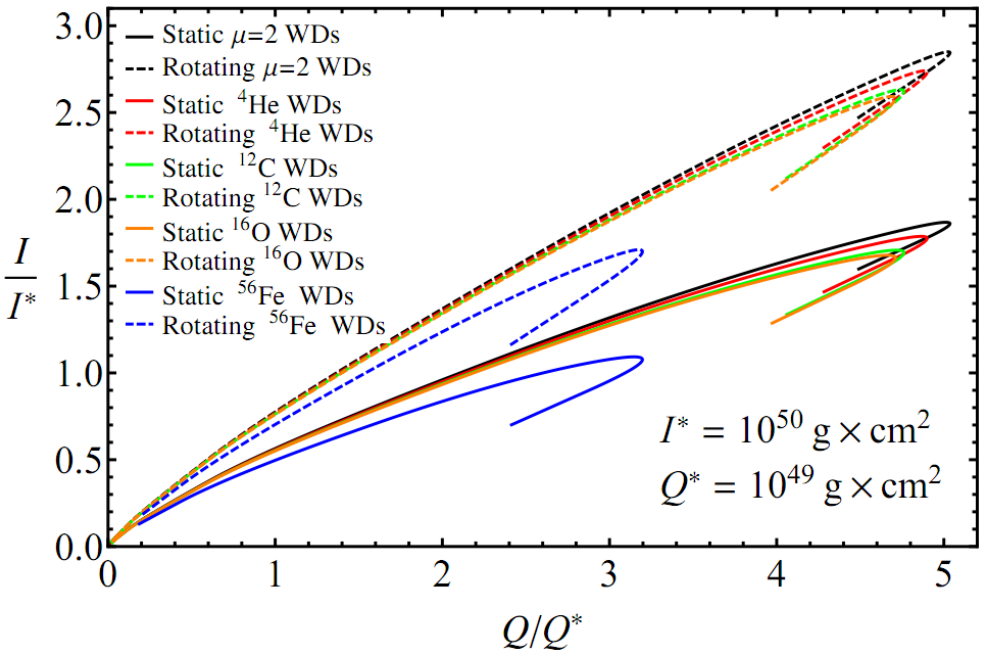


Figure 5.16 – Quadrupole moment versus moment of inertia

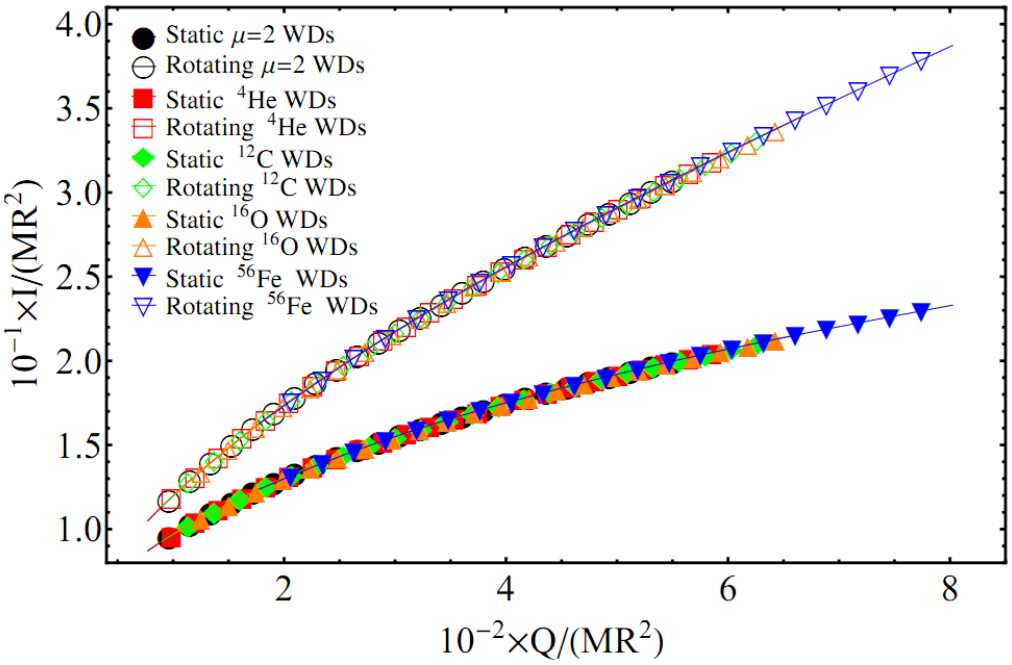


Figure 5.17 – Normalized quadrupole moment versus normalized moment of inertia

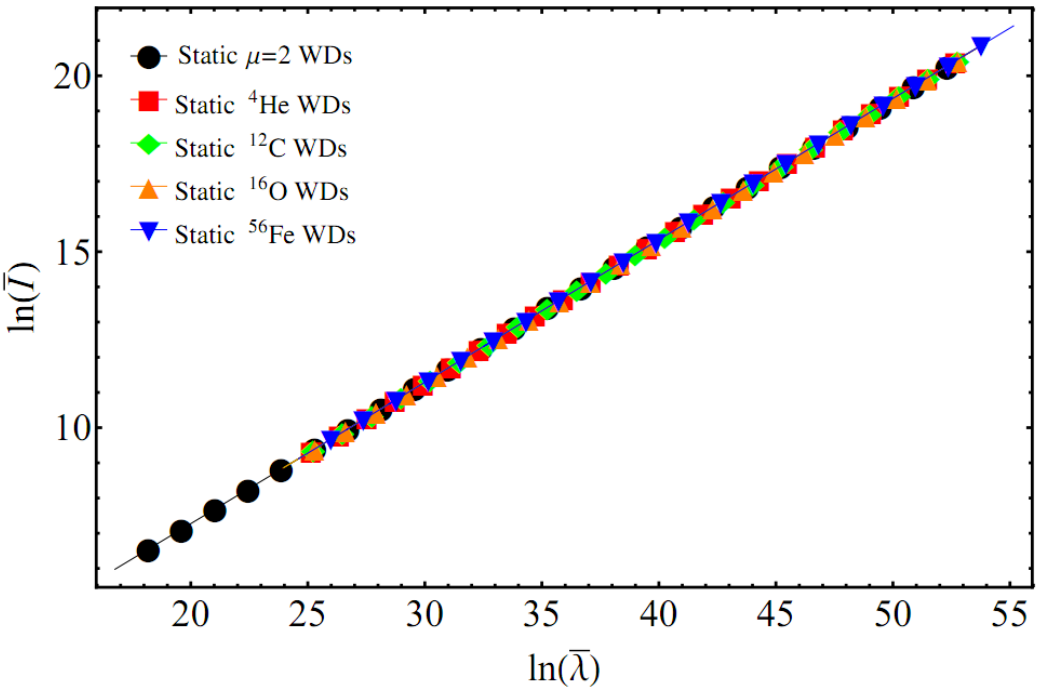


Figure 5.18 – Dimensionless moment of inertia versus dimensionless Love number

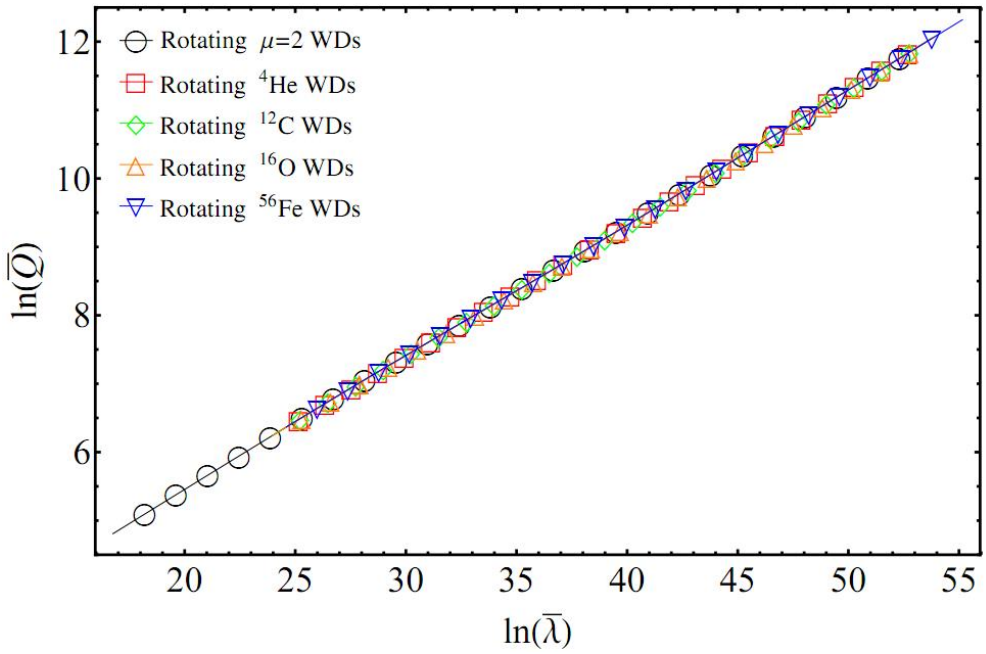


Figure 5.19 – Dimensionless quadrupole moment versus dimensionless Love number

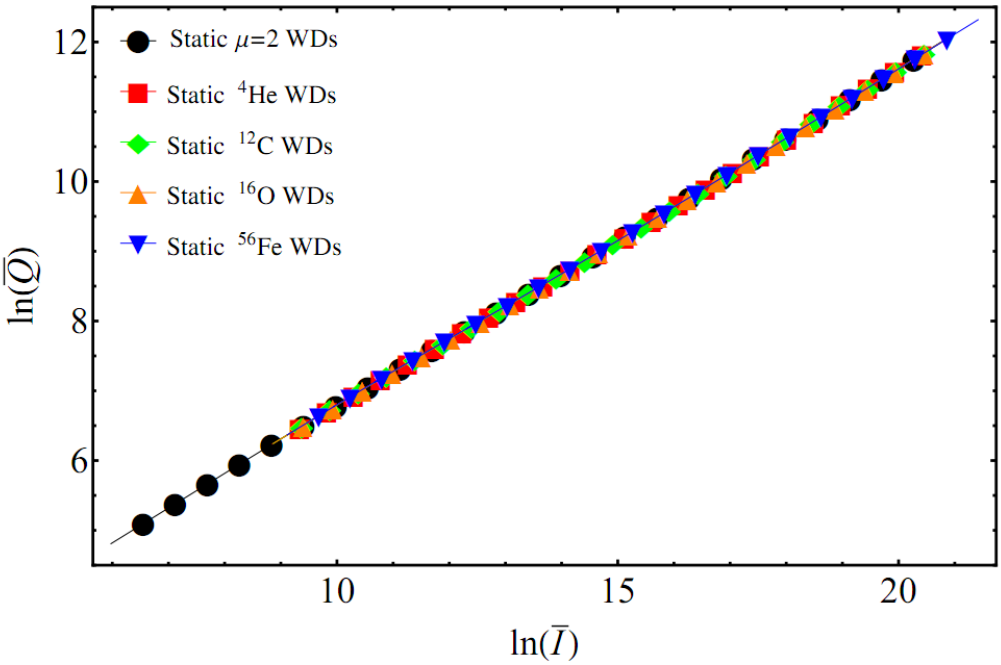


Figure 5.20 – Dimensionless quadrupole moment versus dimensionless moment of inertia

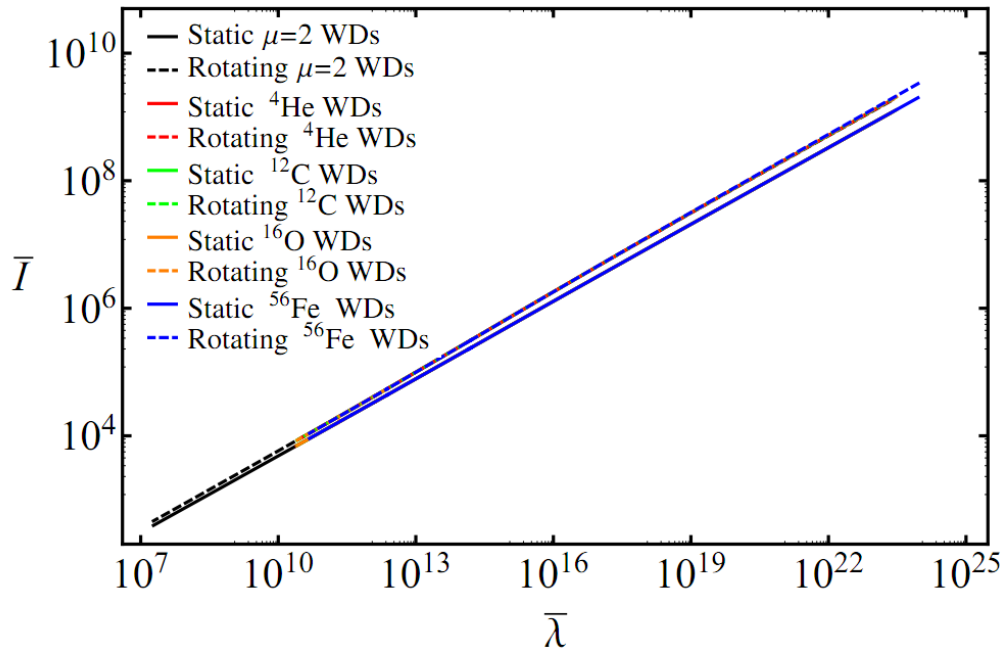


Figure 5.21 – Dimensionless moment of inertia versus dimensionless Love number. Here we included the moment of inertia of rotating WDs for the sake of comparison with the static one

The relation between the dimensionless quantities is given as

$$\bar{\lambda} = \left(\bar{I}^{(0)}\right)^2 \bar{Q}, \tag{5.3}$$

where $\bar{I}^{(0)}$ is the moment of inertia of the static configuration. If we write it in physical units

$$\lambda = \frac{Q}{\Omega^2}, \tag{5.4}$$

where Ω is the angular velocity of the star, this equation is equivalent to Eq. (2.253) of [132, p. 118], namely,

$$GI_{02} = -\frac{2}{3}\sqrt{\frac{5}{4\pi}}\, k_2 \Omega^2 a^5, \tag{5.5}$$

where $-I_{02}\sqrt{4\pi/5} = Q$ is the quadrupole moment, $(2/3)k_2 a^5/G = \lambda$ is the rotational Love number, though it does not directly depend on Ω. Although this relation is very well-known in NG, it is astonishing that it holds also in relativistic regimes [139]. Regarding the relation between the quadrupole moment and eccentricity, it can be confronted with Eq.(2.260) of [132, p. 119], i.e.,

$$J_2 = \frac{2}{3}\frac{k_2}{1+2k_2} e^2, \tag{5.6}$$

where $J_2 = Q/(Ma^2)$ is the dimensionless quadrupole defined as the normalization of the quadrupole moment in terms of the static mass and the square of the static radius. It then follows that there exist Q-e, I-Q and hence I-e-Q relations [154].

5.5 Summary

In section 5, we numerically integrated the underlying differential equations in order to determine the structure of slowly rotating classical WDs in hydrostatic equilibrium. In particular, the relations for the mass, the shapes of rotating stars, the moment of inertia, and the quadrupole moment were established as functions of the central density and angular velocity for the Chandrasekhar and Salpeter equations of state. All these quantities play a fundamental role in describing the equilibrium configurations of uniformly rotating main sequence stars as well as massive stars. The results we obtained for the interdependence between mass, radius, density, etc. are in agreement with other works related to rigidly rotating WDs in NG.

Furthermore, we considered all the stability criteria for rotating WDs and investigated only configurations that are stable against the mass-shedding limit, inverse β-decay instability and the axisymmetric secular instability. Unlike GR, in classical physics all WDs, even those composed of light elements such as helium ^{4}He and carbon ^{12}C, are stable against secular instabilities.

In addition, by solving the Radau-Clairaut equation or, equivalently, by determining the function ξ_2 for the deviation from spherical symmetry, we calculated

the rotational Love number and corroborated the I-Love-Q relations for rotating WDs. In doing this, we worked with the Chandrasekhar and Salpeter equations of state, selecting different nuclear compositions for the latter. In all diagrams, the WDs composed of pure iron ^{56}Fe have very particular distinctive features. Nonetheless, this distinction disappeared in the I-Love-Q relation. We also investigated the dependence of the moment of inertia and the quadrupole in terms of the eccentricity. We found that the I-Q-e relation is universal because it does not depend on the EoS and on the nuclear composition of the WD.

From the astrophysical standpoint, I-Love-Q-e relations are key points as just knowing only two of the parameters, one can extract the rest basic quantities. It would be interesting to investigate in the relativistic regime the I-Q-e relations and test other relations to be independent of the EoS.

CONCLUSION

The PhD dissertation presents results of the theoretical investigation of properties of equilibrium configurations of white dwarfs with a main focus on the effects of general relativity, finite temperatures, nuclear composition and rotation.

The result obtained within the section of the PhD dissertation is presented in more detail at the end of the each section, respectively. The general results of the PhD dissertation in a short form are the following:

1. The comparison of the exterior solutions of Einstein's gravitational field equations is considered. The relation of the approximate Kerr and Hartle-Thorne, Kerr and Fock, Hartle-Thorne and Sedrakyan-Chubaryan solutions were established. We have also proved the mathematical and physical equivalence of the Hartle-Thorne and Sedrakyan-Chubaryan solutions. We conclude that the Sedrakyan-Chubaryan solution can be considered as an alternative approach to describing the gravitational field of a slightly deformed stationary axially symmetric mass distribution in the slow rotation approximation. Moreover, the Sedrakyan-Chubaryan solution with its internal counterpart can be applied to various astrophysical problems together with the Hartle-Thorne solution on equal rights.

2. Equilibrium configuration of static white dwarfs are investigated in general relativity. It is shown that the effects of general relativity play an important role near the Chandrasekhar limit, more precisely, for large masses and small radii, in strong gravitational fields. However, it is also shown that the difference between Newtonian gravity and general relativity decreases for small masses and large radii due to the weakness of the gravitational field. In addition, the analytical expression for the Newtonian and general relativistic mass-radius relation has been found and its accuracy has been estimated.

Equilibrium configuration of static white dwarfs is investigated taking into account the effects of finite temperatures. It is necessary to take into account the effects of finite temperatures in white dwarfs with low masses. The consideration of the effects of temperature can explain observational data from Sloan Digital Sky Survey Data Release 4. Moreover, the core temperatures have been estimated for white dwarfs – satellites of the millisecond pulsars PSR J1738+0333, PSR J1012+5307 and PSR J1911-5958A.

Equilibrium configuration of static white dwarfs is considered taking into account the nuclear composition. It is shown that taking into account nuclear composition, neutronization threshold, the Thomas-Fermi corrections and Coulomb interactions is very important to describe some white dwarfs in the catalogues of the SDSS DR 10 and 12. In addition, the WD characteristics from the SDSS DR 4, 10 and 12 are analyzed. The histogram and the Gaussian distribution of mass and radius are constructed for the catalogues. The maximum, minimum and average values of the logarithm of the surface gravity, effective temperature, mass and radius are defined. The theoretical mass-radius relations are compared with the observational data.

3. Equilibrium configuration of cold and hot rotating white dwarfs is considered both in Newtonian gravity and general relativity. We show that The effects of temperature are more prominent for low-mass white dwarfs while the general

relativistic effects are more important for massive white dwarfs, however, the effects of rotation and nuclear composition affect the structure of white dwarfs in all mass ranges. Thereby, in order to construct a realistic model of white dwarfs the effects of finite temperatures, general relativity and rotation must be accounted for properly.

4. The I-Love-Q relations were corroborated for rotating WDs. In doing this, we worked with the Chandrasekhar and Salpeter equations of state, selecting different nuclear compositions for the latter. In all diagrams, the WDs composed of pure iron have very particular distinctive features. Nonetheless, this distinction disappeared in the I-Love-Q relation. We also investigated the dependence of the moment of inertia and the quadrupole in terms of the eccentricity. We found that the I-Q-e relation is universal because it does not depend on the EoS and on the nuclear composition of the WD.

The research tasks posed at beginning of the PhD dissertation are completely fulfilled and the purpose of the dissertation achieved.

The results obtained in the PhD dissertation can be directly used in the further investigations in astronomy, relativistic astrophysics, physics of compact objetcs and cosmology, thus it is valuable for the development of the field of study.

REFERENCES

1 Fontaine G., Brassard P., Bergeron P. The potential of white dwarf cosmochronology // The Publications of the Astronomical Society of the Pacific. – 2001. – Vol. 113, No. 782. – P. 409-435.

2 Ramos G.L. Evolutionary sequences for H and He atmosphere massive white dwarf stars: PhD thesis. – Porto Alegre, Brasil: Universidade Federal do Rio Grande do Sul, Instituto de Física, 2018. – P. 90.

3 Liebert J., Bergeron P., Eisenstein D., Harris H.C., Kleinman S.J., Nitta A., Krzesinski J. A helium white dwarf of extremely low mass // Astrophys. J. Lett. – 2004. – Vol. 606, No. 2. – P. L147-L149.

4 Werner K., Hammer N.J., Nagel T., Rauch T., Dreizler S. On possible Oxygen/Neon white dwarfs: H1504+65 and the white dwarf donors in Ultracompact X-ray Binaries, https://arxiv.org/pdf/astro-ph/0410690.pdf.

5 Shapiro S.L., Teukolsky S.A. Black holes, white dwarfs, and neutron stars: The physics of compact objects. – New-York: John Wiley & Sons, 1983. – P. 663.

6 Padmanabhan T. Theoretical astrophysics, Volume 2, Stars and stellar systems. – New-York: Cambridge University Press, 2001. – P. 596.

7 Chandrasekhar S. The maximum mass of ideal white dwarfs // Astrophys. J. – 1931. – Vol. 74. – P. 81-82.

8 Van Kerkwijk M.H., Chang P., Justham S. Sub-Chandrasekhar white dwarf mergers as the progenitors of type Ia supernovae // Astrophys. J. Lett. – 2010. – Vol. 722, No.2. – P. L157-L161.

9 Anand S.P.S. On Chandrasekhar's limiting mass for rotating white dwarf stars // Proceedings of the National Academy of Sciences of the USA. – 1965. – Vol. 54, No. 1. – P. 23-26.

10 Roxburgh I.W. On models of non spherical stars II. Rotating white dwarfs // Zeitschrift für Astrophysik. – 1965. – Vol. 62. – P. 134-142.

11 Roxburgh I. W., Durney B.R. Structure, oscillations and stability of rotating white dwarfs // Zeitschrift für Astrophysik. – 1966. – Vol. 64. – P. 504-511.

12 Papoyan V.V., Sedrakyan D.M., Chubaryan E.V. Newtonian theory of rapidly rotating white dwarfs // Astrophysics. – 1971. – Vol. 7, No. 1. – P. 55-61.

13 Geroyannis V.S., Hadjopoulos A.A. Models of white dwarfs under rapid uniform or differential rotation – Numerical results // Astrophys. J. Suppl. Ser. – 1989. – Vol. 70. – P. 661-677.

14 Geroyannis V.S., Papastiriou P.J. An iterative technique for computing rotating white dwarf models // Astrophys. J. Suppl. Ser. – 1994. – Vol. 90, No. 1. – P. 501-510.

15 Arutyunyan G.G., Sedrakyan D.M., Chubaryan E.V. Rotating white dwarfs in general relativity theory // Astrophysics. – 1971. – Vol. 7, No. 3. – P. 274-280.

16 Boshkayev K., Rueda J.A., Ruffini R., Siutsou I. On general relativistic uniformly rotating white dwarfs // Astrophys. J. – 2013. – Vol. 762, No. 2. – ID. 117. – P. 1-14.

17 Boshkayev K., Rueda J.A., Ruffini R., Siutsou I. General relativistic and Newtonian white dwarfs // Proceedings of the Thirteenth Marcel Grossmann Meeting

on General Relativity. – Singapore: World Scientific Publishing Company, 2015. – P. 2468-2474.

18 Ilkov M., Soker N. Type Ia supernovae from very long delayed explosion of core-white dwarf merger // MNRAS. – 2012. – V. 419, No. 2. – P. 1695-1700.

19 Andrew Howell D., Sullivan M., Nugent P.E. and et al. The type Ia supernova SNLS-03D3bb from a super-Chandrasekhar-mass white dwarf star // Nature. – 2006. – V. 443. – P. 308-311.

20 Salpeter E.E. Energy and pressure of a zero-temperature plasma // Astrophys. J. – 1961. – Vol. 134, No. 3. – P. 669-682.

21 Salpeter E.E., Van Horn H.M. Nuclear reaction rates at high densities // Astrophys. J. – 1969. – Vol. 155. – P. 183-202.

22 Feynman R.P., Metropolis N., Teller E. Equations of state of elements based on the generalized Fermi-Thomas theory // Phys. Rev. – 1949. – Vol. 75, No. 10. – P. 1561-1573.

23 Rotondo M., Rueda J.A., Ruffini R., Xue S.-S. Relativistic Thomas-Fermi treatment of compressed atoms and compressed nuclear matter cores of stellar dimensions // Phys. Rev. C. – 2011. – Vol. 83, No. 4. – P. 045805-1 – 045805-15.

24 De Carvalho S.M. Finite temperature effects in the white dwarf structure and neutron star cooling in general relativity: PhD thesis. – Rome: Sapienza University of Rome, 2013. – P. 136.

25 De Carvalho S.M., Rotondo M., Rueda J.A., Ruffini R. Relativistic Feynman-Metropolis-Teller treatment at finite temperatures // Phys. Rev. C. – 2014. – Vol. 89, No. 1. – P. 015801-1 – 015801-10.

26 Carceres Uribe D.L. Massive fast rotating highly magnetized white dwarfs: theory and astrophysical applications: PhD thesis. – Rome: Sapienza University of Rome, 2017. – P. 176.

27 Boshkayev K.A., Zhami B.A., Kalymova Zh.A., Brisheva Zh.N. Static white dwarfs taking into account the effects of finite temperatures and general relativity // News of the NAS of RK, phys.-math. series. – 2017. – Vol. 6, No. 316. – P. 27-38.

28 Migdal A.B., Popov V.S., Voskresenskii D.N. The vacuum charge distribution near super-charged nuclei // J. Exp. Theor. Phys. – 1977. – Vol. 45, No. 3. – P. 436-444.

29 Boshkayev K.A., Zhami B.A., Kalymova Zh.A., Brisheva Zh.N., Taukenova A.S., Aimuratov Y.K. White dwarf stars taking into account nuclear composition in general relativity // Recent Contributions to Physics. – 2017. – Vol. 62, No. 2. – P. 4-12.

30 Fermi E. Un metodo statistico per la determinazione di alcune priorieta dell'atome // Rendicondi Accademia Nazionale de Lincei. – 1927. – Vol. 6, No. 32. – P. 602-607.

31 Thomas L.H. The calculation of atomic fields // Mathematical Proceedings of the Cambridge Philosophical Society. – 1927. – Vol. 23, No. 5. – P. 542-548.

32 Boshkayev K.A., Suleymanova Sh.S., Aimuratov Ye.K., Zhami B.A., Toktarbay S., Taukenova A.S., Kalymova Zh. A. Correspondence of the Kerr and

Hartle-Thorne metrics // News of the NAS of the RK, phys.-math. series. – 2015. – Vol. 5, No. 303. – P. 151-158.

33 Boshkayev K.A., Suleymanova S.S., Zhami B.A., Taukenova A.S., Aimuratov Ye. K. Correspondence of the Fock and the Kerr metrics // News of the NAS of the RK, phys.-math. series. – 2015. – Vol. 3, No. 301. – P. 43-48.

34 Zhami B.A., Aimuratov Ye.K., Boshkayev K.A. Derivation of the Post-Newtonian metric // Международная зимняя школа-семинар по гравитации, астрофизике и космологии «Петровские чтения – 2014»: Аннотации лекций, тезисы докладов. – Казань, 2014, С. 48 – С. 16-17.

35 Boshkayev K., Quevedo H., Toktarbay S., Zhami B., Abishev M. On the equivalence of approximate stationary axially symmetric solutions of the Einstein field equations // Gravitation and Cosmology. – 2016. – Vol. 22, No. 4. – P. 305-311.

36 Boshkayev K., Abutalip M., Toktarbay S., Zhami B. Geodesics in the Hartle-Thorne spacetime // Abstracts of XII-th International Conference on Gravitation, Astrophysics and Cosmology, Dedicated to the centenary of Einstein's General Relativity theory». – PFUR, Moscow, Russia, 2015, P.141. – P. 42.

37 Boshkayev K.A., Quevedo H., Toktarbay S., Zhami B. The Sedrakyan-Chubaryan solution versus the Hartle-Thorne solution // Тезисы докладов 5-международной научной конференции «Физика и Физические Образование: Достижения и Перспективы Развития». – Бишкек, 2015. – С. 53.

38 Kerr R.P. Gravitational field of a spinning mass as an example of algebraically special metrics // Phys. Rev. Lett. – 1963. – Vol. 11, No. 5. – P. 237-238.

39 Boshkayev K.A., Quevedo H., Ruffini R. Gravitational field of compact objects in general relativity // Phys. Rev. D. – 2012. – Vol. 86, No. 6. – P. 064043-1 – 064043-13.

40 Newman E.T., Janis A.I. Note on the Kerr spinning-particle metric // Jour. of Math. Phys. – 1965. – Vol. 6, No. 6. – P. 915-917.

41 Newman E.T., Couch E., Chinnapared K., Exton A., Prakash A., Torrence R. Metric of a rotating, charged mass // Jour. of Math. Phys. – 1965. – Vol. 6, No. 6. – P. 918-919.

42 Ohanian H.C., Ruffini R. Gravitation and Spacetime, 3rd Edition. – New York: Cambridge University Press, 2013. – P. 546.

43 Hartle J.B. Slowly rotating relativistic stars. I. Equations of structure // Astrophys. J. – 1967. – Vol. 150, No. 3. – P. 1005-1029.

44 Hartle J.B., Thorne K.S. Slowly rotating relativistic stars. II. Models for neutron stars and supermassive stars // Astrophys. J. – 1968. – Vol. 153, No. 3. – P. 807-834.

45 Berti E., Stergioulas N. Approximate matching of analytic and numerical solutions for rapidly rotating neutron stars // MNRAS. – 2004. – Vol. 350, No. 4. – P. 1416-1430.

46 Berti E., White F., Maniopoulou A., Bruni M. Rotating neutron stars: an invariant comparison of approximate and numerical space-time models // MNRAS. – 2005. – Vol. 358, No. 3. – P. 923-938.

47 Andersson N., Comer G. L. Slowly rotating general relativistic superfluid neutron stars // Class. Quant. Grav. – 2001. – Vol. 18, No. 6. – P. 969-1002.

48 Stergioulas N. Rotating stars in relativity // Living Reviews in Relativity. – 2003. – Vol. 6, No. 1. – id. 3. – P. 1-109.

49 Bini D., Geralico A., Luongo O., Quevedo H. Generalized Kerr spacetime with an arbitrary mass quadrupole moment: geometric properties versus particle motion // Class. Quant. Grav. – 2009. – Vol. 26, No. 22. – id. 225006. – P. 1-23.

50 Boyer R.H., Lindquist R.W. Maximal analytic extension of the Kerr metric // Jour. of Math. Phys. – 1967. – Vol. 8, No. 2. – P. 265-281.

51 Hernandez W.C. Material sources for the Kerr metric // Phys. Rev. – 1967. – Vol. 159, No. 5. – P. 1070-1072.

52 Glampedakis K., Babak S. Mapping spacetimes with LISA: inspiral of a test body in a 'quasi-Kerr' field // Class. Quant. Grav. – 2006. – Vol. 23, No. 12. – P. 4167-4188.

53 Johannsen T., Psaltis D. Testing the no-hair theorem with observations in the electromagnetic spectrum. III. Quasi-periodic variability // Astrophys. J. – 2011. – Vol. 726, No. 1. – id. 11. – P. 1-10.

54 Johannsen T., Psaltis D. Testing the no-hair theorem with observations in the electromagnetic spectrum. I. Properties of a quasi-Kerr spacetime // Astrophys. J. – 2010. – Vol. 716, No. 1. – P. 187-197.

55 Psaltis D., Johannsen T. A ray-tracing algorithm for spinning compact object spacetimes with arbitrary quadrupole moments. I. Quasi-Kerr black holes // Astrophys. J. – 2012. – Vol. 745, No. 1. – P. 1-6.

56 Broderick A.E., Johannsen T., Loeb A., Psaltis D. Testing the no-hair theorem with event horizon telescope observations of Sagittarius A* // Astrophys. J. – 2014. – Vol. 784, No. 1. – id. 7. – P. 1-14.

57 Chandrasekhar S. The post-newtonian equations of hydrodynamics in general relativity // Astrophys. J. – 1965. – Vol. 142, No. 4. – P. 1488-1512.

58 Абдильдин М.М. О метрике вращающегося жидкого шара, Вопросы теории поля, под ред. С.Е. Ерматова. – Алма-Ата: изд. КазГУ, 1985. – С. 20-25.

59 Абдильдин М.М. Механика теории гравитации Эйнштейна. – Алма-Ата: Наука, 1988. – 199 с.

60 Абдильдин М.М. Проблема движения тел в общей теории относительности. – Алматы: Қазақ университеті, 2006. – 132 с.

61 Landau L.D., Lifshitz E.M. Course of theoretical physics, Volume 2: The classical theory of fields – Oxford: Butterworth-Heinemann, 1987. – P. 402.

62 Бошкаев К.А., Кеведо Э., Абишев М., Токтарбай С., Аймуратов Е. Соответствие метрик Фока и Хартла-Торна // Известия НАН РК, серия физико-мат. – 2013. – Т. 290, № 4. – С. 3-12.

63 Fock V. Theory of Space, Time and Gravitation, 2nd Edition. – Oxford: Pergamon Press, 1964. – P. 460.

64 Brumberg V.A. Essential relativistic celestial mechanics. – Bristol, England: Adam Hilger, 1991. – P. 271.

65 Chandrasekhar S. Ellipsoidal figures of equilibrium – an historical account // Communications on pure and applied mathematics. – 1967. – Vol. 20, No. 2. – P. 251-265.

66 Meinel R., Ansorg M., Kleinwachter A., Neugebauer G., Petroff D., Relativistic figures of equilibrium. – New York: Cambridge University Press, 2008. – P. 230.

67 Yagi K., Kyutoku K., Pappas G., Yunes N., Apostolatos Th. A. Effective no-hair relations for neutron stars and quark stars: Relativistic results // Phys. Rev. D. – 2014. – Vol. 89, No. 12. – P. 124013-1-124013-37.

68 Bradley M., Fodor G., Perjes Z. A slowly rotating perfect fluid body in an ambient vacuum // Class. Quant. Grav. – 2000. – Vol. 17, No. 14. – P. 2635-2640.

69 Fodor G., Perjes Z., Bradley M. Slowly rotating charged fluid balls and their matching to an exterior domain // Phys. Rev. D. – 2002. – Vol. 66, No. 8. – P. 084012-1 – 084012-12.

70 Bradley M., Eriksson D., Fodor G., Racz I. Slowly rotating fluid balls of Petrov type D // Phys. Rev. D. – 2007. – Vol. 75, No. 2. – P. 024013-1 – 024013-14.

71 Bradley M., Fodor G. Quadrupole moment of slowly rotating fluid balls // Phys. Rev. D. – 2009. – Vol. 79, No. 4. – P. 044018-1 – 044018-13.

72 Konno K., Obata T., Kojima Y. Deformation of relativistic magnetized stars // Astronomy & Astrophysics. – 1999. – Vol. 352. – P. 211-216.

73 Konno K., Obata T., Kojima Y. Flattening modulus of a neutron star by rotation and magnetic field // Astronomy & Astrophysics. – 2000. – Vol. 356. – P. 234-237.

74 Konno K. Moments of inertia of relativistic magnetized stars // Astronomy & Astrophysics. – 2001. – Vol. 372, No. 2. – P. 594-600.

75 Ioka K., Sasaki M. Relativistic stars with poloidal and toroidal magnetic fields and meridional flow // Astrophys. J. – 2004. – Vol. 600, No. 1. – P. 296-316.

76 Colaiuda A., Ferrari V., Gualtieri L., Pons J. A. Relativistic models of magnetars: structure and deformations // MNRAS. – 2008. – Vol. 385, No. 4. – P. 2080-2096.

77 Mallick R., Schramm S. Deformation of a magnetized neutron star // Phys. Rev. C. – 2014. – Vol. 89, No. 4. – P. 045805-1 – 045805-7.

78 Folomeev V., Dzhunushaliev V. Magnetic fields in anisotropic relativistic stars // Phys. Rev. D. – 2015. – Vol. 91, No. 4. – P. 044040-1 – 044040-10.

79 Sedrakyan D.M., Chubaryan E.V. Stationary axially symmetric gravitational fields // Astrofizika. – 1968. – Vol. 4, No. 2. – P. 239-255.

80 Sedrakyan D.M., Chubaryan E.V. Internal solution for stationary axially symmetric gravitational fields // Astrofizika. – 1968. – Vol. 4, No. 4. – P. 551-565.

81 Arutyunyan G.G., Sedrakyan D.M., Chubaryan E.V. Rotating superdense configurations in general relativity // Soviet Astronomy-AJ. – 1971. – Vol. 15, No. 3. – P. 390-395.

82 Arutyunyan G.G., Sedrakyan D.M., Chubaryan E.V. Internal structure of rotating baryon configurations // Soviet Astronomy-AJ. – 1973. – Vol. 17, No. 1. – P. 38-41.

83 Quevedo H. Multipole moments in general relativity: static and stationary vacuum solutions // Fortschritte der Physik. – 1990. – Vol. 38, No. 10. – P. 733-840.

84 Pappas G., Apostolatos Th.A. An all-purpose metric for the exterior of any kind of rotating neutron star // MNRAS. – 2013. – Vol. 429, No. 4. – P. 3007-3024.

85 Ryan F.D. Gravitational waves from the inspiral of a compact object into a massive, axisymmetric body with arbitrary multipole moments // Phys. Rev. D. – 1995. – Vol. 52, No. 10. – P. 5707-5718.

86 Boshkayev K.A., Zhami B.A., Kalymova Zh.A., Balgimbekov G.Sh., Taukenova A.S., Brisheva Zh.N., Koyshybaev N. Theoretical calculation of the main parameters of white white dwarfs // News of the NAS of the RK, physico-mathematical series. – 2016. – Vol. 3, No. 307. – P. 49-60.

87 Boshkayev K.A., Zhami B.A., Kalymova Zh.A. Application of Wolfram Mathematica program to the determination of the main parameters of white dwarf stars // Recent Contributions to Physics. – 2017. – Vol. 60, No. 1. – P. 136-146.

88 Калымова Ж.А., Жами Б.А., Бошкаев К.А. Исследование белых карликов в общей теории относительности // Тезисы докладов 5-международной научной конференции «Физика и Физические Образование: Достижения и Перспективы Развития». – Бишкек, 2015. – С.55.

89 Zhami B.A., Kalymova Zh.A., Balgimbekov G.Sh., Boshkayev K.A. Static Newtonian and general relativistic white dwarf stars // Book of Abstracts: International Scientific Conference of Students and Young Scientists «Farabi alemi». – Almaty, 2016. – P. 10.

90 Boshkayev K.A., Rueda J.A., Zhami B.A., Kalymova Zh.A., Balgymbekov G. Sh. Equilibrium structure of white dwarfs at finite temperatures // International Journal of Modern Physics: Conference Series. – 2016. – Vol. 41. – P. 1660129-1 – 1660129-7.

91 Boshkayev K., Rueda J.A., Ruffini R., Zhami B. Mass-radius relations of white dwarfs at finite temperatures // Proceedings of the 14th Marcel Grossmann Meeting on Recent Develop. in Theor. and Exp. GR, Astrophys., and Rel. Field Theories, University of Rome “La Sapienza”, Italy. – Singapore: World Scientific Publishing, 2018. – P. 4287-4290.

92 Zhami B., Boshkayev K., Kalymova Zh., Balgimbekov G., Taukenova A. Hot white dwarf stars in general relativity // Book of abstracts of the 9-th International Scientific Conference «Modern achievements of physics and fundamental physical education». – Almaty: Kazakh University, 2016. – P. 53.

93 Жәми Б.А., Бошкаев К.А. Ыстық ақ ергежейлі жұлдыздар жайлы // Book of Abstracts: International Scientific Conference of Students and Young Scientists «Farabi alemi». – Almaty, 2015. – P. 42.

94 Қалымова Ж.А., Макхамова Ж., Жәми Б., Балғымбеков Ғ., Бошқаев Қ.А. Қос жүйедегі ақ ергежейлі жұлдыздарды параметрлерін анықтау // Book of Abstracts: International Scientific Conference of Students and Young Scientists «Farabi alemi». – Almaty, 2017. – P. 54.

95 Zhami B.A., Kalymova Zh.A., Boshkayev K.A. Static hot relativistic white dwarf stars at finite temperatures // Book of Abstracts: International Scientific

Conference of Students and Young Scientists «Farabi alemi». – Almaty, 2018. – P. 31.

96 Баратова С.С., Жәми Б.А., Қалымова Ж.А., Бошқаев Қ.А. Ядролық құрамы әр түрлі ыстық ақ ергежейлі жұлдыздар // Book of Abstracts: International Scientific Conference of Students and Young Scientists «Farabi alemi». – Almaty, 2019. – P. 37.

97 Zhami B.A., Boshkayev K.A., Kalymova Zh.A., Brisheva Zh.N., Balgimbekov G.Sh. Static cold equilibrium white dwarf relativistic stars with known nuclear compositions // Materials of the International Scientific Conference dedicated to the 80th anniversary of Academician of the NAS RK Abdildin M.M. Abdildin readings: Actual Problems of Modern Physics. – Almaty, 2018. – P. 52-53.

98 Sagert I., Hempel M., Greiner C., Schaffner-Bielich J. Compact stars for undergraduates // Eur. J. Phys. – 2006. – Vol. 27, No. 3. – P. 577-610.

99 Misner Ch.W., Thorne K.S., Wheeler J.A. Gravitation. – San Francisco: W.H. Freeman and Company, 1973. – P. 1279.

100 Schutz B.F. A first course in general relativity, 2nd Edition. – New York: Cambridge University Press, 2009. – P. 406.

101 Tolman R.C. Static solutions of Einstein's field equations for spheres of fluid // Phys. Rev. – 1939. – Vol. 55, No. 4. – P. 364-373.

102 Oppenheimer J.R., Volkoff G.M. On massive neutron cores // Phys. Rev. – 1939. – Vol. 55, No. 4. – P. 374-381.

103 Zel'dovich Y.B., Novikov I.D. Relativistic astrophysics, Volume 1. – Chicago, IL: University of Chicago Press, 1971. – P. 540.

104 Chandrasekhar S. On stars, their evolution and their stability // Reviews of Modern Physics. – 1984. – Vol. 56, No. 2. – P. 137-147.

105 Rotondo M., Rueda J.A., Ruffini R., Xue S.-S. Relativistic Feynman-Metropolis-Teller theory for white dwarfs in general relativity // Phys. Rev. D. – 2011. – Vol. 84, No. 8. – P. 084007-1 – 084007-16.

106 Carvalho G., Marinho R., Malheiro M. The importance of GR for the radius of massive white dwarfs // AIP Conference Proceedings. – 2015. – Vol. 1693, No. 1. – P. 030004-1-030004-4.

107 Haensel P., Potekhin A.Y., Yakovlev D.G. Neutron Stars I: Equation of State and Structure. – New York: Springer-Verlag New York, 2007. – P. 620.

108 Antoniadis J., Van Kerkwijk M.H., Koester D., Freire P.C.C., Wex N., Tauris T.M., Kramer M., Bassa C.G. The relativistic pulsar-white dwarf binary PSR J1738+0333 – I. Mass determination and evolutionary history // MNRAS. – 2012. – Vol. 423, No. 4. – P. 3316-3327.

109 Koester D. Convective mixing and accretion in white dwarfs // Astronomy & Astrophysics. – 1976. – Vol. 52, – P. 415-425.

110 Panei J.A., Althaus L.G., Chen X., Han Z. Full evolution of low-mass white dwarfs with helium and oxygen cores // MNRAS. – 2007. – Vol. 382, No. 2. – P. 779-792.

111 Tremblay P.-E., Bergeron P., Gianninas A. An improved spectroscopic analysis of DA white dwarfs from the Sloan Digital Sky Survey Data Release 4 // Astrophys. J. – 2011. – Vol. 730, No 2. – P. 1-28.

112 Kepler S.O., Pelisoli I., Koester D., Ourique G. et al, New white dwarf stars in the Sloan Digital Sky Survey Data Release 10 // MNRAS. – 2015. – Vol. 446, No. 4. – P. 4078-4087.

113 http://astro.if.ufrgs.br/keplerDR10.html.

114 Kepler S.O., Pelisoli I., Koester D., Ourique G., Romero A.D., Reindl N., Kleinman S. J., Eisenstein D.J., Valois A.D.M., Amaral L. A. New white dwarf and subdwarf stars in the Sloan Digital Sky Survey Data Release 12 // MNRAS. – 2016. – Vol. 455, No. 4. – P. 3413-3423.

115 http://astro.if.ufrgs.br/keplerDR12.html.

116 Kepler S.O., Romero A.D., Pelisoli I., Ourique G. White dwarf stars // Int. J. Mod. Phys.: Conf. Ser. – 2017. – Vol. 45. – P. 1760023-1-1760023-23.

117 Meynet G., Maeder A. Stellar evolution with rotation. V. Changes in all the outputs of massive star models // Astronomy & Astrophysics. – 2000. – Vol. 361. – P. 101-120.

118 Meynet G., Maeder A. Stellar evolution with rotation. X. Wolf-Rayet star populations at solar metallicity // Astronomy & Astrophysics. – 2003. – Vol. 404. – P. 975-990.

119 Ekstrom S., Meynet G., Chiappini C., Hirschi R., Maeder A. Effects of rotation on the evolution of primordial stars // Astronomy & Astrophysics. – 2008. – Vol. 489, No.2. – P. 685-698.

120 Boshkayev K., Rueda J.A., Ruffini R., Siutsou I. General relativistic white dwarfs and their astrophysical implications // J. Kor. Phys. Soc. – 2014. – Vol. 65, No. 6. – P. 855-860.

121 Belvedere R., Boshkayev K., Rueda J.A., Ruffini R. Uniformly rotating neutron stars in the global and local charge neutrality cases // Nucl. Phys. A. – 2014. – Vol. 921. – P. 33-59.

122 Boshkayev K., Quevedo H., Kalymova Zh., Zhami B. Hartle formalism for rotating Newtonian configurations // European Journal of Physics. – 2016. – Vol. 37, No. 6. – id. 065602. – P. 1-30.

123 Boshkayev K., Rueda J.A., Ruffini R., Zhami B., Kalymova Zh., Balgimbekov G. Non-rotating and slowly rotating white dwarfs in classical physics // Physical Science and Technology. – 2015. – Vol. 2, No. 1. – P. 66-71.

124 Boshkayev K., Toktarbay S., Zhami B., Taukenova A., Suleymanova Sh., Kalymova Zh., Abutalip M. Equilibrium configurations of slowly rotating stars // Вестник КазНУ, серия физическая. – 2015. – Т. 52, № 1. – С. 78-95.

125 Қалымова Ж.А., Бошқаев Қ.А., Жами Б.А., Балгимбеков Г.Ш., Бришева Ж.Н. Классикалық физикадағы статикалық және айналмалы ақ ергежейлі жұлдыздар // Book of abstracts of the 9-th International Scientific Conference «Modern achievements of physics and fundamental physical education». – Almaty: Kazakh University, 2016. – P. 60.

126 Zhami B.A., Kalymova Zh.A., Balgymbekov G.Sh., Makhkamova Zh., Boshkayev K.A. On rotating white dwarf stars // Book of Abstracts: International Scientific Conference of Students and Young Scientists «Farabi alemi». – Almaty, 2017. – P. 15.

127 Boshkayev K.A., Rueda J.A. Zhami B.A. Rotating hot white dwarfs // Proceedings of the Twelfth Asia-Pacific International Conference on Gravitation, Astrophysics, and Cosmology. – Moscow: World Scientific Publishing, 2016. – P. 189-190.

128 Boshkayev K., Rueda J.A., Ruffini R., Zhami B. Induced compression of white dwarfs by angular momentum loss // Proceedings of the 14th Marcel Grossmann Meeting on Recent Develop. in Theor. and Exp. GR, Astrophys., and Rel. Field Theories, University of Rome "La Sapienza", Italy. – Singapore: World Scientific Publishing, 2018. – P. 4379-4384.

129 Zhami B.A., Boshkayev K.A., Kalymova Zh.A., Brisheva Zh.N., Balgimbekov G.Sh. Rotating white dwarfs at finite temperatures // Materials of the International Scientific Conference dedicated to the 80th anniversary of Academician of the NAS RK Abdildin M.M. Abdildin readings: Actual Problems of Modern Physics. – Almaty, 2018. – P. 47-52.

130 Zhami B.A., Kalymova Zh.A., Baratova S.S., Boshkayev K.A. Investigation of hot rotating white dwarfs in general relativity // Book of Abstracts: International Scientific Conference of Students and Young Scientists «Farabi alemi». – Almaty, 2019. – P. 25.

131 Chandrasekhar S., Roberts P. The ellipticity of a slowly rotating configuration // Astrophys. J. – 1963. – Vol. 138. – P. 801-808.

132 Poisson E., Will C.M. Gravity: Newtonian, Post-Newtonian, Relativistic, 1st edition. – New York: Cambridge University Press, 2014. – P. 792.

133 Chandrasekhar S. An introduction to the study of stellar structure. – Chicago, Ill: University of Chicago Press, 1939. – P. 509.

134 Jeffreys H. The Earth, 4th Edition. – Cambridge: Cambridge University Press, 1959. – P. 420.

135 Tassoul J.-L. Theory of rotating stars. – Princeton, NJ: Princeton University Press, 2015. – P. 524.

136 Chandrasekhar S. The equilibrium of distorted polytropes. I. The rotational problem // MNRAS. – 1933. – Vol. 93. – P. 390-406.

137 James R.A. The structure and stability of rotating gas masses // Astrophys. J. – 1964. – Vol. 140, No. 2. – P. 552-582.

138 Hartle J.B. Slowly rotating relativistic stars // Astrophys. and Space Sci. – 1973. – Vol. 24, No. 2. – P. 385-405.

139 Yagi K., Yunes N. I-Love-Q relations in neutron stars and their applications to astrophysics, gravitational waves, and fundamental physics // Phys. Rev. D. – 2013. – Vol. 88, No. 2. – id. 023009. – P. 1-28.

140 Yagi K., Yunes N. I-Love-Q: Unexpected universal relations for neutron stars and quark stars // Science. – 2013. – Vol. 341, No. 6144. – P. 365-368.

141 Lo K-W., Lin L-M. The spin parameter of uniformly rotating compact stars // Astrophys. J. – 2011. – Vol. 728, No. 1. – id. 12. – P. 1-6.

142 Cipolletta F., Cherubini C., Filippi S., Rueda J.A., Ruffini R. Fast rotating neutron stars with realistic nuclear matter equation of state // Phys. Rev. D. – 2015. – Vol. 92, No. 2. – P. 023007-1-023007-14.

143 Qi B., Zhang N.-B., Sun B.-Y., Wang S.-Y., Gao J.-H. A key factor to the spin parameter of uniformly rotating compact stars: crust structure // Reseacrh in Astronomy & Astrophysics. – 2016. – Vol. 16, No. 4. – P. 60-1-60-8.

144 Boshkayev K., Rueda J. A., Muccino M. Theoretical and observational constraints on the mass-radius relations of neutron stars, https://arxiv.org/pdf/1606.07804.pdf.

145 Friedman J.L., Ipser J. R., Sorkin R. D. Turning-point method for axisymmetric stability of rotating relativistic stars // Astrophys. J. – 1988. – Vol. 325. – P. 722-724.

146 Prodan S., Murray N. On the dynamics and tidal dissipation rate of the white dwarf in 4U 1820-302012 // Astrophys. J. – 2012. – Vol. 747, No. 1. – id. 4. – P. 1-15.

147 Boshkayev K., Rueda J.A., Ruffini R. On the maximum mass of general relativistic uniformly rotating white dwarfs // Int. J. Mod. Phys. E. – 2011. – Vol. 20, No. supp. 1. – P. 136-140.

148 Boshkayev K., Izzo L., Rueda J.A., Ruffini R. SGR 0418+5729, Swift J1822.3-1606, and 1E 2259+586 as massive, fast-rotating, highly magnetized white dwarfs // Astronomy & Astrophysics. – 2013. – Vol. 555. – id. A151. – P. 1-9.

149 Rueda J.A., Boshkayev K., Ruffini R., Loren-Aguilar P., Kulebi B., Aznar-Siguan G., Garcia-Berro E. A white dwarf merger as progenitor of the anomalous x-ray pulsar 4U 0142+61? // Astrophys. J. Lett. – 2013. – Vol. 772, No. 2. – id. L24. – P. 1-4.

150 Weber F., Glendenning N.K. Application of the improved Hartle method for the construction of general relativistic rotating neutron star models // Astrophys. J. – 1992. – Vol. 390, No. 2. – P. 541-549.

151 Glendenning N.K. Compact stars: Nuclear physics, particle physics, and general relativity. – New York: Springer, 2000. – P. 468.

152 Mathew A., Nandy M.K. General relativistic calculations for white dwarfs // Research in Astronomy and Astrophysics. – 2017. – Vol. 17, No.6. – P.61-1-61-10.

153 Boshkayev K. Non-rotating and slowly rotating stars in classical physics // Inter. J. of Math. and Phys. – 2014. – Vol. 5, No. 1. – P. 69-80.

154 Boshkayev K., Quevedo H., Zhami B. I-Love-Q relations for white dwarfs // Monthly Notices of the Royal Astronomical Society. – 2017. – Vol. 464, Iss. 4. – P. 4349-4359.

155 Hamada T., Salpeter E.E. Models for zero-temperature stars // Astrophys. J. – 1961. – Vol. 134. – P. 683-698.

156 Harrison B.K., Wakano M., Wheeler J.A. “Matter-energy at high density; end point of thermonuclear evolution,” In Onzieme Conseil de Physique Solvay, La Structure et l’evolution de l’univers. – Brussels: Stoops, 1958. – P. 124.

157 Audi G., Wapstra A.H., Thibault C. The AME2003 atomic mass evaluation: (II). Tables, graphs and references // Nuc. Phys. A. – 2003. – Vol. 729, No. 1. – P. 337-676.

158 Wapstra A.H., Bos K. The 1977 Atomic mass evaluation // Atomic Data and Nuclear Data Tables. – 1977. – Vol. 19. – P. 175-295.

159 Eisenstein D.J. et al. A catalog of spectroscopically confirmed white dwarfs from the Sloan Digital Sky Survey Data Release 4 // Astrophys. J. Suppl. Ser. – 2006. – Vol. 167, No. 1. – P. 40-58.

160 Kepler S.O., Kleinman S.J., Nitta A., Koester D., Castanheira B.G., Giovannini O., Costa A.F.M., Althaus L. White dwarf mass distribution in the SDSS // MNRAS. – 2007. – Vol. 375, No. 4. – P. 1315-1324.

161 Koester D., Kepler S.O. DB white dwarfs in the Sloan Digital Sky Survey data release 10 and 12 // Astron.&Astrophys. – 2015. – Vol. 583. – id. A86. – P. 1-9.